University of Alberta

Kinematically singular pre-stressed mechanisms as new semi-active variable stiffness springs for vibration isolation

by

Mojtaba Azadi Sohi

A thesis submitted to the Faculty of Graduate Studies and Research
in partial fulfillment of the requirements for the degree of

Doctor of Philosophy

Department of Mechanical Engineering

Fall 2010
Edmonton, Alberta

EXAMINING COMMITTEE

Dr. Saeed Behzadipour (Supervisor) – Mechanical Engineering

Dr. Gary Faulkner (Co-supervisor) – Mechanical Engineering

Dr. Donald Raboud – Mechanical Engineering

Dr. Gilbert Grondin – Civil and Environmental Engineering

Dr. Clément Gosselin – Mechanical Engineering, Laval University

To my Family

Kinematically singular pre-stressed mechanisms as new semi-active variable stiffness springs for vibration isolation

ABSTRACT

Researchers have offered a variety of solutions for overcoming the old and challenging problem of undesired vibrations. The optimum vibration-control solution that can be a passive, semi-active or active solution, is chosen based on the desired level of vibration-control, the budget and the nature of the vibration source. Mechanical vibration-control systems, which work based on variable stiffness control, are categorized as semi-active solutions. They are advantageous for applications with multiple excitation frequencies, such as seismic applications. The available mechanical variable stiffness systems that are used for vibration-control, however, are slow and usually big, and their slowness and size have limited their application. A new semi-active variable stiffness solution is introduced and developed in this thesis to address these challenges by providing a faster vibration-control system with a feasible size.

The new solution proposed in this thesis is a semi-active variable stiffness mount/isolator called the antagonistic **V**ariable **S**tiffness **M**ount (VSM), which uses a variable stiffness spring called the **A**ntagonistic **V**ariable stiffness **S**pring (AVS). The AVS is a kinematically singular prestressable mechanism. Its stiffness can be changed by controlling the prestress of the mechanism's links. The AVS provides additional stiffness for a VSM when such stiffness is needed and remains inactive when it is not needed. The damping of the VSM is constant and an additional constant stiffness in the VSM supports the deadweight. Two cable-mechanisms - kinematically singular cable-driven mechanisms and Prism Tensegrities - are developed as AVSs in this thesis. Their optimal configurations are identified and a general formulation for their prestress stiffness is provided by using the notion of infinitesimal mechanism.

The feasibility and practicality of the AVS and VSM are demonstrated through a case study of a typical engine mount by simulation of the mathematical models and by extensive experimental analysis. A VSM with an adjustable design, a piezo-actuation mechanism and a simple on-off controller is fabricated and tested for performance evaluation. The performance is measured based on four criteria: (1) how much the VSM controls the displacement near the resonance, (2) how well the VSM isolates the vibration at high frequencies, (3) how well the VSM controls the motion caused by shock, and (4) how fast the VSM reacts to control the vibration. For this evaluation, first the stiffness of the VSM was characterized through static and dynamic tests. Then performance of the VSM was evaluated and compared with an equivalent passive mount in two main areas of transmissibility and shock absorption. The response time of the VSM is also measured in a realistic scenario.

ACKNOWLEDGMENT

During my graduate studies, many people have helped and inspired me to complete this thesis. I cannot mention them all here, but I will always be grateful to them.

I owe a particular debt of gratitude to my PhD supervisor, Dr. Behzadipour, and the other members of my thesis committee. Dr. Behzadipour was a pleasure to work with: he was knowledgeable and insightful, friendly and truthful, and helpful and inspiring. I always enjoyed our conversation and benefited from high many suggestions. I was very fortunate to have Dr. Faulkner as my co-supervisor. He is renowned for his teaching and from his Biomechanics course I learned what no teaching seminar had taught me — how to treat every student with respect. In addition, I would like to thank Dr. Raboud and Dr. Gosselin for their valuable comments on my research and thesis.

I am also grateful for the support of all the technicians, non-academic and academic staff in the Mechanical Engineering Department. They created a friendly and supportive work environment that was very encouraging for graduate students. I thank all the staff particularly Gail Dowler for her helps and Bernie Faulkner, Roger Marchand and Andrew Campbell for sharing their technical knowledge and helping me to make a vibration isolator for my research.

Throughout my PhD program, I also benefited immeasurably from the friendship and support of Vahid Hosseii, Mahdi Shahbakhti, Mehdi Saffarian, Siavash Rezazadeh, Mohsen Eslami, Iman Izadi, Reza Mohammadi, Sepehr Pourrezaei, Marc Evans, Ahmad Ghazi, Omid Ghasemalizadeh, Mohammadreza Mirzaee, Masoud Mashkournia, Touqeer Sohail and …. Thank you all for giving me many happy memories of my life at the University. I want to particularly thank Saeed Ahmadi my old friend in Iran, who provided me with long-distance support by keeping me in good spirits whenever he telephoned me.

Finally, I cannot thank my family enough. Sharifeh and Morteza, my dear mother and father, without your continuous love and encouragement, I never could have accomplished my dreams. My memories of how unconditionally you dedicated your lives to me and my sister leave me speechless. I can only say that I love you both with all my heart. I also want to thank my dear wife, Maryam. My life would be incomplete without the blessing of your continuous patience, support, and love. Negar, my beautiful daughter, you were just a baby when I began my PhD studies. Now, you are beginning your education, just when I am finishing mine. Good luck *Negare baba*. I love you "one hundred million thousand." I am also thankful to my sister, Bahar, and my brother-in- low Arshia, for their support and hospitality during my work at University of Cambridge as visiting student.

Thanks you, Almighty God, for giving me all these wonderful people in my life.

CONTENTS

LIST OF TABLES

LIST OF FIGURES

LIST OF SYMBOLS AND NOMENCLATURE

Abbreviation	Phrase	Definition/Description
AVS	**A**ntagonistic **V**ariable stiffness **S**pring	The semi-active variable stiffness spring made with a kinematically singular prestressed mechanism.
VSM	antagonistic **V**ariable **S**tiffness **M**ount	The vibration mount/isolator made with an **AVS** in parallel with a soft rubber mount.
VSM-C	**VSM** that uses **C**ables	The **VSM** made based on a cable-driven mechanism in which cables are used for maintaining the prestress.
VSM-P	**VSM** that uses **Pl**ates	The **VSM** made based on a cable-driven mechanism in which plates are used for maintaining the prestress.
FOIM	**F**irst-**O**rder **I**nfinitesimal **M**echanism	Differential motions at the joints of a mechanism that do not change the lengths of the links. FOIM is also called first-order infinitesimal flex.
TP	**T**ensegrity **P**rism	One type of tensegrity
TPS	**T**ensegrity **P**rism **S**pring	The **AVS** made with a **TP**.

Symbols	Definition
n	Number of cables in cable-driven mechanism, Number of bars in Tensegrity Prisms
N_m	Number of members in a pin-jointed structure
N_j	Number of nodes in a pin-jointed structure
N_c	Number of displacement constraints in a pin-jointed structure
m	Number of mechanism in a pin-jointed structure
s	Number of states of prestress in a pin-jointed structure
m_{cf}	Number of the infinitesimal mechanisms in a pin-jointed structure
R	Stiffness ratio
f	Frequency of Excitation
f_n	Natural frequency
θ	Top n-gon twist in a n-gon truncated pyramid
β	Top n-gon twist in a n-gon TP
φ	Phase response
$\hat{\mathbf{u}}_i$	Unit direction vector of the i^{th} cable in a cable-driven mechanism
$\hat{\mathbf{q}}$	Unit direction vector
$\hat{\mathbf{e}}_1, \hat{\mathbf{e}}_2, \hat{\mathbf{e}}_3$	Unit vectors of the global coordinate frame
L_c	Length of cable
L_b	Length of platform
l_i	Lengh of i^{th} cable in a cable-driven mechanism
$\mathbf{r}_i$	Moment arm vector of the i^{th} cable in a cable-driven mechanism
r_{ix}	Component of $\mathbf{r}_i$ along x axis
r_{iy}	Component of $\mathbf{r}_i$ along y axis
r_{iz}	Component of $\mathbf{r}_i$ along z axis
d	Diameter of cables in a cable-driven mechanism
L_e	Effective length of cable or plate in a VSM
L_d	Dead length of cable in a VSM-C
r_h	Radius of the circumscribing circles in the top n-gon TP

r_o	Radius of the circumscribing circles in the base n-gon TP
h	Height of TP
h_p	Height of TP at the tensegrity state
L	Length of vertical cables in a TP
L_p	Length of vertical cables in a TP at the tensegrity state
b	Length of bars in a TP
L_N	Natural length of the cable
$\mathbf{d}$	Small nodal displacement vector of a pin-jointed structure
$\mathbf{e}$	Small vector of member elongations in a pin-jointed structure
m_s	Sprung mass
m_e	Engine mass
E	Elastic modulus
τ_p	Antagonistic force / Prestress
$\mathbf{f}$	External force vector (on the platform of a cable-driven mechanism or on the nodes of a pin-jointed structures)
τ	Internal forces of components of a mechanism
$\boldsymbol{\tau}$	Internal force vector of components of a pin-jointed structure
F_z	Force along z axis
M_z	Moment about z axis
W_o	Deadweight
c	General symbol for viscous damping
C_r	Constant damping of the passive mount
c_r	Constant damping of the soft rubber mount
c_{sf}	Front suspensions' damping
c_{sr}	Rear suspensions' damping
k	General symbol for stiffness
k_T	Translational stiffness
k_R	Rotational stiffness
k	General symbol for stiffness
K_r	Constant stiffness of the passive mount
k_r	Constant stiffness of the soft rubber mount
k_{AVS}	Total stiffness of AVS
$\mathbf{K}$	Tensor of total stiffness of cable-driven mechanisms
$\mathbf{K}_e$	Tensor of elastic stiffness of cable-driven mechanisms
$\mathbf{K}_p$	Tensor of prestress stiffness (antagonistic stiffness) of cable-driven mechanisms
k_i	Elastic stiffness of i^{th} cable in cable-driven mechanism
k_{sf}	Front suspensions' stiffness
k_{sr}	Rear suspensions' stiffness
K_T	Stiffness of a translational TPS
k_c	Stiffness of cable
$K_{T_{\tau_p}}$	Translational prestress stiffness of a TPS
$K_{T_{\tau_l}}$	Translational load stiffness of a TPS
K_{T_e}	Translational elastic stiffness of a TPS
K_R	Stiffness of a rotational TPS
$K_{R_{\tau_p}}$	Rotational prestress stiffness of a TPS
$K_{R_{\tau_l}}$	Rotational load stiffness of a TPS

K_{R_e}	Rotational elastic stiffness of a TPS
k_D	Dynamic stiffness
J_T	Jacobian matrix of a translational TPS
J_R	Jacobian matrix of a rotational TPS
$\mathbf{A}$	Equilibrium matrix of a pin-jointed structure

Chapter 1 INTRODUCTION

Variable stiffness is widely used for two major applications: vibration-control [1,2,3] and robotics applications where the robot interacts with delicate environments [4,5,6,7]. In robotics, stiffness is usually determined by the stiffness of the robot's actuators and, hence, the power consumption is proportional to the external excitation. For this reason, this stiffness control is called active stiffness control. The vibration-control systems, such as vibration isolators or vibration absorbers, are usually classified into three main groups: passive, active and semi-active systems. The passive systems can be optimized for use in a certain frequency range. However, they have significant limitations where broadband disturbances are encountered.

Active and semi-active mounts/isolators are used for demanding and challenging vibration-control applications where passive mounts do not provide an adequate response. The core of an active system is a variable force actuator that exerts an adjustable force to counteract the undesired vibration. Active systems have broad bandwidth and higher control authority and usually require major control efforts since they use the external power directly to suppress the mechanical energy of the vibration. These systems may also suffer from control-induced instability. As a result, active systems are considered as expensive solutions and their cost limits their industrial usage.

Semi-active systems, on the other hand, tend to overcome the disadvantages of passive and active systems by using variable stiffness elements/springs or variable damping elements integrated with an uncomplicated control algorithm to tune the stiffness and damping for optimum performance. The power consumption in semi-active systems is much lower than that in the active systems because the power is used indirectly to adjust the system's vibration properties by changing the stiffness and damping coefficients. The semi-active systems can be designed to achieve the majority of the performance characteristics of the active systems. In summary, semi-active mounts use uncomplicated control systems, consume less energy than active mounts, and provide a cost-efficient solution. Therefore, they are widely utilized in industrial applications [1,2,3].

In this thesis, a new semi-active vibration mount/isolator called the antagonistic **V**ariable **S**tiffness **M**ount (VSM) is introduced. Vibration mounts have two fundamental vibration characteristics: damping and stiffness. The VSM consists of a soft rubber mount which is in parallel with a variable stiffness spring called the **A**ntagonistic **V**ariable stiffness **S**pring (AVS). The AVS provides stiffness when it is needed and remains inactive when it is not

needed. The soft rubber mount provides a constant damping and an additional constant stiffness to support the deadweight. This soft rubber mount also acts as a safety component for a real situation where the AVS or the control system fails to operate properly.

The AVS is a kinematically singular prestressable mechanism with a stable **F**irst-**O**rder **I**nfinitesimal **M**echanism (FOIM). The stiffness of an AVS can be changed by controlling the antagonistic forces (prestress) of the mechanism's links. Unlike other mechanical variable stiffness springs, which vary the stiffness based on the geometry change [3,8], the proposed AVS uses force control to change the stiffness and, as a result, provides a faster response [9,10].

In the literature, antagonistic stiffness has not yet been reported as a semi-active variable stiffness for vibration-control systems.

1.1 Problem Statement

Vibration is often undesirable and harmful. Powered mechanical devices are usually sources of vibrations that may significantly influence the devices' performance as well as jeopardizing the surroundings. Earthquakes are another source of harmful vibrations that have fatal and devastating results. Undesired vibrations may also waste energy, decrease the service life of machinery and produce unwanted noise.

Researchers have offered a variety of solutions for overcoming the old problem of undesired vibrations. Reducing the vibrations at the source (e.g., balancing the mechanical systems), isolating the vibrations through appropriate mounting of sensitive equipment and reducing the response (e.g., dissipating the energy) are the three solutions normally implemented [11]. All the vibration-control systems that implement the latter two techniques are classified into three categories: passive, semi-active and active. Each solution has its own advantages, limitations and disadvantages. Choosing the right solution depends on several parameters such as the desired level and speed of vibration-control, the budget and the nature of the vibration source. Mechanical vibration-control systems which work based on variable stiffness control are one of the available semi-active solutions. They are advantageous for applications with multiple excitation frequencies, such as seismic applications. The available mechanical variable stiffness vibration-control systems, however, are slow and massive, and their slowness and size have limited the application of these systems. The variable stiffness springs and mounts developed in this thesis address this challenge by providing a fast response and a smaller mechanical variable stiffness vibration-control system.

1.2 Motivation

The initial component of this work began with the study of the stiffness of special cases of parallel mechanisms, i.e., cable-driven manipulators/mechanisms. Cable-driven manipulators/ mechanisms are redundant parallel manipulators in which cables are used to provide the motion of the moving platform. Since cables are unilateral force elements, one should ensure all the cables in a cable-driven mechanism are in tension; otherwise, it will collapse. The cables can be kept in tension by redundant actuation and maintaining prestress in the cables (i.e., antagonistic cable forces). The cable's prestress creates an additional stiffness component called prestress stiffness (or antagonistic stiffness). This new stiffness coexists with two other sources of stiffness: elastic stiffness and load stiffness. The latter two originate from the elasticity of the links and the external load. Changing the level of the

prestress changes the prestress stiffness and eventually changes the total stiffness felt on the platform of the cable-driven mechanism. However, the prestress stiffness is usually thought to be "inferior" and hence negligible. However, in [12], Behzadipour et. al. showed by an example that the effect of the prestress on the total stiffness can be significant. These researchers found that a planar cable-driven mechanism became unstable for a certain level of prestress. Consideration of similar planar geometries in [13] showed redundant cable-driven mechanisms, near their kinematically singular positions, demonstrated this effect. Again in [9,14], the effects of prestress in a singular cable-driven mechanism were found to be profound. These results led to investigations of another type of prestressable and kinematically singular cable-based mechanism known as Tensegrities.

1.3 CHALLENGES

Up to the present, the use of prestress stiffness as a semi-active variable spring for vibration applications is a relatively novel idea. The existence of similar attempts and studies could have been helpful for this thesis, which became an opportunity for carrying out a novel research.

This work takes advantage of the prestress stiffness in kinematically singular configurations, even though singular configurations are usually judged as problematic and avoided in robotics and mechanism design. In addition, prestress stiffness is usually considered and reported as a negligible portion of the total stiffness, whereas in this thesis, prestress stiffness is used as an effective source for stiffness control for real industrial applications. Some of the major concerns expressed by others in the mechanisms and robotics community regarding the use of an AVS include:

1. The prestress stiffness is small, therefore the total stiffness of the AVS may not be significant enough to be used in a real application.
2. Because of singularity of the geometry, the stiffness of AVS will be very nonlinear.
3. The total stiffness of the AVS will be small unless special cables or actuators are used.

While these concerns are genuine, this thesis shows that by using feasible components in a feasible space, an AVS can be designed with a simple geometry. One possible design was detailed and prototyped as a proof of concept and to demonstrate its viability. In the prototype, the prestress stiffness of the AVS could rise to more than three times that of a regular passive engine mount. It is also shown that the AVS, in general, is a nonlinear spring. However, the nonlinearity can be tailored by using the geometry appropriate for an AVS 's application.

1.4 CONTRIBUTION

The main contribution of this thesis is that it develops a new variable stiffness spring called the AVS for vibration applications. The characteristics of the AVS that make it practical and advantageous for industrial applications include the following:

- Semi-active solution.
- Fast response.
- Simple On-off control.
- Full stiffness controllability.

- Large stiffness magnitude.
- Simple geometry.
- Feasible size.
- Simple motions: Translation or Rotation.

The specific contributions of this thesis are the following:

- The novel concept of making a variable stiffness spring by using kinematically singular prestressed cable mechanisms is presented, and the fundamental challenges are addressed.
- The optimal configurations of cable-driven mechanisms are identified for achieving effective variable prestress stiffness.
- The prism tensegrities are developed as a second option for achieving effective variable prestress stiffness.
- A general formulation for the prestress stiffness of the implemented singular mechanisms is provided by using the notion of infinitesimal mechanism/infinitesimal flex.
- The feasibility of the concept is demonstrated through a case study of a typical engine mount by simulation of the mathematical model and by extensive experimental analysis.

1.5 THESIS OVERVIEW

Chapter 2 describes the key concepts such as the antagonistic force and stiffness. This chapter also introduces the process of making an AVS and a VSM. The variable stiffness springs discussed in the literature are reviewed, as well as the desired characteristics of a variable stiffness spring. In addition, Chapter 2 explains why cable-based mechanisms are superior for making an and how a VSM works and how it improves the vibration response at different frequency ranges.

Chapter 3 presents the AVS developed from cable-driven mechanisms. The stiffness of cable-driven mechanisms is studied in order to find the geometries that provide the desired characteristics for the variable stiffness spring explained in Chapter 2.

Chapter 4 presents the development of an AVS from tensegrities called the TPS. This chapter reviews the literature about pin-jointed structures, showing that a subgroup of prestressed pin-jointed structures such as tensegrities can be used as an AVS for vibration-control applications. Tensegrity prisms are recognized as an applicable tensegrity for making an AVS. A comprehensive formulation of the stiffness is derived and presented for the proposed tensegrity-based AVS.

At the end of Chapter 3 and Chapter 4, in order to study the feasibility of the developed AVSs and VSMs in a real application, two similar case studies are presented on the engine mount of a typical vehicle. In these case studies, the VSM acts as a semi-active engine mount, and its performance is compared with that of a passive engine mount designed for the same application.

In Chapter 5, the performance of the VSM as predicted by the case studies in Chapter 3 and Chapter 4 is experimentally evaluated. For this reason, a VSM was built, set as an engine mount, and tested. In this chapter, the design of the VSM and the testing setup are briefly explained, and experimental results are presented and analyzed.

Chapter 6 summarizes and discusses the contributions of this thesis and suggests some possible applications and directions for extending it.

1.6 RELATED PUBLICATIONS

This research has been presented at several conferences held by the Automotive Engineering, and Mechanism and Robotics communities [13,14,15,16,17]. The development of an AVS by using cable-driven mechanisms which is presented in Chapter 3, has been published in the *Journal of Mechanism and Machine Theory* [9]. The research presented in Chapter 4 about the development of an AVS by using tensegrity prisms has been submitted as a paper to the ASME *Journal of Mechanisms and Robotics* and has been accepted for publication [10]. Some aspects of the experimental analysis and results for the performance of the AVS mentioned in Chapter 5 have been described in a paper submitted for publication to the *Journal of Sound and Vibration* [18]. Finally, a provisional patent [19] has been filed for a novel variable stiffness spring made by using tensegrity prisms.

Chapter 2 ANTAGONISTIC VARIABLE STIFFNESS FOR VIBRATION APPLICATIONS

In order to explain the significance of antagonistic variable stiffness, the desired characteristics of a variable stiffness spring and some of the available variable stiffness springs are reviewed in this chapter. In addition, it will be explained why cable-driven mechanisms and tensegrities are superior for making an AVS. An AVS when used in parallel with a soft rubber mount forms a vibration mount/isolator called a VSM. It will be explained at the end of this chapter how a VSM works and how it improves the vibration response at different frequency ranges.

2.1 ANTAGONISTIC FORCE (PRESTRESS)[1]

The word "antagonistic" originates from the Greek verb *antagonizesthai*, which means "struggle against". This word is used in physiology to describe the antagonistic muscles and has been adopted in Engineering to convey a similar concept in mechanisms. The human body, which can be seen as a mechanism formed by rigid elements (bones) and elastic elements (muscles), moves and works by antagonistic actuation. Since muscles can exert only a pulling force, antagonistic pairs are needed in the body. An example of this kind of muscle pairing is the biceps and triceps (Figure 2-1).

[1] The term "prestress" will be preferred to "antagonistic force" in this work as this term can be used as both noun and verb. However, "prestress" and "antagonistic force" are equivalent.

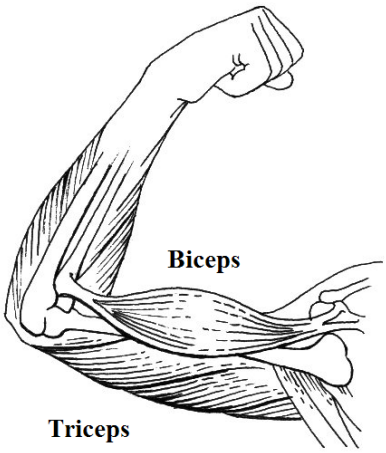

Figure 2-1. Biceps and triceps are antagonistic pair muscles that can apply antagonistic forces (Courtesy Pearson Scott Foresman)

In kinematics, antagonistic forces (prestress forces) are the internal forces in the links of a mechanism where the externally applied force/moment is zero. It is clear that not every mechanism can posses antagonistic forces. The existence of antagonistic forces requires a mechanism to be either kinematically singular or redundantly actuated. In Figure 2-2a, a 4-bar linkage is shown at a singular position. The links of this mechanism can be axially preloaded (e.g., by creating equal tensile forces in links 2 and 4) while there is no external load. These axial forces (τ_p) in the links are antagonistic forces since they internally satisfy the static equilibrium and result in no external force. Figure 2-2b shows a planar cable-driven mechanism formed by a rigid moving platform restrained by four variable length cables. The mechanism has three degrees of freedom provided by four actuators, which control the lengths of the cables. There is one degree of actuation redundancy. The force of the redundant cable, which can be any of the four, is balanced by properly selected forces in the other three cables. As a result, a set of antagonistic forces (prestresses) is formed in the cables that correspond to zero external force and moment on the plarform.

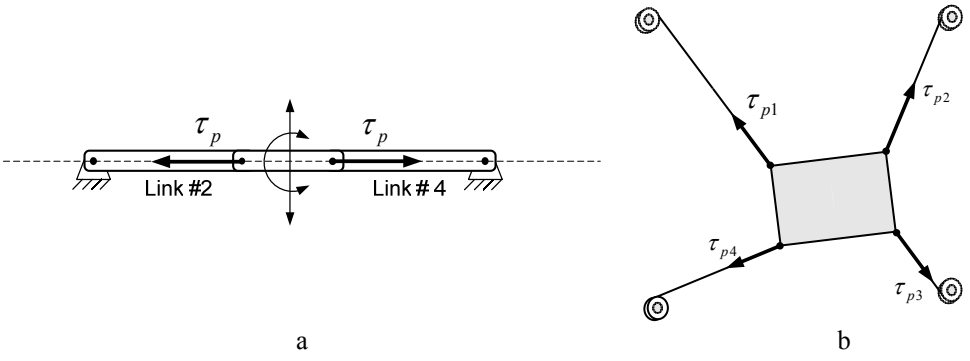

Figure 2-2 Antagonistic stiffness of a 4-bar linkage

2.2 ANTAGONISTIC STIFFNESS (PRESTRESS STIFFNESS)

Prestress (antagonistic force), when present in a mechanism, creates a stiffness which is called prestress stiffness (antagonistic stiffness). It will be shown in sections 3.1 and 4.4 that this stiffness is merely a function of the geometry and prestresses in the links. From Figure

2-2a, the reader can intuitively realize that when the links are axially prestressed, the middle link will demonstrate some stiffness in the vertical and rotational directions as shown. For example, it becomes harder to move the middle link up and down vertically when the prestress of the links increases to higher magnitudes. As a result, this mechanism (Figure 2-2a) can be said to have variable stiffness in this configuration that can be changed by the level of the prestress. In other words, this mechanism acts as a translational spring (Figure 2-3.a) in the vertical direction, but has variable stiffness set by the level of prestress. In a similar way, this mechanism (Figure 2-2.a) demonstrates variable rotational stiffness in its middle link and acts as a rotational spring (Figure 2-3.b).

a **b**

Figure 2-3. a. Example of translational spring b. Example of rotational spring

The redundant mechanism of Figure 2-2b has also prestress stiffness, which depends only on the prestress of the cables and can be expressed by a tensor (a 3-by-3 matrix in planar coordinates).

Prestress stiffness, as will be shown in section 3.2, may have either a stabilizing or destabilizing influence (i.e., it may or may not tend to restore the original geometry when the mechanism undergoes a displacement). Therefore, increasing the prestress, in an unstable prestress stiffness, decreases the overall stiffness.

Note that the prestress stiffness generally (not always) coexists with the elastic stiffness of the mechanism caused by the elasticity of the links and joints. These two stiffness components are in parallel. As a result, in general, the total stiffness of an unloaded mechanism is the summation of the antagonistic and elastic stiffness.

The relative magnitude of prestress stiffness versus the total stiffness determines its influence on the overall stiffness. In many mechanisms, the prestress stiffness is small relative to the elastic one [20] and, hence, is ignored [21,22] or even referred to as “inferior” [20] in the stiffness analysis. Nevertheless, in some configurations such as the one shown in Figure 2-2.a, the geometry of the mechanism makes the prestress stiffness the dominant stiffness in the directions shown. Furthermore, this author has shown in [9,10] that the magnitude of the prestress stiffness can be designed to be comparable with the other sources of the stiffness components and can also be large enough to be used for a wide range of industrial applications.

In the literature, prestress stiffness has not yet been explored as a variable stiffness for vibration-control. Some other applications of prestress stiffness that have been reported in the literature includes stiffness modulation in parallel manipulators with redundant actuation [79], grasping [4,5,80,81], tensegrity mechanisms [23,24,82] and bio-mechanics [83,84,85]. In most of these works, kinematics and virtual work are used for deriving the stiffness formulations while in some others [25,26,27,28], the stiffness is found by linearizing the dynamic equations of motion. The prestress stiffness has been also studied in structural engineering as prestress stiffness and is found from linearizing the static equilibrium equations and using the theory of virtual work [23,29].

In this thesis, the prestress stiffness of certain mechanisms is utilized to obtain an effective variable stiffness spring suitable for a wide range of vibration-control applications. This spring is called the Antagonistic Variable stiffness Spring (AVS) in this thesis. Almost all of the available industrial springs are either translational or rotational springs (e.g., Figure 2-3). This simplicity, facilitates their application in mechanical machinery and systems. For this reason, an AVS was also devised to work as either a translational or a rotational spring.

2.3 ANTAGONISTIC VARIABLE STIFFNESS SPRING (AVS)

Antagonistic variable stiffness springs (AVSs) are prestressable mechanisms with singular kinematics. The basic concept of an AVS is presented in the simplest form in Figure 2-4.a which shows a four-bar planar mechanism in a kinematically singular configuration. This configuration has two key characteristics that makes it ideal for making an AVS: prestressability and possessing infinitesimal mechanisms/infinitesimal flex. The prestressability in this mechanism enables it to maintain an arbitrary prestress of τ_p in its links. Prestress in a prestressable mechanism can improve or deteriorate its stability. For example in the mechanism shown in Figure 2-4.a, a tensile prestress improves the stability, but a compressive prestress makes the mechanism unstable.

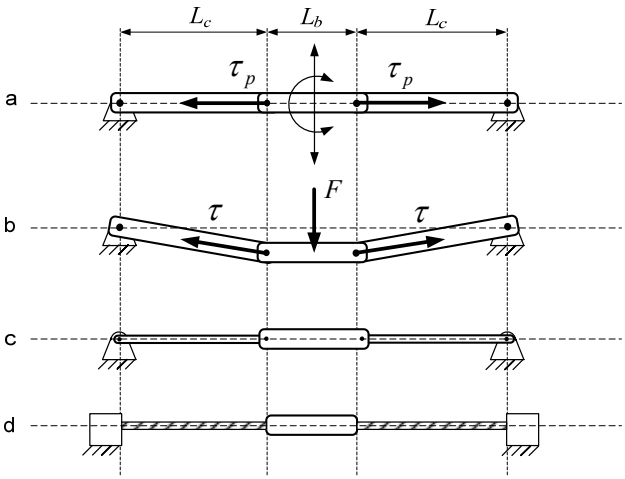

Figure 2-4. a. Four-bar mechanism in a kinematically singular and prestressable configuration b. The same mechanism deflected under external load c. Side links are substituted with thinner links that have lower elasticity d. To eliminate joints, cables are used as side links

In terms of kinematics, this configuration of a four-bar mechanism is locked, so that it does not have any finite mechanism, but does have a first-order infinitesimal mechanism (an infinitesimal flex). The first-order infinitesimal mechanism/infinitesimal flex is the second key characteristic of this mechanism for making variable stiffness. First-order infinitesimal mechanisms are the differential motions at the joints of a mechanism that do not change the lengths of the links.[2] The singular four-bar linkage (Figure 2-4.a) has two first-order infinitesimal mechanisms in the directions shown in the figure. The first one is a pure differential translation of the middle link vertically in the up and down directions and the second one is a pure differential rotation of the middle link either C.W. or C.C.W.

It will be shown later that the stiffness of an unloaded prestressable mechanism (such as the one shown in Figure 2-4.a), in general, is a function of the elasticity of the links, the

[2] For complete and mathematical definition of first order mechanisms see [20]

geometry of the mechanism and the prestress. In a special case, the elasticity of the links does not contribute to the stiffness of the prestressable mechanism. This unique characteristic is found only for prestressable mechanisms with a FOIM (First-order infinitesimal mechanism) along their FOIM. In other words, the stiffness of an unloaded prestressable mechanism with a FOIM along its FOIM is independent of the elasticity of the links and merely a function of the prestress and the geometry of the mechanism. This is an interesting characteristic that provides full control of the stiffness by prestress control from zero to a level limited by the strength of the links. For example, the stiffness along the vertical FOIM of the four-bar mechanism (called translational stiffness, k_T), shown in Figure 2-4.a, is

$$k_T = \frac{2\tau_p}{L_c}. \tag{2.1}$$

As expected, this stiffness is a function of prestress τ_p and the geometry of the mechanism that is represented by $\frac{2}{L_c}$. Note that the relation between the stiffness and the prestress is linear.

In summary, the mechanism shown in Figure 2-4.a along its vertical infinitesimal mechanism has a variable stiffness (Eq.(2.1)) that can be controlled by the level of the prestress. By considering these facts, one can consider this mechanism as a translational variable stiffness spring along the vertical direction.

The stiffness described by Eq. (2.1) is valid only at the singular configuration. When this mechanism deflects under an external vertical load (F) to a new position such as the one shown in Figure 2-4.b, the stiffness increases to higher values because at the new configuration. In addition to the stiffness caused by the prestress, the elasticity of the links creates an additional elastic stiffness. As a result, the stiffness of the AVS is nonlinear as this stiffness changes with the mechanism's deflection. It will be shown later in sections 3.4.1 and 4.6.3 that nonlinearity can be adjusted to some extent by adjusting the geometry of the AVS. For example, increasing the lengths of the side links (L_c) results in a more linear stiffness. The downside of improving linearity by increasing (L_c) is decreasing the magnitude of the prestress stiffness for the same prestress level (see Eq.(2.1)). Another technique that increases linearity without decreasing the stiffness is using side links with lower elastic stiffness. For example, decreasing the thickness of the side links to smaller values will decrease their elastic stiffness (Figure 2-4,c). For this thesis, cables were used to replace some of the links. Using flexible cables, such as wire ropes (aircraft cables), significantly decreases the lateral elastic stiffness of these links. The use of these cables also simplifies the manufacturing of the AVS as they can be connected to other components directly without using revolute joints. As a result, using cables eliminates the joints as well (Figure 2-4.d).

The stiffness observed on the middle link of the mechanism (Figure 2-4.a) along the second FOIM is a rotational stiffness. This rotational stiffness (k_R) is found as

$$k_R = \left(\frac{{L_b}^2}{L_c} + L_b\right)\tau_p . \tag{2.2}$$

This mechanism, along its rotational FOIM, can be thought of as a rotational AVS with similar characteristics as those discussed above.

The four-bar mechanism is a simple example to show the concept of an AVS with prestressed cable mechanisms. In this thesis, two designs for an AVS are proposed. First, an

AVS based on a cable-driven mechanism is studied, and the optimum configuration for a translational AVS and rotational AVS are found. Then, tensegrity prisms are utilized to make translational and rotational AVSs.

2.4 AVAILABLE VARIABLE STIFFNESS FOR VIBRATION APPLICATIONS

Several variable stiffness elements have been developed by using various techniques such as employing "smart materials", which can respond rapidly to a stimulus. These materials include shape memory alloys, magnetorheological elastomers, piezoelectrics, and electro active polymers. As well, mechanical methods can be used to obtain variable stiffness: changing the number of the active coils in a coil spring or changing the geometry of a compliance mechanism. In the following, some of the properties of the available variable stiffness elements used in semi-active control systems are briefly reviewed.

2.4.1 SHAPE MEMORY ALLOYS

Shape memory alloys (SMAs) are a class of alloys whose mechanical properties, including the modulus of elasticity, change with the temperature. The elasticity of SMAs is not a linear function of the temperature and switches between two distinct values corresponding to low-temperature and high-temperature phases. The elasticity of the SMAs in the high-temperature phase is up to four times as large as that of the low-temperature phase. Therefore, the spring constant (stiffness) of a spring made of a SMA can vary by a factor of three to four.

The change in the stiffness of a SMA is the result of temperature change and therefore has a relatively long response time. This property has limited the bandwidth of these materials to a few hertz. In addition, SMAs cannot be actuated efficiently without a complex control system and have large temperature hysteresis. Therefore, they are more suitable for quasi-static vibration-control applications [86,87,88,89].

2.4.2 MAGNETORHEOLOGICAL ELASTOMERES

Magnetorheological (MR) elastomers consist of rubber filled with micron-sized magnetizable particles. During the curing stage of the elastomer, an applied magnetic field aligns the particles into chains. The mechanical properties of MR elastomers, including the elasticity, can be then controlled reversibly and rapidly (in a millisecond time scale) by using an applied magnetic field. Semi-active systems that use MR elastomers benefit from a fast dynamic response and, consequently, a higher bandwidth. However, for an effective range of stiffness change, a rather strong variable magnetic field is required, and this requirement can limit the feasibility of this method. Nonlinearity and hysteresis are among other disadvantages of these materials [90,91,92].

2.4.3 PIEZOELECTRIC SYSTEMS

Piezoelectric elements, which sometimes are referred to as variable stiffness elements, are actually force actuators with small strokes. Changing the force of these elements in a timely manner by using a control algorithm provides a virtual variable stiffness [93]. Therefore, these systems should be included among the active methods of vibration-control.

2.4.4 MECHANICAL SYSTEMS

2.4.4.1 Mechanical springs by changing the geometry of the system

A variety of mechanical methods has been developed and reported in the literature. These springs change the stiffness by changing the system's geometry by, for example: controlling the effective number of active coils in a coil spring, using adjustable pitching stiffness, adjusting the tuning ratio by moving the masses, adjusting the effective inertia [3], adjusting the gap between two leaf springs, controlling the curvature of beams by using piezoelectric actuators, altering the geometry by using a tunable fluid-filled beam [8], and altering the orientation of a set of coil springs [30]. All of the mechanical devices work based on changing the shape or geometry of a mechanism. Doing so requires the finite movement of the parts and/or links of the system, and results in a relatively long response time. Therefore, similar to SMAs, the mechanical methods usually suffer from their low bandwidth and, hence, are not suitable for higher-frequency applications.

2.4.4.2 Mechanical springs without changing the geometry of the system

The AVS introduced in this research is a force-controlled spring. Unlike other mechanical variable stiffness springs, the AVS is not based on finite motion or geometry change and hence can provide a faster response than that of other springs. These properties of the AVS seem promising for a range of vibration-control applications with relatively low energy consumption at low cost.

2.5 DESIRED CHARACTERISTICS OF A VARIABLE STIFFNESS SPRING

The following characteristics can be identified as desirable in any variable stiffness, including that of the AVS, for their effectiveness in practical vibration-control applications:

- Fast response.
- High stiffness controllability.
- Linearity.
- Sufficient stiffness magnitude.

In the following sections, these characteristics are explained briefly, and in the following chapters, they are discussed in detail for the AVS .

2.5.1 FAST RESPONSE

Semi-active springs are used for demanding and challenging applications where passive springs do not provide an adequate response. They are usually required to change the stiffness quickly in order to maintain vibration-control in the working range.

2.5.2 HIGH STIFFNESS CONTROLLABILITY

The stiffness controllability is defined as the ratio of the controllable (variable) stiffness to the total stiffness. High stiffness controllability means that large changes in the total stiffness of the variable stiffness spring can be achieved. Large changes of the stiffness of an isolator can significantly change the response of the vibrating system and is, consequently, desired.

2.5.3 LINEARITY

The change of the total stiffness with displacement is understood as the nonlinearity of a variable stiffness spring. Under an external load, springs deflect to a new static equilibrium.

In a nonlinear spring, the stiffness at the new equilibrium differs from the spring's initial stiffness. According to this definition, all of the available springs are actually nonlinear. Even industrial coil springs, that are usually assumed as linear springs, demonstrate a small changes in stiffness when displaced. However, if the change of the stiffness with displacement is negligible for the desired application, the spring is considered as a linear one. The linearity assumption simplifies the formulation and facilitates the study of the vibration system. On the other hand, in some engineering applications, a nonlinear stiffness with repeatable stiffness value (low hysteresis) is desired. For example, the available passive engine mounts are intentionally designed with nonlinear stiffness. The stiffness of these mounts increases when deflection is imposed. As a result, they have lower stiffness when they isolate low-amplitude vibrations caused by an engine and become stiffer when displaced further under shock waves caused by sudden braking.

2.5.4 SUFFICIENT STIFFNESS MAGNITUDE

In addition to wanting to have complete control over the stiffness (stiffness controllability), spring designers want to provide a sufficiently large range of variable stiffness. The ability to do so will facilitate the use of a spring for a wide variety of industrial applications.

2.6 SUITABLE MECHANISMS FOR MAKING AN AVS

It was explained in section 2.3 that the antagonistic variable stiffness spring (AVS) is a prestressable mechanism. Prestress creates stiffness (prestress stiffness) that is a function of the prestress and the geometry. As a result, any prestressable mechanism has variable stiffness and can be thought of as a variable stiffness spring. However, all prestressable mechanisms cannot make a useful variable spring because the total stiffness of a general prestressable mechanism, in addition to the prestress stiffness, has other components including elastic stiffness which depends on the geometry and elasticity of the links. If the geometry is not correctly devised, the prestress stiffness might be very small or even negligible when compared with the elastic stiffness. Also, if the elasticity of the links is not selected properly, the resultant prestress stiffness might be very nonlinear and not suitable for some applications in which high linearity is desired.

This research utilizes a subgroup of prestressed mechanisms to develop an AVS. These mechanisms are kinematically singular prestressed mechanisms with first-order infinitesimal mechanism (FOIM).

As a platform to develop and study the AVS, two special cases of cable mechanisms, which can retain prestress, are used in this research: cable-driven mechanisms (Figure 2-7) and prestressable pin-jointed mechanisms such as tensegrities (Figure 2-10). These mechanisms are prestressable and have first-order infinitesimal mechanism. Using cable-mechanisms for making an AVS has the following benefits:

1. Cable-mechanisms are easy to build. The bending flexibility of the cables replaces the mechanical joints and facilitates the multiplication of the links and/or the use of complex configurations at a low cost.
2. In cable-driven mechanisms, all the links and, in tensegrities, most of the links are in tension. The links under tension are not subject to buckling and are designed for the required strength, without any limit on their lengths. This property can lead to designing slimmer elements that can apply the desired amount of force at lower inertia (mass-

based inertia) and elastic stiffness. Furthermore, using links with low elasticity improves the linearity of the AVS.

The concept of making an AVS is not restricted to cable-driven mechanisms and tensegrities. An AVS such as one studied in [17] and shown in Figure 2-5 can be developed with other types of kinematically singular mechanisms that are prestressable and have FOIM. When the platform of this mechanism is loaded, it deflects along the guide. Changing the prestress of the cables changes the magnitude of this deflection.

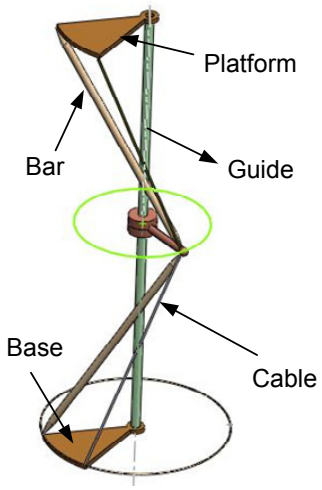

Figure 2-5. An AVS made with a kinematically singular prestressed mechanism other than cable-driven mechanism and tensegrity

In the following sections, cable–driven mechanisms and tensegrities are reviewed, and geometries for making useful AVSs are discussed.

2.6.1 CABLE-DRIVEN MECHANISMS

Cable-driven mechanisms are categorized as a class of parallel manipulators. Figure 2-6 shows a Stewart mechanism, which is a spatial parallel manipulator with 6 adjustable rigid links. Cable-driven mechanisms use cables instead of adjustable rigid links to move the platform around [31,32,33]. A spatial cable-driven mechanism needs at least 7 cables to deliver a motion similar to Stewart mechanism (Figure 2-7).

Figure 2-6. A parallel manipulator with six adjustable rigid links. Links carry both compression and tension (Courtesy Physik Instrumente (PI) GmbH & Co.)

The position and orientation of the moving platform can be determined by controlling the lengths of the cables. In order to maintain the rigidity of the mechanisms, all cables should carry tensile forces. In non-singular kinematics, at least one redundant cable is required to

guarantee the existence of tensile forces in all cables. These cable forces are internally in equilibrium and hence are called antagonistic forces. Antagonistic forces (prestresses) are the sources of prestress stiffness.

To build an AVS, the winches do not move the platform in space. Instead, they set and control the internal forces by pulling the cables. The stiffness of a cable-driven mechanism depends on several parameters including the prestress of the cables. As a result, if the prestress changes, the stiffness changes, and, consequently, the platform's deflection under an external force **f** also changes (Figure 2-8).

In general, the stiffness of a cable-driven mechanism, in addition to be depending on the prestress, also depends on the geometry and the elasticity of the cables. It will be shown later in Chapter 3 that the contribution of prestress to the total stiffness of the cable-driven mechanism depends on the geometry and is maximized in singular configurations. For instance, the stiffness of the kinematically singular configuration shown in Figure 2-9 along its FOIM (direction **q**) is only prestress stiffness. Other sources of stiffness such as the elasticity of the cables do not contribute to the total stiffness of this mechanism along direction **q**. As a result, the total stiffness can be controlled from zero to any desired value by the prestress as long as the links stand the pretension.

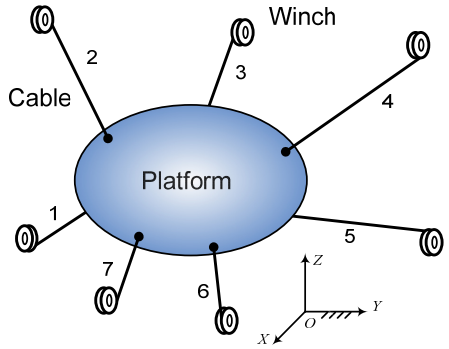

Figure 2-7. Cable-driven mechanism with one degree of kinematic redundancy

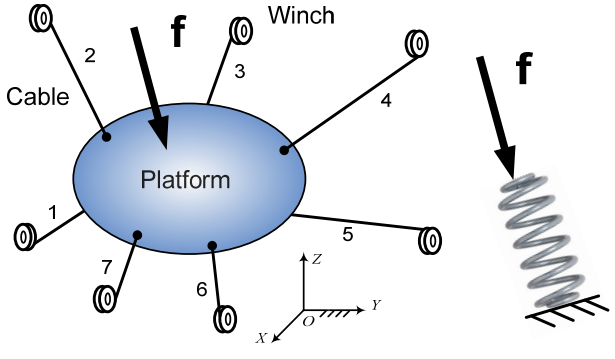

Figure 2-8. Cable-driven mechanism can work as a spring.

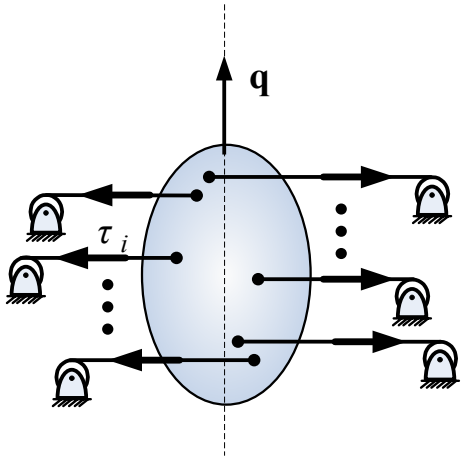

Figure 2-9. Desired configuration of a translational AVS.

The stiffness of cable-driven mechanisms is studied in [12]. As well, some studies on the stiffness of parallel manipulators [6,25,27,33] can be used to study the stiffness of cable-driven mechanisms. These studies consider the effects of the internal loads of the links, including the prestress.

2.6.2 TENSEGRITIES

Research on tensegrity structures began about 60 years ago when Buckminster Fuller was inspired by artist Kenneth Snelson's sculptures [34,35,36]. Figure 2-10 shows two sculptures made by this artist. Buckminster Fuller invented the word "tensegrity" as a contraction of "tensional integrity" [37,38]. Tensegrities are structures/mechanisms composed of cable elements that carry tensile forces, and some bars that carry compressive forces. The bars are distributed in the tension network of cables in a stable configuration which is prestressed. "Prestressed" means that the tension is built up in the cables and that compression is built up in the rods such that the structure's equilibrium and stability is maintained.

The high strength-to-weight ratio of these systems and the simplicity in their fabrication drew the attention of structural engineers wanting to build large structures such as huge domes for sport fields, emergency shelters [38], and deployable structures for space applications [39]. Several books discuss the tensegrity structures [34,40,41]. One of these [41], which is widely used by researchers, was written by the literary critic Hugh Kenner in 1976. This book provides helpful formulations for a general one-stage tensegrity prism such as that shown in Figure 2-11.

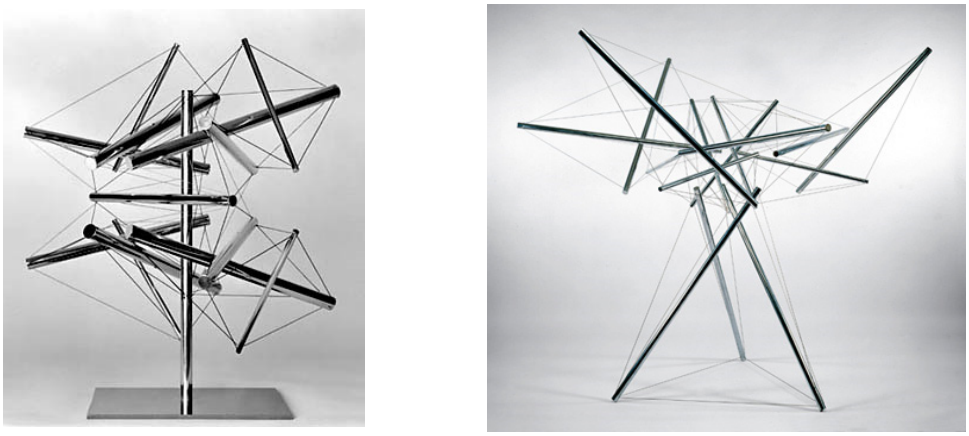

Figure 2-10. Tensegrity Sculptures of K. Snelson (Courtesy K.Snelson) [42]

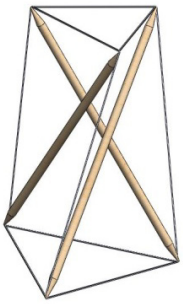

Figure 2-11. One-stage tensegrity prism (simplest form of spatial tensegrities)

Although the idea of tensegrity systems was introduced in the middle of the last century, most of the first publications on this issue are limited to structural and topological analysis [43,44] and to attempts to introduce these structures to the science and engineering community [45,46]. In recent decades, the tensegrities have received new attention, and several attempts have been made to use these systems in their simple configurations for the purpose of manipulation and robotics (cable-based manipulators) [47,48,49]. Joseph Duffy and Carl D. Crane and their colleagues at the University of Florida have studied a group of tensegrities (one-stage tensegrities) as a class of parallel mechanisms [50,51].

The early works on the stiffness of tensegrities was done in civil engineering, where they were considered as special cases of pin-jointed structures. As a result, the knowledge that had already been developed about pin-jointed structures advanced the understanding of tensegrities quickly. Some works such as [53] used finite element analysis but considered large deflections for the components. [52, 53] considered large deflections by using higher-order terms of a Taylor expansion of static equilibrium.

Other researchers such as Calladine, Pellegrino and Guest from the Deployable Structures Laboratory of University of Cambridge assumed the presence of small deflections. These researcheres have used linear static equilibrium equations and virtual work theory to study the kinematics and mechanics of prestressed pin-jointed structures and extended their research to tensegrities as prestressed pin-jointed structures with first-order infinitesimal mechanisms [20,24,72,].

Mathematicians have also worked on the rigidity and stability of the tensegrity structures under the mathematical rigidity theory [55,54]. These works are often neglected by engineers because of its difficult notations and different underlying aims [24]. In 2001, Murakami et al. [23,56,57] at the University of California in San Diego were the first to use continuum mechanics to present the total stiffness by linearizing the equations of motion.

Skelton and his team at the University of California at San Diego studied the mechanics of tensegrities in order to actively or semi-actively control the shape, stiffness and vibration of the tensegrities. The essence of their works was recently published in [58]. These researchers presented tensegrities as unique controllable structures that maintain an extremely high degree of "controllability" during all phases of the structure design. Moreover, Skelton et al. showed that in tensegrity structures, structural design and control design can be integrated into one process in order to require less power from the control system to change the shape to the new desired shape.

The mechanics of simple tensegrities such as planar tensegrities are studied in the literature in order to explore the possible advantages of tensegrities for new applications such as locomotion [59], deployable structures [60], and manipulation [61]. Oppenheim and Williams have worked on the analytical stiffness of the 3-bar tensegrity shown in Figure 2-11 [52,62]. In [82], these authors focused on the vibration along the FOIM of the tensegrity and studied the stiffness and the effects of the pretension on the stiffness. These researchers suggested that the effects of the infinitesimal motion should not be overlooked, but that at higher pre-stress levels and in tensegrities with members showing high extensibility, these effects may no longer dominate the vibration response.

The stiffness of tensegrities was formulated in [23,24,58]. In these works, it is clearly stated that prestress of the cables and bars affects the stiffness of the tensegrity. The researchers who studied the mechanics of tensegrity including the stiffness followed different approaches and had different assumptions. Some of looked at tensegrities as structures with small deflections of the components. The assumption of small deflections enabled these researchers to linearize the equations of motion and, consequently, find a general equation that could describe complex tensegrities with a large number of components [23,24,58]. This method is very insightful and useful for understanding the general characteristics of tensegrities. In this approach, the end of the bars (nodes) are considered as end-effectors, and the stiffness matrix that maps the displacements of the nodes to the forces applied on the nodes is found. This approach, however, is not always adopted as the generality of the equations make understanding and studying the effects of parameters difficult. The present thesis has benefited from these works, but in order to present a straightforward stiffness formulation, this thesis defines "stiffness" as it is common in Robotics. The stiffness described in Robotics maps the displacement caused by the applied force on only one end-effector, which can be a node, a bar, or a rigid body that connects several nodes.

Tensegrities, similar to cable-driven mechanisms, have a set of characteristics required for their use as a variable stiffness spring. For this thesis, tensegrity prisms (such as the one shown in Figure 2-12.a) were designed as variable stiffness springs for vibration-control applications. Tensegrity prisms have a relatively simple geometry, which facilitates their manufacturing and application in industrial applications. Figure 2-12.b shows the translational variable stiffness spring developed based on the octagonal tensegrity prism shown in Figure 2-12.a. The top and bottom octagonal plates constrain the relative motion of

the top and bottom nodes, correspondingly. A vertical guide confines the tensegrity prism spring to move along its FOIM. Increasing the prestress of the cables increases the stiffness of this spring. Similar to the stiffness of the spring developed with cable-driven mechanisms, the stiffness of the spring developed with a tensegrity prism can be controlled effectively by the level of the prestress.

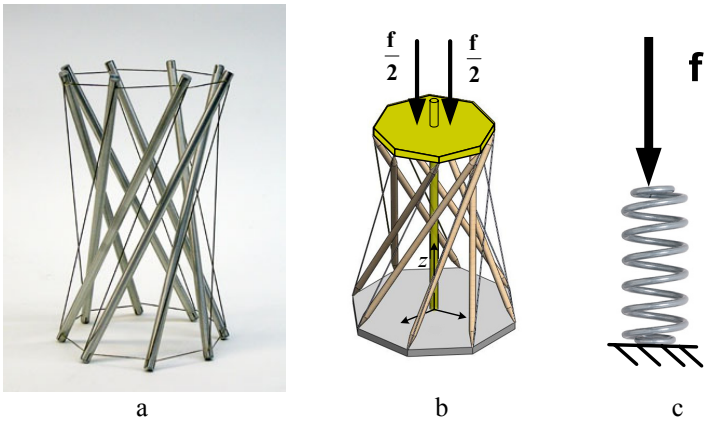

Figure 2-12. a. An Octagonal Tensegrity Prism (Courtesy K.Snelson) b. Spring developed by tensegrity prism, this spring can works as a translational spring c. Translational coil Spring

2.7 ANTAGONISTIC VARIABLE STIFFNESS MOUNT (VSM)

The concept of making an AVS, supported by the preliminary simulation results [13,15], seemed promising. In order to determine the concept's practicality, it was decided to investigate the application of an AVS in an existing industrial vibration problem.

A Variable Stiffness Mount (VSM) is a vibration isolator that consists of an AVS and a soft rubber mount (Figure 2-13). The AVS provides variable stiffness while the soft rubber mount provides constant small values for the damping and stiffness. The soft rubber mount also supports the deadweight of the vibrating system. This soft rubber mount also acts as a safety component for a situation where the AVS or the control system fails to operate properly. In such a situation, the VSM will work as a passive mount and the system that uses the VSM will not need to be stopped and fixed immediately. Therefore, the system will be able to continue its operation and to be fixed later.

Vibration-control in a dynamic systems was found to be an ideal challenge for examining the concept of an AVS. Selecting a vibration-control problem had several advantages. First, this problem is still a challenging problem and an effective solution based on the variable stiffness could benefit a variety of applications. Second, several studies have been published in this area, and the proposed research could benefit from them. Third, different vibration-control solutions are available in the market and the performance of the vibration-control system designed with an AVS could be easily compared with their performance. For these reasons, the AVS was used to design a new vibration mount/isolator called the VSM for vibration-control applications. The VSM is a general vibration mount useful for isolating the vibration and controlling the vibration displacement near the resonance. In this research, a VSM was designed, built, set as an engine mount, and tested. The performance of the VSM was compared with that of a regular passive engine mount. The simulation results for the VSM as an engine mount are discussed in Chapters 3 and 4. The test results are presented in Chapter 5.

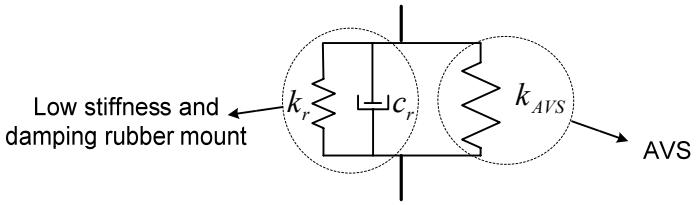

Figure 2-13. Variable Stiffness Mount (VSM)

Spring and dampers are the main components in any vibration mount or vibration absorber. However, they act differently in attenuating the undesired vibration. In order to explain the significance of a VSM, this section compares how a variable damping mount and a VSM as a variable stiffness mount work in vibration isolation. Consider a simple passive one DoF vibration mount. The passive mount can be implemented either for isolating the base excitation vibrations or for isolating the forced vibrations (Figure 2-14). The displacement transmissibility of the base excitations and the force transmissibility of forced vibrations are shown in Figure 2-15. It is known that these two transmissibilities, while defined differently, have identical formulations [63]. The stiffness determines the resonance frequency (f_n) and the frequency where the isolation starts ($f > \sqrt{2}f_n$). Damping limits the vibration before resonance by dissipating the energy. However, in the isolation region ($f > \sqrt{2}f_n$), the damping negatively affects the isolation (see Figure 2-15).

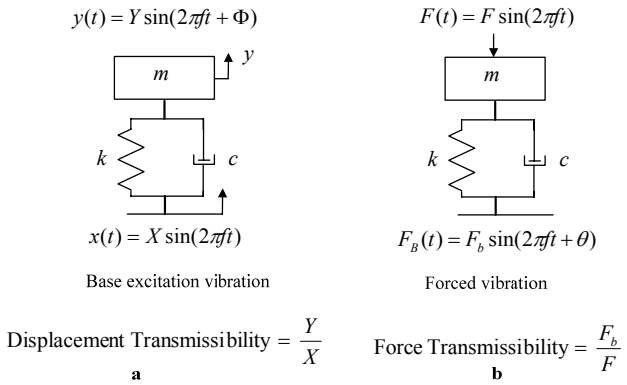

Figure 2-14. Displacement and force transmissibility of a one degree of freedom vibrating system

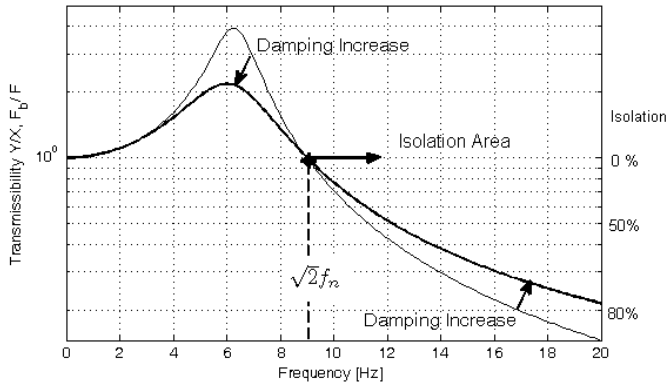

Figure 2-15. Displacement and Force Transmissibility curves of one degree of freedom vibration model when damping changes

Passive designs provide satisfactory vibration attenuation for applications with fixed working frequencies, such as AC electrical motors. The passive mounts of an AC electrical motor have enough damping to control the motor's bounce during the starting while the frequency quickly passes the natural frequency and reaches the working frequency at the isolation region.

On the other hand, there are some applications such as vibration-control of combustion engines or seismic excitations in which the working frequency is variable. In these cases, a passive mount is not an optimum design. The engine vibration control can be considered as an example. Passive engine mounts are designed for better isolation in driving mode of the engine (when engine frequency is around 30-50 Hz) rather idling mode (about 20 Hz) as an engine is used mainly for driving. As a result, when the car is idling, the engine vibration is quite noticeable but when it starts moving, the perceived vibration is much weaker.

Semi-active or active vibration mounts provide better solutions than passive mounts for demanding applications such as engine isolation applications. The former work by changing the damping or stiffness in different frequency ranges. The damping is set higher for low frequencies to provide lower transmissibility and, consequently, better vibration displacement control. In higher frequency ranges, the damping is set lower to provide better isolation (see Figure 2-15). Other types of semi-active mounts implement a stiffness change [30,64,65]. In this technique, the stiffness is set to high values in low frequencies and low values for high frequencies. As a result, better displacement control (lower transmissibility) in low frequencies and better isolation (lower transmissibility) in high frequencies are achieved. The VSM presented in this thesis falls into this category.

Most of the semi-active isolators/mounts are based on damping change; however, the stiffness has more effect on the optimum operation of a mount [66,67]. Jalili in [66] explains that the available variable stiffness springs are unpopular due to their high energy requirement. Even low-power designs of variable stiffness elements usually suffer from a limited frequency range, fabrication complexities, and high costs, Mainly because the stiffness of most of these available variable stiffness mounts is changed by changing the geometry [66,64,30,65]. Geometry change is accompanied by high actuation power, slow response and high costs. The proposed VSM works based on a force change in the links rather than a geometry change. The result is a faster response by a simpler mechanism.

To explain how the VSM works, a one DOF vibrating system is compared with a passive mount in Figure 2-16.a and an equivalent VSM in Figure 2-16.b. These mounts are assumed to be designed for similar requirements so that they can be compared. K_r and C_r are the constant stiffness and constant damping of the passive mount, respectively. In Figure 2-17, Curve 4 is the transmissibility of the passive mount with the natural frequency at 6 Hz. The VSM (Figure 2-16.b) consists of a soft rubber mount (with k_r and c_r) working in parallel with an AVS with a variable stiffness of k_{AVS}. k_r and c_r are lower than K_r and C_r for reasons that will be explained in Chapter 3 and Chapter 4. The main function of the embedded passive mount is to support the deadweight of the mass. The VSM has two states: active and inactive. It is active when the AVS is prestressed ($k_{AVS} > 0$) and is inactive when the prestress of the AVS is set to zero ($k_{AVS} = 0$). If the VSM always remains active its transmissibility will be similar to that represented by Curve 2 in Figure 2-17. If the AVS of the VSM is always kept inactive, its transmissibility will be similar to that represented curve 1 in the same figure. In the active state (Curve 2), the total stiffness of the VSM ($k_r + k_{AVS}$) is designed to be higher than the stiffness of the equivalent passive mount (K_r). As a result, the

natural frequency of the active VSM (here 12 Hz) is bigger than that of the passive mount (6 Hz). As previously mentioned, in the always inactive state (Curve 1), the total stiffness of the VSM (k_r) was intentionally selected lower than the stiffness of the equivalent passive mount (K_r). As a result, the natural frequency of the always inactive VSM (here, 4 Hz) becomes smaller than that of the passive mount (6 Hz). When a VSM is operating as a semi-active mount, depending on the frequency of the excitation, either active or inactive states are used (Figure 2-17, Curve 3). In low-frequency excitations, close to the natural frequency of the passive mount (6 Hz), the transmissibility is high, and the passive mount provides a poor displacement control. Therefore, the VSM is set to work in the active state (Curve 2) to provide significant vibration displacement control. When the frequency of the excitation increases beyond the intersection of Curves 1 and 2 (at about 5 Hz), the inactive state provides better displacement control and isolation. As a result, in the high-frequency range, the inactive state is chosen. As previously mentioned, the damping of the VSM (c_r) is selected to be lower than the damping of the equivalent passive mount (C_r). As Curve 3 reveals that using the soft rubber mounts in the VSM with lower damping (Curve 3) provides better vibration isolation in the high-frequency range (see also Figure 2-15).

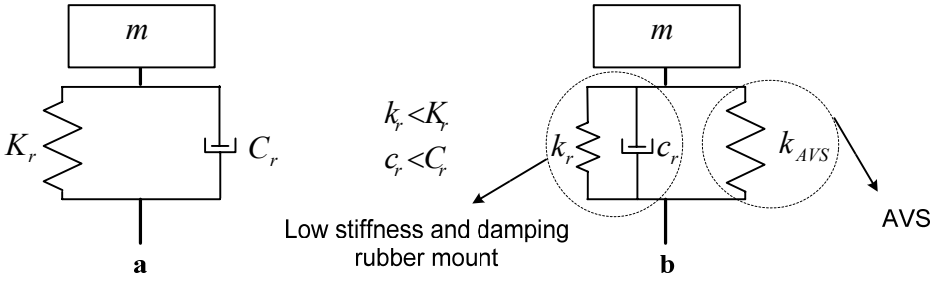

Figure 2-16. Schematics of one DOF vibrating system a. with passive mount b. with variable stiffness spring mount (VSM)

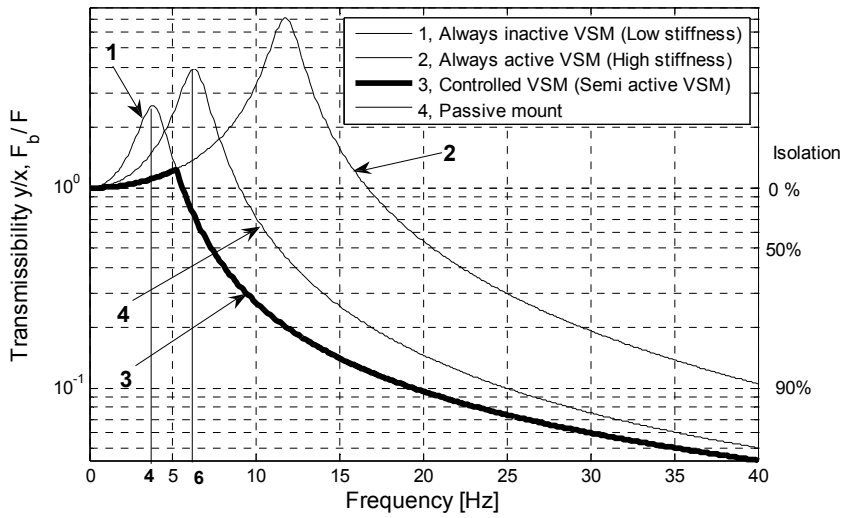

Figure 2-17. Semi-active vibration-control by varying the stiffness

2.8 SUMMARY

The spring developed in this research, the AVS, is a prestressable mechanism that can maintain prestress (antagonistic forces). The prestress of the links in an AVS create a stiffness which is called prestress stiffness (antagonistic stiffness). The stiffness of an AVS can be controlled and changed by the level of prestress. The desired characteristics of any variable stiffness spring including the AVS were explained in this chapter. The available variable stiffness springs were discussed, and the AVS was categorized as a new mechanical spring that works without any finite change in its geometry.

Any kinematically singular and prestressed mechanism can be used as an AVS. In this thesis, however, two types of prestressed mechanisms are chosen for making an AVS: cable-driven mechanisms and tensegrities. The AVS, when used in parallel with a soft rubber mount forms an isolator called a VSM. The general characteristics of a VSM and the way it works were explained in this chapter.

In the following chapters, the developed AVSs will be studied in detail, the desired characteristics of variable stiffness springs will be checked for the developed AVS, and the performance of the VSM will be examined in a realistic industrial situation.

Chapter 3 DEVELOPING AN ANTAGONISTIC VARIABLE STIFFNESS SPRING BY USING CABLE-DRIVEN MECHANISMS[3]

It was explained in Chapter 2 that cable-driven mechanisms are one of the suitable mechanisms for making an antagonistic variable stiffness spring. In this chapter, an AVS (antagonistic variable spring) is developed from cable-driven mechanisms. The stiffness of cable-driven mechanisms is studied in order to find the geometries that provide the desired characteristics for the variable stiffness spring explained in 0. In order to elaborate on the feasibility of the AVS in real applications, as discussed in section 2.7, a case study is presented at the end of this chapter on the engine mount of a typical vehicle. The designed engine mount is a semi-active VSM that uses an AVS built from a cable-driven mechanism.

3.1 STIFFNESS OF A CABLE-DRIVEN MECHANISM

Consider a general cable-driven mechanism shown in Figure 3-1, with *6* degrees of freedom. The moving platform is restrained by *n* cables, whose lengths can be controlled by active winches.

It is assumed that the mechanism is tensionable, meaning that the arrangement of the cables and the moving platform is such that prestress (the antagonistic tensile forces) can be created in all cables at the same time and these prestress forces can be scaled to any desired level. As a result, all the cables remain taut. Small displacements of the moving platform can be determined by vector $d\mathbf{P} = (dp_1, dp_2, \ldots, dp_m)^t$ where p_i is the i^{th} coordinate variable (since small displacements are involved, angular displacements are also considered as vector quantities). The corresponding joint displacements (i.e. cable lengths) are represented by $d\mathbf{l} = (dl_1, dl_2, \ldots, dl_n)^t$where l_i's are cables' lengths. It is also assumed that an external wrench $\boldsymbol{W_e}$ which consists of external force $\boldsymbol{F_e}$ and moment external $\boldsymbol{M_e}$ is applied on the moving-platform. The stiffness of the mechanism sensed at the moving platform is a tensor $\mathbf{K}$ which is found by dividing the deferential change of the external wrench ($\boldsymbol{W_e}$) over the corresponding differential displacement of the platform ($d\mathbf{P}$).

[3] Most of the materials in this chapter are taken from the paper published in [9].

$$\mathbf{K} = \frac{d\mathbf{W}_e}{d\mathbf{P}} \tag{3.1}$$

In the most general case where platform have all three translational and three rotational motions ($d\mathbf{P}_{6\times1}$), the stiffness matrix will be a six by six tensor. Along an arbitrary direction, presented by a general unit vector $\hat{\boldsymbol{q}}_{6\times1}$, the stiffness of the cable-driven mechanism is expressed by an scalar (k) found from $k = \hat{\boldsymbol{q}}_{6\times1}{}^{t}\,\mathbf{K}_{6\times6}\,\hat{\boldsymbol{q}}_{6\times1}$.

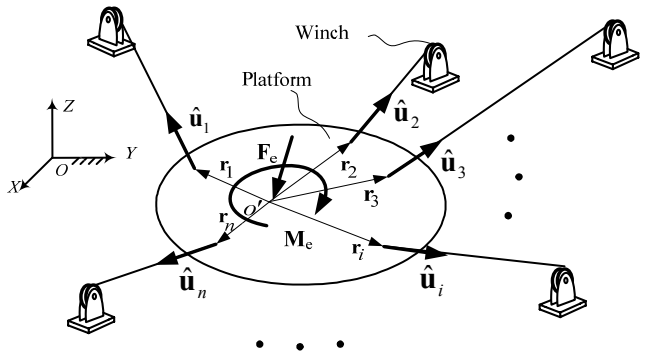

Figure 3-1 General model of a cable-driven mechanism

The stiffness matrix of cable-driven mechanisms has been derived and reported in the literature [12,68]. In [12], the stiffness of the cable-driven mechanism (Figure 3-1) is found by summing the stiffness effects of individual cables. The contribution of each cable to the total stiffness is two-fold: (1) elastic stiffness, which acts along the direction of the cable, and (2) internal force stiffness, which is perpendicular to the direction of the cable similar to the lateral stiffness of a pendulum.

In this present thesis, the following assumptions are made for the modelling and analysis:

1. It is assumed that the internal forces are merely prestress (antagonistic forces), or that the external load is zero. In its most general case, the stiffness of such a mechanism changes slightly when an external load is applied because the mechanism settles at a different equilibrium point with different internal cable forces. However, in vibration-control applications, it can be assumed that the vibration occurs around a constant equilibrium point and the cable forces required to balance the external force are negligible compared to the prestress in the cables. A previous study by the author confirmed this assumption in a planar system [13]. As a result, the stiffness formulation will be presented for an unloaded cable-driven mechanism.
2. This model is based on small deflections for the definition of the stiffness. It is clear that in a real system, the stiffness changes when the moving platform is displaced. For the present work, it is assumed that the desired displacement is small enough not to violate the linearity assumption. The effects of nonlinearity will be investigated later by considering the variation of the stiffness.
3. Platform is rigid.

The stiffness of the mechanism, measured at the moving platform, can be written as

$$\mathbf{K} = \mathbf{K}_e + \mathbf{K}_p \quad , \tag{3.2}$$

where $\mathbf{K}$ is the total stiffness, $\mathbf{K}_e$ is the elastic stiffness caused by the elasticity of the cables, and $\mathbf{K}_p$ is the prestress stiffness (antagonistic stiffness) generated by the internal prestress (antagonistic forces). $\mathbf{K}_e$ and $\mathbf{K}_p$ can be expressed in terms of the geometry of the mechanism and the cable properties. For this purpose, let $\hat{\mathbf{u}}_i$ and $\mathbf{r}_i$ be the direction vector and the moment arm vector of the i^{th} cable, respectively, as shown in Figure 3-1. Also, let k_i, l_i, and τ_i be the coefficient of elastic stiffness, the length and the force of the i^{th} cable, respectively, where a positive τ_i indicates a tensile cable force. $\mathbf{K}_e$ and $\mathbf{K}_p$ can be expressed as [12]

$$\mathbf{K}_e = \sum_{i=1}^{n} k_i \begin{bmatrix} \hat{\mathbf{u}}_i \hat{\mathbf{u}}_i^t & \hat{\mathbf{u}}_i \hat{\mathbf{u}}_i^t [\mathbf{r}_i \times]^t \\ [\mathbf{r}_i \times] \hat{\mathbf{u}}_i \hat{\mathbf{u}}_i^t & [\mathbf{r}_i \times] \hat{\mathbf{u}}_i \hat{\mathbf{u}}_i^t [\mathbf{r}_i \times]^t \end{bmatrix} \tag{3.3}$$

$$\begin{aligned} \mathbf{K}_p = & \sum_{i=1}^{n} \frac{\tau_i}{l_i} \begin{bmatrix} I - \hat{\mathbf{u}}_i \hat{\mathbf{u}}_i^t & [\mathbf{r}_i \times]^t - \hat{\mathbf{u}}_i \hat{\mathbf{u}}_i^t [\mathbf{r}_i \times]^t \\ [\mathbf{r}_i \times] - [\mathbf{r}_i \times] \hat{\mathbf{u}}_i \hat{\mathbf{u}}_i^t & [\mathbf{r}_i \times][\mathbf{r}_i \times]^t - [\mathbf{r}_i \times] \hat{\mathbf{u}}_i \hat{\mathbf{u}}_i^t [\mathbf{r}_i \times]^t \end{bmatrix} \\ & - \sum_{i=1}^{n} \tau_i \begin{bmatrix} \mathbf{0} & \mathbf{0} \\ \mathbf{0} & [\hat{\mathbf{u}}_i \times][\mathbf{r}_i \times] \end{bmatrix}, \end{aligned} \tag{3.4}$$

where $[\mathbf{r}_i \times]$ is the matrix operator of the cross product:

$$[\mathbf{r}_i \times] = \begin{bmatrix} 0 & -r_{iz} & r_{iy} \\ r_{iz} & 0 & -r_{ix} \\ -r_{iy} & r_{ix} & 0 \end{bmatrix}. \tag{3.5}$$

The elastic stiffness, $\mathbf{K}_e$ in Eq. (3.3), can be easily shown to be symmetric by demonstrating that $\mathbf{K}_e^t = \mathbf{K}_e$. The prestress stiffness, $\mathbf{K}_p$, is composed of two parts according to Eq. (3.4):

$$\mathbf{K}_p = \mathbf{K}_p^s - \mathbf{K}_p^f \ , \tag{3.6}$$

where

$$\begin{aligned} \mathbf{K}_p^s = & \sum_{i=1}^{n} \frac{\tau_i}{l_i} \begin{bmatrix} I - \hat{\mathbf{u}}_i \hat{\mathbf{u}}_i^t & [\mathbf{r}_i \times]^t - \hat{\mathbf{u}}_i \hat{\mathbf{u}}_i^t [\mathbf{r}_i \times]^t \\ [\mathbf{r}_i \times] - [\mathbf{r}_i \times] \hat{\mathbf{u}}_i \hat{\mathbf{u}}_i^t & [\mathbf{r}_i \times][\mathbf{r}_i \times]^t - [\mathbf{r}_i \times] \hat{\mathbf{u}}_i \hat{\mathbf{u}}_i^t [\mathbf{r}_i \times]^t \end{bmatrix} \\ \mathbf{K}_p^f = & \sum_{i=1}^{n} \tau_i \begin{bmatrix} \mathbf{0} & \mathbf{0} \\ \mathbf{0} & [\hat{\mathbf{u}}_i \times][\mathbf{r}_i \times] \end{bmatrix}. \end{aligned} \tag{3.7}$$

$\mathbf{K}_p^s$ can be easily found to be symmetric by showing that it is equal to its transpose. For $\mathbf{K}_p^f$ which is a purely rotational stiffness, the anti-symmetric part is found:

$$(\mathbf{K}_p^f)^t - \mathbf{K}_p^f = \sum_{i=1}^{n} \tau_i \begin{bmatrix} \mathbf{0} & \mathbf{0} \\ \mathbf{0} & [\mathbf{r}_i \times][\hat{\mathbf{u}}_i \times] - [\hat{\mathbf{u}}_i \times][\mathbf{r}_i \times] \end{bmatrix}. \tag{3.8}$$

Using the Jacobi identity, we have $[\mathbf{r}_i \times][\hat{\mathbf{u}}_i \times] - [\hat{\mathbf{u}}_i \times][\mathbf{r}_i \times] = [(\mathbf{r}_i \times \hat{\mathbf{u}}_i) \times]$, and, hence,

$$(\mathbf{K}_p^f)^t - \mathbf{K}_p^f = \sum_{i=1}^{n} \tau_i \begin{bmatrix} \mathbf{0} & \mathbf{0} \\ \mathbf{0} & [(\mathbf{r}_i \times \hat{\mathbf{u}}_i) \times] \end{bmatrix}, \tag{3.9}$$

which can be written as:

$$\left(\mathbf{K}_p^f\right)^t - \mathbf{K}_p^f = \begin{bmatrix} \mathbf{0} & \mathbf{0} \\ \mathbf{0} & \left[\left(\sum_{i=1}^{n}\left(\tau_i \mathbf{r}_i \times \hat{\mathbf{u}}_i\right)\right)\times\right] \end{bmatrix}. \tag{3.10}$$

Eq. 3.9 shows that the anti-symmetric part of $\mathbf{K}_p$ depends on the total moment of the cable forces on the moving platform. However, since all the cable forces are antagonistic, the summation of their moments is zero, and, therefore,

$$\left(\mathbf{K}_p^f\right)^t - \mathbf{K}_p^f = \mathbf{0}, \tag{3.11}$$

which shows that the prestress stiffness is symmetric.

3.2 STABILITY OF THE STIFFNESS COMPONENTS

A stiffness matrix is said to be stable here if and only if the stiffness in any arbitrary direction such as $\hat{\mathbf{q}}$ is not negative. In other words, the stiffness tends to restore the original geometry or remains neutral when the element is displaced for small values in any direction.

For the elastic stiffness found in Eq. (3.3), the matrix can be written in the following form:

$$\mathbf{K}_e = \sum_{i=1}^{n} k_i \, \mathbf{c}_i \mathbf{c}_i^t \ , \tag{3.12}$$

where

$$\mathbf{c}_i = \begin{bmatrix} \hat{\mathbf{u}}_i \\ \mathbf{r}_i \times \hat{\mathbf{u}}_i \end{bmatrix} \quad i = 1, 2, \ldots, n \quad . \tag{3.13}$$

Therefore, the elastic stiffness in the arbitrary direction of $\hat{\mathbf{q}}$ becomes

$$k_e^{\mathbf{q}} = \hat{\mathbf{q}}^t \mathbf{K}_e \hat{\mathbf{q}} = \sum_{i=1}^{n} k_i \left(\hat{\mathbf{q}}^t \mathbf{c}_i\right)^2 \quad . \tag{3.14}$$

Eq. (3.14) shows that k_e^q is always non-negative. As a result, $\mathbf{K}_e$ is stable (positive semi-definite).

The prestress stiffness $\mathbf{K}_p$ shown in Eq. (3.4), is composed of two matrices: $\mathbf{K}_p^s$ and $\mathbf{K}_p^f$. $\mathbf{K}_p^s$ can be shown to be stable. For this purpose, $\mathbf{K}_p^s$ can be expressed as [12]:

$$\mathbf{K}_p^s = \sum_{i=1}^{n} \sum_{j=1}^{3} \frac{\lambda_i^j \tau_i}{l_i} \mathbf{d}_i^j \left(\mathbf{d}_i^j\right)^t, \tag{3.15}$$

where

$$\lambda_i^j = \left\| \hat{\mathbf{e}}_j - (\hat{\mathbf{e}}_j \cdot \hat{\mathbf{u}}_i)\hat{\mathbf{u}}_i \right\| \quad j = 1, 2, 3 \tag{3.16}$$

$$d_i^j = \frac{1}{\lambda_i^j} \begin{bmatrix} \hat{\mathbf{e}}_j - (\hat{\mathbf{e}}_j \cdot \hat{\mathbf{u}}_i)\hat{\mathbf{u}}_i \\ \mathbf{r}_i \times \left(\hat{\mathbf{e}}_j - (\hat{\mathbf{e}}_j \cdot \hat{\mathbf{u}}_i)\hat{\mathbf{u}}_i\right) \end{bmatrix} \quad j = 1, 2, 3 \ ,$$

and $\hat{\mathbf{e}}_1, \hat{\mathbf{e}}_2, \hat{\mathbf{e}}_3$ are the unit vectors of the global coordinate frame. Therefore, the stiffness due to $\mathbf{K}_p^s$ in the arbitrary direction of $\hat{\mathbf{q}}$ is found to be

$$\left(k_p^s\right)^q = \hat{\mathbf{q}}^t \mathbf{K}_p^s \hat{\mathbf{q}} = \sum_{i=1}^{n} \sum_{j=1}^{3} \frac{\lambda_i^j \tau_i}{l_i} \left(\mathbf{d}_i^j \cdot \hat{\mathbf{q}}\right)^2 . \tag{3.17}$$

Since λ_i^j and τ_i are both non-negative, $\left(k_p^s\right)^q$ is also non-negative, and, therefore, the first part of the prestress stiffness is positive semi-definite and hence stable.

The second part of the prestress stiffness, $\mathbf{K}_p^f$, is a rotational stiffness, and, in general, it can be stable or unstable even if all the cable forces are positive (tensile). Therefore, $\mathbf{K}_p^f$ is indefinite. In some configurations, an unstable $\mathbf{K}_p^f$ may dominate and result in the instability of the prestress stiffness and even the instability of the total stiffness [12].

In conclusion, the prestress stiffness is always stable if constrained and used in translational directions. In general, it may be unstable in rotational directions. Another conclusion is that in an unstable prestress stiffness, a higher prestress level results in decay in the total stiffness (see examples in [15]). In other words, cable-driven mechanisms stiffen by increasing the cable tensions only if their prestress stiffness is stable.

3.3 RELATIVE SIGNIFICANCE OF STIFFNESS COMPONENTS

As is mentioned in section 2.5.2, prestress stiffness needs to be significant relative to the passive elastic stiffness in order to be used as an effective variable stiffness element. To elaborate on the relative significance of prestress stiffness, the stiffness ratio, $R(\hat{\mathbf{q}})$, is defined as the ratio between the prestress stiffness and total stiffness for a given geometry of a cable-driven mechanism in a particular displacement direction $\hat{\mathbf{q}}$ of the moving platform:

$$R(\hat{\mathbf{q}}) = \frac{k_p^q}{k_e^q + k_p^q} . \tag{3.18}$$

The stiffness ratio has a value between zero and one where one indicates that the elastic stiffness is zero, and the total stiffness is determined merely by the prestress stiffness, which is active and controllable. As a result, a higher stiffness ratio implies higher stiffness controllability through prestress control and is highly desired for an AVS.

In order to effectively control the stiffness through prestress control, a high stiffness ratio is required. For this purpose, the structures of the elastic and prestress stiffness matrices are analyzed in order to determine their extreme values and maximum stiffness ratio.

It is evident from Eq. (3.14) that $k_e^{\mathbf{q}}$ vanishes if $\hat{\mathbf{q}}$ is normal to all $\mathbf{c}_i$'s. This can be realized in many configurations such as those shown in Figure 3-2a and b. In these configurations, the mechanism is kinematically singular, as can be detected from the rank of their Jacobian. Having zero elastic stiffness $k_e^{\mathbf{q}}$ in a certain direction may lead to a stiffness ratio of one if the prestress stiffness is not zero in the same direction.

The configuration shown in Figure 3-2a has zero elastic stiffness in the direction of $\hat{\mathbf{q}}_x$. This displacement is a translational displacement and normal to all the cables. The prestress stiffness in this direction is found from Eqs. (3.4) and) to be

$$k_p^x = \sum_{i=1}^{n} \frac{\tau_i}{l_i} \hat{\mathbf{q}}_x^t \left(I - \hat{\mathbf{u}}_i \hat{\mathbf{u}}_i^t\right) \hat{\mathbf{q}}_x = \sum_{i=1}^{n} \frac{\tau_i}{l_i} \left(\left\|\hat{\mathbf{q}}_x\right\|^2 - \left(\hat{\mathbf{q}}_x^t \hat{\mathbf{u}}_i\right)^2\right) . \tag{3.19}$$

Note that $\hat{\mathbf{q}}_x^t \hat{\mathbf{u}}_i = 0$ for all cables, and $\|\hat{\mathbf{q}}_x\| = 1$; therefore, k_p^x becomes

$$k_p^x = \sum_{i=1}^{n} \frac{\tau_i}{l_i} \ . \tag{3.20}$$

k_p^x is not only nonzero in this direction (assuming $\tau_i > 0$), but also is at maximum over all configurations since $\left(\hat{\mathbf{q}}_x^t \hat{\mathbf{u}}_i\right)^2$ in Eq. (3.19) vanishes for all cables. As a result, in this configuration, the stiffness ratio is one, and, at the same time, the prestress stiffness is at maximum, so that the range of the controllable stiffness is further increased.

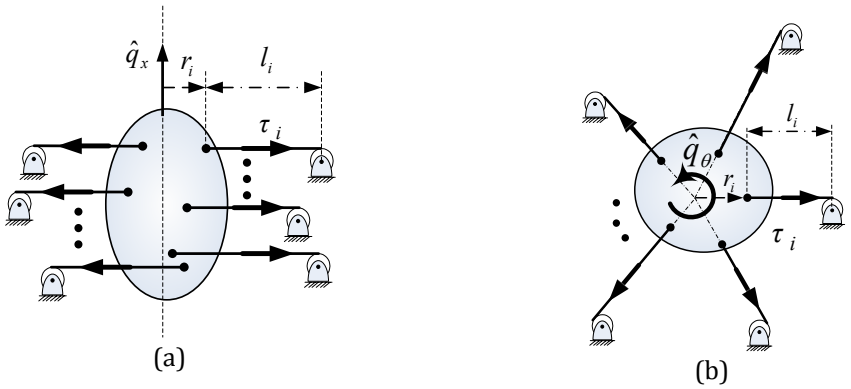

Figure 3-2 Two possible mechanisms with zero elastic stiffness and maximum prestress stiffness along the shown directions

A rotational prestress stiffness with a stiffness ratio of one is depicted in Figure 3-2.b. The prestress stiffness in the rotational direction of $\hat{\mathbf{q}}_\theta$ is found from Eqs. (3.4) and **Error! Reference source not found.**) to be

$$k_p^\theta = \sum_{i=1}^{n} \frac{\tau_i}{l_i} \left(\left\| \mathbf{r_i} \times \hat{\mathbf{q}}_\theta \right\|^2 - \left(\mathbf{r_i} \times \hat{\mathbf{u}}_i \cdot \hat{\mathbf{q}}_\theta \right)^2 \right) + \sum_{i=1}^{n} \tau_i \left(\hat{\mathbf{u}}_i \times \hat{\mathbf{q}}_\theta \right) \cdot \left(\mathbf{r_i} \times \hat{\mathbf{q}}_\theta \right) . \tag{3.21}$$

which can be further simplified in this particular configuration by noting that $\mathbf{r}_i \times \hat{\mathbf{u}}_i = \mathbf{0}$, $\mathbf{r}_i \perp \hat{\mathbf{q}}_\theta$ and $\mathbf{r}_i = r_i \hat{\mathbf{u}}_i$ for *i*=1,2,...,*n*. Therefore, we have

$$k_p^\theta = \sum_{i=1}^{n} \frac{\tau_i}{l_i} r_i^2 + \sum_{i=1}^{n} \tau_i r_i \ . \tag{3.22}$$

The rotational prestress stiffness in this configuration is at maximum since both summations in Eq. (3.22) are at their maximum values over all possible configurations of $\mathbf{r}_i$'s and $\hat{\mathbf{u}}_i$'s.

In summary, a stiffness ratio of one , that implies full control of the total stiffness through the prestress, is possible. A stiffness ratio of one corresponds to singular configurations of cable-driven mechanisms in which the elastic stiffness vanishes. In certain singular configurations, not only the stiffness ratio is one but also the prestress stiffness, in either translational or rotational directions, is at maximum. This property further increases the range of the controllable stiffness.

The range of the stiffness in singular configurations such as those shown in Figure 3-2 is found from Eqs. (3.20) and (3.22) to be determined by the maximum yield strength, the

number of the cables, and the dimensions of the mechanism. For instance, the number of the cables in such configurations can be increased while maintaining the maximum stiffness ratio. In Figure 3-3, an arrangement is shown in which the multiplicities of the cables are used to increase the stiffness range by using one actuator. The configurations shown in Figure 3-2 are two examples of possible configurations for an AVS.

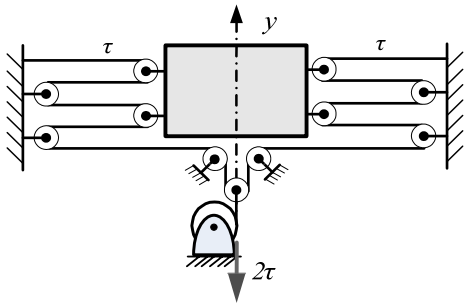

Figure 3-3 The number of the cable forces can be increased to increase the maximum prestress stiffness or the range of the controllable stiffness

Please note that, some prestressable mechanisms such as those shown in Figure 3-2 and Figure 3-3 have several stable kinematically singular directions (FOIMs). All of these FOIMs can be considered as a possible direction for developing an AVS. However, in the design process of an AVS, only one of the FOIMs is selected as the working direction of the designed AVS. For example, consider the singular prestressable mechanism shown in Figure 3-4. All of the links of this mechanism are in *xy* plane and the joints of this mechanism falls on four straight lines as shown in Figure 3-4 along *y* axis. This mechanism has four stable FOIMs (four kinematically singular directions): (1) along *x* axis (translational, similar to $\hat{q}_x$ in Figure 3-2.a), (2) along *z* axis (translational, out of *xy* plane), (3) about *x* axis (rotational), and (4) about *y* axis (rotational). The AVS will be designed to work along one of these FOIMs while three other FOIMs still exist. These three FOIMs can be eliminated by constraining the AVS to move along the selected FOIM. If the prestress level in the AVS stiffens these three FOIMs enough that the AVS can be used along the selected FOIM, there is no need to eliminate them.

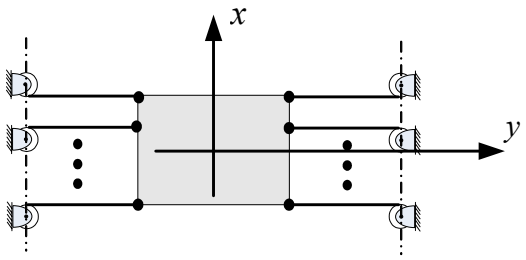

Figure 3-4 A kinematically singular prestressable mechanism with four FOIM (four singular directions).

3.4 CASE STUDY: APPLICATION OF AVS TO ENGINE MOUNT

In order to elaborate on the feasibility of the AVS in real applications, a case study is presented here on the engine mount of a typical vehicle. Engine mounts have relatively small displacements (less than 0.3 mm [71]) which help in avoiding the nonlinear stiffness effects of the AVS. The design of a simple AVS as an engine mount is proposed here and its

performance is compared with that of an equivalent[4] passive mount. The purpose is to show that with realistic assumptions and feasible dimensions and forces, an AVS can be built to significantly outperform existing mount designs.

Engine mounts connect the engine to the chassis and are designed to provide two major vibration functions:

1. Controlling the bouncing of the engine from the low-frequency shock excitations (0-20 Hz) caused by sudden acceleration and braking and riding on bumpy roads.
2. Isolating the chassis from the high-frequency (20-200 Hz) engine excitations caused by the firing pulse and rotating parts inside the engine [69].

Designing for the first property results in a high stiffness (hard) mount in the low-frequency range while the second property requires low stiffness (soft) in the higher frequencies. Commonly used passive mounts with constant stiffness and damping cannot provide this desired performance. On the other hand, an adaptive element with variable stiffness and fast response can adjust the stiffness of the mount according to the frequency of the excitation and hence make significant improvements.

The AVS made by a cable-driven mechanism, explained above, is explored here as an antagonistic **V**ariable **S**tiffness **M**ount (VSM). As was explained in section 2.7, this VSM is a semi-active mount that consists of a translational AVS and a soft rubber mount. A schematic of this VSM is shown in Figure 3-5. The translational AVS is a cable-driven mechanism which uses the concept shown in Figure 3-2.a. The minimum overall stiffness is that of the soft rubber mount where the cable forces are set at zero. The stiffness can be then increased by pulling the cables that generate the prestress stiffness. The soft rubber mount provides a damping effect to limit the magnitude of the transient response near the resonance frequency and also supports the weight of the engine. As Figure 3-5 shows, each cable has a vertical extension called the dead length (L_d). The dead length of each cable reduces its elastic stiffness (by increasing its length) while having no effect on its prestress stiffness. This property is used here to improve the linearity of the element for the displacement range of the application.

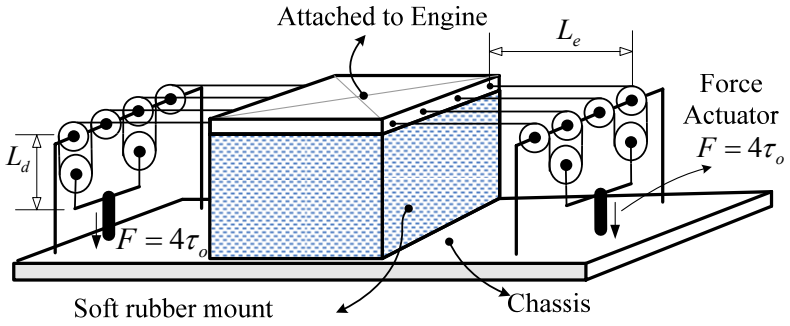

Figure 3-5 Schematic of the VSM developed with cable-driven mechanism

[4] An "equivalent passive mount" in this chapter means a passive rubber mount that has the same static stiffness.

3.4.1 MODELING

As was explained in Chapter 2, the VSM can be modeled as the stiffness (k_r) and viscous damping (c_r) of the rubber mount in parallel with the stiffness of the cable mechanism (k_{AVS}) (Figure 3-6.b). The performance of this VSM will be compared with the performance of an equivalent passive mount modeled as a constant stiffness (K_r) and constant damping (C_r) (Figure 3-6.a).

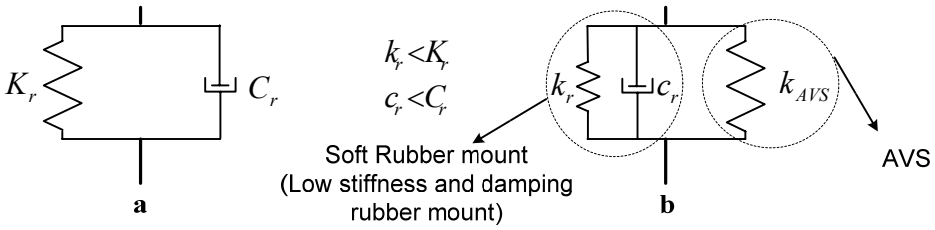

Figure 3-6 a. Model of a typical passive mount b. Model of the VSM

Table 3-1. Specifications of VSM (Figure 3-5)

Mount's type	Specification	Variable	Value	Unit
VSM	Number of cable connections	n	8	-
	Diameter of cables	d	2	mm
	Effective length	L_e	20	mm
	Dead length	L_d	20	mm
	Yield strength	S_y	1690	MPa
	Safety factor at maximum cable force	N_s	5.7	-
	Elastic modulus	E	200	GPa
	Stiffness of the soft rubber mount of VSM	k_r	$0.5\text{x}10^5$	N/m
	Damping of the soft rubber mount of VSM	c_r	300	N.s/m
Passive mount	Damping of the passive mount	C_r	610	N.s/m
	Stiffness of the passive mount	K_r	$1.3\text{x}10^5$	N/m

The specifications of the passive mount are of a typical mount used in passenger cars [70]. The parameters of the VSM are selected such that its overall stiffness range will be comparable with that of the passive mount and the maximum force in the cables will be less than 20% of its yield strength. The details of the parameters of both systems are given in Table 3-1.

In order to obtain the desired stiffness in the VSM, the cable forces are assumed to be set by a control system as a function of the dominant frequency of the disturbance. In practice, this task will be accomplished by using a sensor to measure the dominant excitation frequency on the chassis, and a control loop to set the desired force in the cable actuators. The overall scheme of the desired stiffness as a function of the frequency is depicted in Figure 3-7. As seen in this figure, the total stiffness of the VSM (K) and the stiffness of the passive mount (K_r) are equal at the beginning of the frequency range. The stiffness of the

VSM increases as a second-order polynomial up to three times the stiffness of the passive mount $3\,K_r$ at around the half of the natural frequency of the system ($f_n/2$) and then remains constant up to $1.5f_n$. For frequencies above $1.5\,f_n$, the stiffness is decreased to the stiffness of the passive mount by removing the cable forces.

As is mentioned above, a desired engine mount has frequency-dependent characteristics to control the engine bounce in low frequencies and to isolate the engine vibration in the higher-frequency range. To compare the performance of the VSM and the passive mount, they are simulated in the following frequency ranges: low frequencies (0-20 Hz) and high frequencies (20-200 Hz).

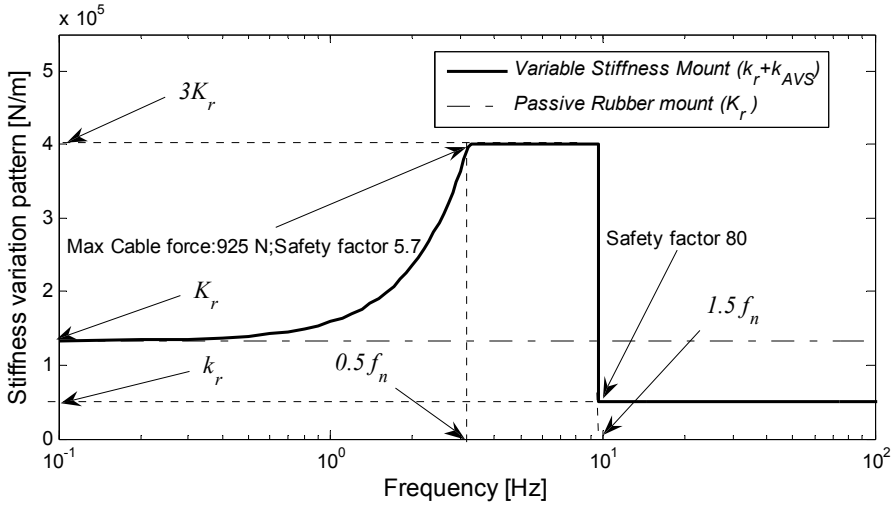

Figure 3-7 Frequency dependent stiffness of VSM

3.4.2 *Comparing the performance of the VSM with the performance of equivalent passive mount in low frequencies*

Sudden accelerations, braking, and riding on bumpy roads cause the engine to bounce at low frequencies and result in relatively large displacements of the engine with respect to the chassis, especially near the resonance frequency of the engine and mount. It is desired to limit this relative displacement to a value of about 0.2 mm [71]. As a result, the relative displacement of the engine and the chassis is a quantitative measure of the performance of the mount in the low-frequency range. To find the relative displacement, a quarter model of a car based on the full model given in [70] is used. This model, along with the passive mount and the VSM, is shown in Figure 3-8, and the model parameters are given in Table 3-2. The complete dynamic equations of the model are given in Appendix A. Note that the VSM is modeled by its nonlinear governing equations, which accommodate both elastic and prestress stiffness effects. It is clear that the prestress stiffness can be derived from the nonlinear dynamic equations of the system by linearization around the static equilibrium point.

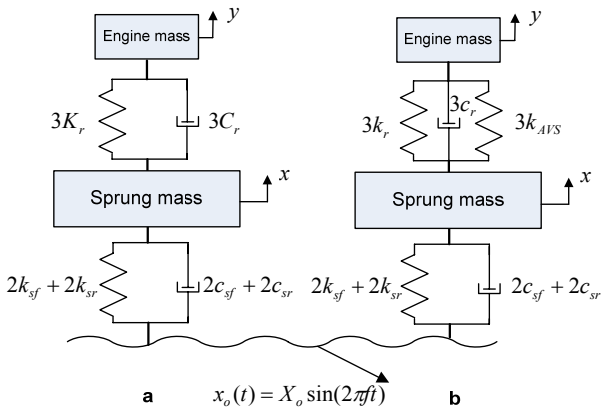

Figure 3-8 Quarter model of a passenger car with a. the equivalent passive mount b. The VSM

Table 3-2. Vehicle model parameters [71]

Specification	Variable	Value	Unit
Sprung mass	m_s	868	kg
Engine mass	m_e	244	kg
Front suspensions' stiffness	k_{sf}	20580	N/m
Rear suspensions' stiffness	k_{sr}	19600	N/m
Front suspensions' damping	c_{sf}	3200	N.s/m
Rear suspensions' damping	c_{sr}	1700	N.s/m

The road surface irregularity is considered as a sinusoidal curve. Figure 3-9 shows the engine's response to the road's displacement occurring at a frequency of 10 Hz. This figure shows that, due to the nonlinearities in the VSM, the engine's steady state oscillation is not a pure sinusoidal; however, it is close to a sinusoidal function with the dominant frequency equal to the road's frequency. In order to compare the response at different frequencies, it is assumed that the velocity of excitation represented by $X_o f$ remains constant at 0.01 m/s for the low-frequency range (0-20 Hz). This assumption results in a realistic mount deflection (less than 0.3 mm) over this frequency range.

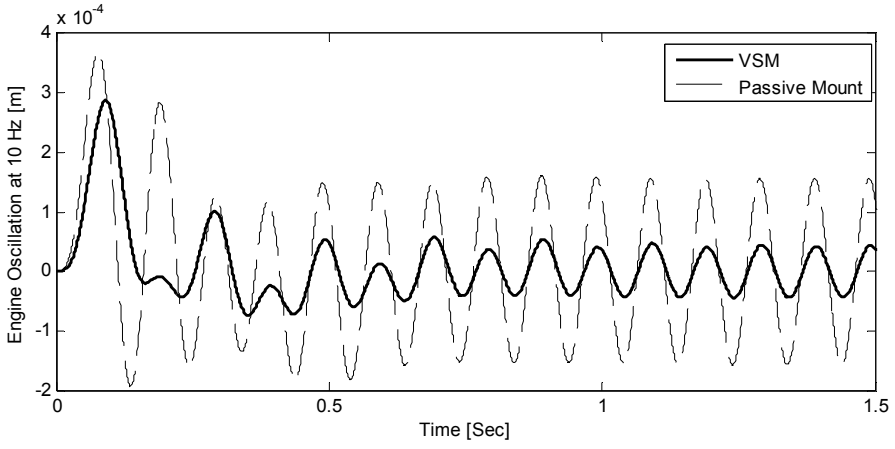

Figure 3-9 The oscillation of the engine

Figure 3-10 shows the relative displacement of the engine with respect to the chassis over the low-frequency range, clearly showing that the AVS improves the relative displacement by limiting the maximum relative displacement to about one-quarter of that of the passive mount.

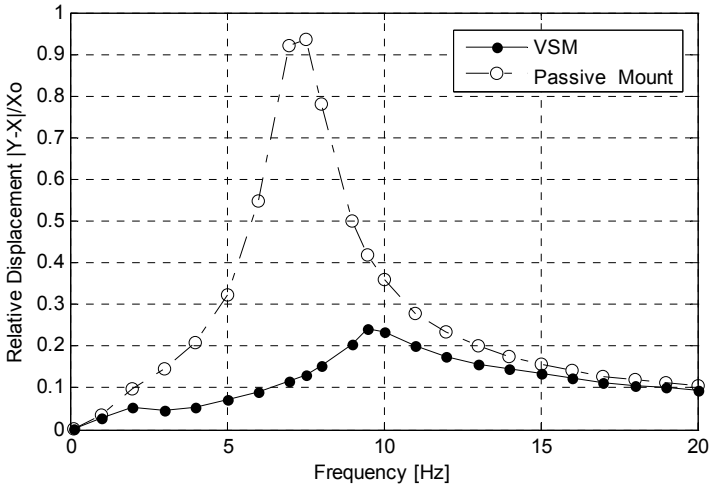

Figure 3-10 Relative displacement of the engine and chassis

3.4.3 *Comparing the performance of the VSM with that of the performance of the equivalent passive mount in high frequencies*

Engine mounts are also supposed to isolate the high-frequency unbalanced forces of the engine from the chassis. In order to compare the isolating ability of the mounts, the force transmissibility ratio of the mounts in the one-quarter car model of Figure 3-8 is used. Since, the displacements of the mounts caused by the engine unbalanced forces are small (due to the high-frequency), a linear model of the VSM is sufficiently accurate and hence used.

The frequency range of 20-200Hz in a four-cylinder engine corresponds to engine speeds of 600-6000 rpm. The stiffness of both mounts is constant at 1×10^5 N/m for the VSM (k_r) and 1.3×10^6 N/m for the passive mount (K_r) (Figure 3-7). The force transmissibility is plotted for both systems in Figure 3-11, which shows that the VSM provides lower transmissibility and better isolation. For example, at the idling speed of 20 Hz, the VSM improves the isolation by 10%. Note that at higher frequencies, the passive mount is already quite efficient in isolating the vibration. For example, at high operating speed (4500 rpm/150 Hz), the passive mount provides 98.3% isolation. At this frequency, the VSM provides 99.1% isolation, or about a 1% isolation improvement.

A major contributing factor to the better performance of the VSM at high frequencies, other than the lower stiffness, is the lower damping. Note that the damping of the mount at high-frequency acts similarly to the stiffness and increases the transmissibility. However, damping is necessary for passive mounts since it limits the resonance displacement at low frequencies. In a VSM, however, the low-frequency resonance oscillation is avoided by using the change in the stiffness, and, hence higher damping is not necessary anymore. As a result, a soft rubber with lower damping improves the isolation of the VSM.

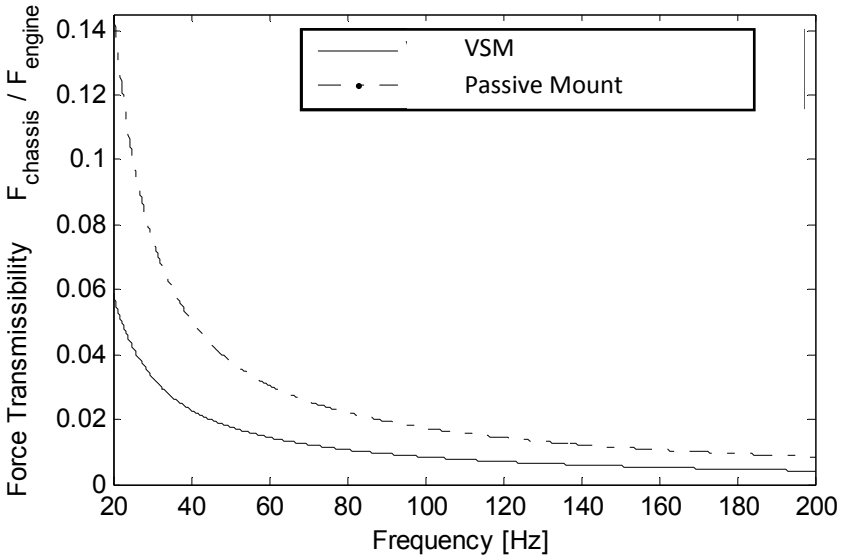

Figure 3-11 Force transmissibility of VSM and the passive mount

3.5 CONCLUSIONS

The idea of using the prestress stiffness as a variable stiffness spring (AVS) for vibration-control applications was proposed, and some of its fundamental issues were addressed. An AVS can change its stiffness much faster than other available mechanical systems since an AVS relies on force change and minimal motions in the links.

Cable-driven mechanisms were used as the development platform, mainly for the kinematics advantages of the cables and simplicity of the fabrication. A suitable stiffness model of cable-driven mechanisms was given, and the stability conditions were discussed.

Two main criteria for an AVS as an effective solution for vibration-control were determined: (1) The prestress stiffness should be dominant in the overall stiffness of the element, and (2) the stiffness magnitude should be significant. It was shown that in kinematically singular configurations of the mechanism, both criteria can be met. In such configurations, the overall stiffness is merely prestress stiffness and hence fully controllable. Also, it was shown in section 3.3 that the number of the cables can be increased to extend the stiffness range to virtually any desired level.

To elaborate on the feasibility of the concept in small displacement applications, a case study was presented with some detailed analysis. An engine mount design based on an AVS was compared with a commercial passive mount by using numerical simulations of the nonlinear model. It was shown that under feasible conditions such as the feasible size and force of the cables, the AVS improves the performance of the engine mount both in low-frequency and high-frequency excitations. The VSM controls the vibration displacement at the resonance frequency four times more than the equivalent passive mount. At the idling frequency of the engine, a VSM provides 94% vibration isolation, or 10% more than the isolation that passive mount provides. These improvements are obtained for the price of a small amount of power used to stretch the cables and set prestress in them.

The development of the AVS concept is based on small displacement along infinitesimal mechanism. Many applications in vibration-control, such as the one selected in this work, deal with small displacements of less than a millimeter. The effectiveness of such an AVS for vibration application was shown by the simulation results. For larger displacements, however, none of the stiffness components remains constant. As a result, in order to use AVS's in large displacement applications such as suspension springs, the nonlinearity effects due to large displacements need to be studied.

Chapter 4 DEVELOPING AN ANTAGONISTIC VARIABLE STIFFNESS SPRING BY USING TENSEGRITY MECHANISMS[5]

In 0Chapter 2, the fundamentals of semi-active variable stiffness springs including the mechanical ones were reviewed. It was argued that one of the main challenges is to decrease the response time. A new idea for building variable stiffness originated from the fact that in prestressed mechanisms the stiffness can be changed by varying the amount of the prestress in the cables. This change can potentially lead to a quick responding variable spring since the force change in the cables requires small displacements. The idea was further explored in Chapter 3 by showing that when prestressable cable-driven mechanisms are in singular configurations, they demonstrate enhanced characteristics for effective and fast-responding mechanical semi-active springs. This spring was called the antagonistic variable stiffness spring (AVS). In this chapter, the idea of creating an AVS is applied to tensegrities as a special case of pin-jointed structures.

Tensegrities demonstrate a similar potential for variable stiffness since they are prestressable, have kinematic singularities, and possess first-order infinitesimal mechanisms (FOIMs). It will be explained later in this chapter that tensegrity prisms (TP) can be designed and used as variable stiffness springs for vibration-control applications. Similar to the stiffness of the spring developed in Chapter 3 with cable-driven mechanisms, the stiffness of a TP can be controlled effectively by the level of prestress. The AVS explained in this chapter is also called the Tensegrity Prism Spring (TPS).

In the first part of this chapter, the literature on pin-jointed structures including tensegrities is briefly reviewed. Tensegrity prisms are then investigated to identify an optimal configuration for creating a variable stiffness spring. A comprehensive formulation of the stiffness for this tensegrity is given by using the Jacobian method. A detailed discussion of the characteristics of the proposed variable spring is presented, followed by an example and conclusions.

[5] Most of this chapter's material was taken from the paper published in [10].

4.1.1 *STATICS AND KINEMATICS OF PIN-JOINTED STRUCTURES*

A spatial pin-jointed structure with N_m members, N_j nodes (joints) and N_c displacement constraints on the nodes has $N_v = 3N_j - N_c$ unknown displacement components in an arbitrary fixed Cartesian coordinate system (X, Y, Z). The static equilibrium equation relates the external nodal force vector $\mathbf{f}_{N_v \times 1}$ to the internal forces of the members $\boldsymbol{\tau}_{N_m \times 1}$ by the "Equilibrium Matrix" $\mathbf{A}_{N_v \times N_m}$:

$$\mathbf{A}\boldsymbol{\tau} = \mathbf{f}\,. \tag{4.1}$$

The equilibrium matrix ($\mathbf{A}$) depends on the geometry and configuration of the structure at the equilibrium. In other words, $\mathbf{A}$ is a function of the positions of the nodes and their connectivities. Now let $\mathbf{d}_{N_v \times 1}$ be the (small) nodal displacement vector, and $\mathbf{e}_{N_m \times 1}$ be the (small) vector of the member elongations corresponding to $\mathbf{f}_{N_v \times 1}$ and $\boldsymbol{\tau}_{N_m \times 1}$, respectively. The principal of virtual work states that the virtual work of the external nodal force vector ($\mathbf{f^t d}$) equals with the virtual work of the internal forces of the members ($\boldsymbol{\tau}^t\mathbf{e}$). By using the principal of virtual work and static equation (Eq.(4.1)), the kinematic equation for small deflections is found as

$$\mathbf{A}^t\mathbf{d} = \mathbf{e}\,, \tag{4.2}$$

in which, $\mathbf{A}^t$ is known as the "Kinematic Matrix" and is the transpose of the equilibrium matrix. Note that the sign convention in this thesis is such that tensile force and elongations in the members are assumed to be positive, and, therefore $\mathbf{A}$ and $\mathbf{A}^t$ are defined accordingly.

4.1.2 *SUBSPACES OF EQUILIBRIUM MATRIX*

The physical properties of a pin-jointed structure including the states of the prestress and the modes of the inextensional mechanisms can be derived from the subspaces of the equilibrium matrix [72]. The four subspaces of $\mathbf{A}$ and their physical implications are summarized in Table 4-1.

Table 4-1: Summary of the information provided by the four subspaces of A [72]

Name of subspace	Description	Dimension	Static information (Eq.(4.1))	Kinematic information (Eq.(4.2))
Column space of **A**	The space spanned by the columns of **A**. Also called range or image of **A.**	rank(**A**)	Column space of **A** gives admissible load vectors **f** which can be supported by structure and hence called "fitted loads".	Column space of **A** (row space of $\mathbf{A}^t$) includes all modes of nodal displacement which results in the elongation or contraction of the components.
Null space of **A**	The space normal to the column space of **A**. It represents the component forces that result in zero external load (prestress).	s	Null space of **A** provides s states of prestress.	Nullspace of **A** gives member elongations that are not feasible and cannot be realized in the structure ("forbidden elongations").
Row space of **A** or Column space of $\mathbf{A}^t$	The space spanned by the rows of **A.**	rank(**A**)	Row space of **A** gives the component forces that correspond to "fitted loads".	Row space of **A** represents any geometrically compatible elongations induced by displacement of nodes.
Left Nullspace of **A** or Nullspace of $\mathbf{A}^t$	The space spanned by mechanisms modes.	m	Left Nullspace of **A** gives the range of external forces **f** that cannot be carried out by the structure.	Left Nullspace of **A** gives m independent inextensional mechanisms (i.e. nodal displacements that do not correspond to any length change in the members. These mechanisms can be either finite or infinitesimal.

The two subspaces of **A** which are most helpful in this study are the s-dimensional null space of **A** and the m-dimensional left null space of **A** where

$$s = N_m - \text{rank}\left(\mathbf{A}_{N_v \times Nm}\right), \tag{4.3}$$

and

$$m = N_v - \text{rank}\left(\mathbf{A}_{N_v \times Nm}\right). \tag{4.4}$$

4.1.3 INEXTENSIONAL MECHANISMS

When the left null space of **A** exists ($m > 0$), the structure has inextensional mechanisms/deformations. An inextensional mechanism is a deformation of the structure that does not change the length of the members. Inextensional mechanisms can be finite or infinitesimal. When the deformation is a finite mechanism (see Table 4-2, Fig.b), the nodes can move freely in a finite distance without changing the lengths of the members. In an infinitesimal mechanism (Table 4-2, Fig.d), on the other hand, when the nodes move, the lengths of the members slightly change. These changes, however, are not of first-order of the node displacements, therefore, these mechanisms are called "infinitesimal". If the changes are of second order, they are called "first-order infinitesimal mechanisms" and referred to as FOIM. Higher-order infinitesimal mechanisms are associated at least with the third-order changes of the members' lengths. First-order and higher order infinitesimal mechanisms are studied in [20,23,72,73,74]. It is notable that the left null space of **A** determines only whether or not the structure has inextensional mechanisms. It cannot distinguish between first-order, higher-order infinitesimal, or finite mechanisms. In order to distinguish first-order infinitesimal from higher-order and finite mechanism, Pellegrino and Calladine [72] introduced the "product-force" method. They suggested that if the "product-force" vector does not lie in the column space of **A**, then the corresponding mechanism is first-order infinitesimal and that otherwise, it is a higher-order infinitesimal or finite mechanism.

The first-order infinitesimal mechanisms exhibit useful characteristics in a prestressable structure ($s > 0$), including a stiffening property and stability, while on the other hand, higher-order infinitesimal mechanisms and finite mechanisms cannot be stabilized by a state of prestress [20,74]. These useful characteristics can be seen in any structure with a first-order infinitesimal mechanism, such as tensegrites, which will be discussed in the following section.

4.1.4 CLASSIFICATION OF PIN-JOINTED STRUCTURES

Every pin-jointed (reticulated) structure belongs to one and only one class of the four classes given in Table 4-2, based on the number of independent state of prestress (s) and the number of independent inextensional mechanisms (m) [75]. s and m are natural numbers that define the static and kinematic properties of the pin-jointed structures, respectively. As the defining equations of s and m given in Eqs.(4.3) and (4.4) show, s and m are functions of the numbers of the members (N_m) and nodes (N_j) as well as the topology and geometry represented by the rank of the equilibrium matrix (**A**).

Table 4-2: Four classes of pin-jointed structures[6][75]

Class	**1**	**2**	**3**	**4**
s	s=0	s=0	$s \geq 1$	$s \geq 1$
m	m=0	$m \geq 1$	m=0	$m \geq 1$
Class	Statically and kinematically determinate structures	Statically overdeterminate and kinematically indeterminate structures	Statically indeterminate and kinematically overdeterminate structures	statically and kinematically indeterminate structures
Example	Truss	Four bar linkage mechanism	Enforced trusses, tensionable cable mechanisms	Singular cable-driven mechanism[20], Tensegrities
Figure (2D Example)	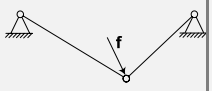	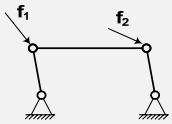	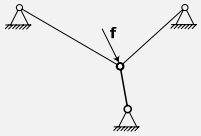	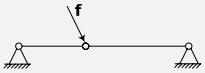
	(a)	(b)	(c)	(d)
Have Inextensional mechanism	No	Yes Finite Mechanism	No	Yes Infinitesimal mechanism
		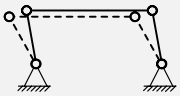		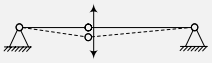
		(e)		(f)
Prestressable	No	No	Yes	Yes
			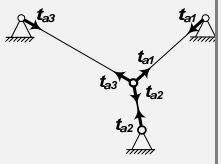	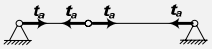
			(g)	(h)

Among the four classes, classes 3 and 4 are prestressable structures; i.e., even without external forces, internal forces can be developed in the members that satisfy the equilibrium. These forces are known as prestress or antagonistic forces. It is well known that the stiffness of a prestressable structure is a function of its prestress that can be selected from the null space of its corresponding Equilibrium matrix (**A**) [23,29]. In other words, the stiffness of the prestressable structures can be changed and controlled by changing the prestress forces.

[6] Note that all figures in this table are planar mechanisms (2D).

Therefore, prestressable structures (Classes 3 and 4) have variable stiffness and hence can be used as variable stiffness springs.

Classes 3 and 4 are similar in the sense that they are both prestressable, but Class 4 also has infinitesimal mechanisms. They give an advantage to Class 4 over Class 3 for creating a variable stiffness spring. The advantage is that the stiffness of a stable prestressable mechanism at equilibrium and along the direction of the infinitesimal mechanism is not a function of the elasticity of the members but of the prestress and the geometry only [29,56]. This property implies that, by controlling the prestress, not only the stiffness can be changed but also the stiffness can be changed from zero (when the prestress is zero) to, theoretically, infinity (when the prestress increases to infinity). Therefore, fully controllable variable stiffness can be potentially obtained. Note that the stiffness can be changed from zero to large values only at the equilibrium state and along the infinitesimal mechanism. When the structure undergoes a finite deflection due to the external load, the infinitesimal mechanism will no longer exist, and, therefore, the abovementioned advantage will be lost. However, as long as the deflections due to the external load are designed to be "sufficiently" small, the stiffness made by the prestress is the dominant stiffness, and the structure will demonstrate an acceptable performance as a variable spring.

Not all mechanisms in Class 4 are stable. "Stability", here, refers to the fact that the mechanism tends to return to its original geometry when deformed under an external load. For this reason, and to obtain stable variable stiffness, a subset of Class 4 with "First-order infinitesimal mechanism" (FOIM) that is stable [20] is considered. As mentioned in section 4.1.3, higher-order infinitesimal mechanisms are unstable and therefore are excluded from this study.

Murakami [23] suggested that the tangent stiffness matrix (the total stiffness matrix) be used to recognize the FOIMs from higher-order infinitesimal mechanisms. If it is positive definite, then the prestressable structure is a first-order infinitesimal mechanism; otherwise, it is of higher orders. As well, Murakami showed that in Class 4 structures with a FOIM, if the prestress is non-zero in every member, it stiffens all infinitesimal mechanisms.

4.2 TENSEGRITY STRUCTURES

a. Vortex study, 1967 Aluminum & Steelon b. Tetra Tower

Figure 4-1 Two examples of tensegrity structures(Courtesy of K.Snelson) [42]

Tensegrity structures can be seen in a variety of configurations such as the inspiring works of Kenneth Snelson, who made the first tensegrity about 60 years ago. Since new tensegrities are still being discovered by the researchers in different fields, a comprehensive definition of tensegrities is not yet agreed upon. However, based on structural studies such as [40,52,56,76], a "tensegrity" is a prestressed and freestanding pin-jointed structure with first-order infinitesimal mechanism (FOIM) in which components (bars and cables) are rectilinear elements. The bars are disconnected elements under only compression against interconnected cables which are only under tension.

"Freestanding" means that tensegrities are stable structures that can maintain their configurations without being constrained to the ground. Structures that comply with the above definition are known as "pure" tensegrities and form a subset of Class 4 structures. However, in the literature, some structures similar to pure tensegrities are also called "tensegrities". For example, sometimes pure tensegrities are augmented by adding extra bars or cables in order to increase the structural stiffness. This, in some cases, results in the elimination of the infinitesimal mechanisms and turns the pure tensegrity to an "over-constrained tensegrity" which belongs to class 3. However, it may be still known as a tensegrity in the literature. These cases are not considered in this research, since the FOIMs are the key for creating an effective variable spring.

4.2.1 SELECTING THE TYPE OF TENSEGRITY

The simplicity of the tensegrity and its infinitesimal mechanisms are two main criteria for a practical spring in industrial applications. A tensegrity can have more than one infinitesimal mechanisms, and some of them may be associated with complex deformations. Therefore, only those with simple forms are desired. The number of bars (n) and cables and how they configure the tensegrity determine the number of the infinitesimal mechanisms. For example, consider the ten-stage cyclic frustum tensegrity shown in Figure 4-1.b. This tensegrity has 40 bars, 120 cables and 80 nodes (joints). Nishimura and Murakami [77] showed that the number of the infinitesimal mechanisms (m_{cf}) of a general cyclic frustum tensegrity with n bars is independent of the stages and is

$$m_{cf} = 2n - 5 \,. \tag{4.5}$$

Therefore, the tensegrity shown in Figure 4-1.b has 75 infinitesimal mechanisms. As explained in the previous section, this tensegrity, if deformed along any of its infinitesimal mechanisms, demonstrate a spring which depends merely on the amount of the prestress. This property means that theoretically, 75 variable springs can be made by this structure. However, the associated displacements in most of these springs are very complex and not practical. To elaborate, let us consider equilibrium matrix **A** and infinitesimal mechanism vectors of this tensegrity. Assume the tensegrity is not constrained to the ground (N_c =0). **A** is a 240x160 matrix with a rank of 159. As a result, the number of mechanisms is found to be 81 ($m = N_v - \text{rank}(\mathbf{A})$). Among these mechanisms, six finite mechanisms represent six rigid body motions of the tensegrity, and the 75 remaining mechanisms are first-order infinitesimal mechanisms (FOIMs). Any infinitesimal mechanism of this tensegrity can be expressed in Cartesian coordinates, by a 240x1 column vector that contains the small displacements of 80 nodes. As another example, consider the regular truncated icosahedral tensegrity (Figure 4-2) studied in [57]. It is a spherical tensegrity with 60 nodes, 30 bars and 90 cables and has 55 FOIMs. Any infinitesimal mechanism described in Cartesian

coordinates (*XYZ*) is a 180x1 column vector that contains the displacement of 60 nodes. Such mechanisms have complex geometry and are difficult to use in a variable spring. Nevertheless, a complex FOIM and the resulting stiffness is still fully controllable and may have suitable applications. In this study, we seek tensegrities whose FOIMs benefit from simpler geometries such as linear or rotational deformations that better resembles a regular spring. This search leads us to tensegrity prisms, which are discussed in the following section.

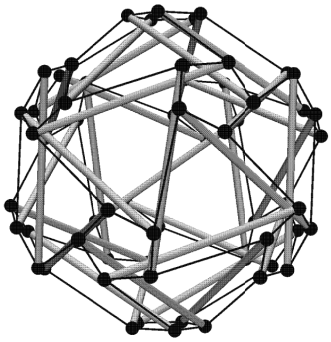

Figure 4-2 A regular truncated icosahedral tensegrity (Courtesy of Dr.Murakami and Dr.Nishimura)

As was explained, in tensegrities, such as those shown in Figure 4-1.b, and Figure 4-2, infinitesimal mechanisms involve the complex motion of numerous nodes. As a result, for this study, we target tensegrity prisms (such as those shown Figure 4-3) that possess simpler FOIMs and, hence, are more appropriate for use as a general purpose variable spring.

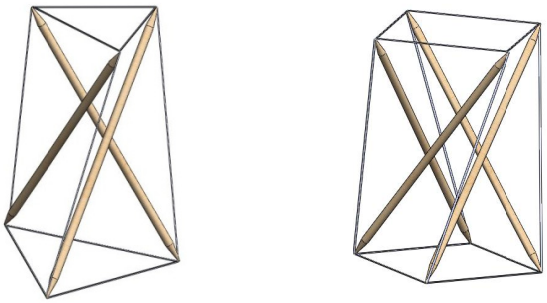

Figure 4-3. Two tensegrity Prisms (TP) a.Triangular TP b. Square TP

4.3 TENSEGRITY PRISM (TP)

Tensegrity prisms (such as those shown in Figure 4-1.a and Figure 4-3) were first introduced by David Emmerich in 1958 [40]. They have been studied as special forms of symmetrical braced rings [75,76], as cyclic frustum tensegrity [23,77,78] , and as "tensegrity prisms" by Kenner [41]. They are formed as one-stage cyclic frustum tensegrities with nodes, bars and cables, and are also called "simplex tensegrities"[40] (see Figure 4-4.b,c). All bars and vertical cables connect two top and base n-gons. Each of the top and base n-gons consists of cables and nodes. The n-gons are equilateral polygons. The

radius of the circumscribing circles are r_h and r_o for the top and base n-gons, respectively. If r_h and r_o are equal, the tensegrity can be enclosed in a cylinder; otherwise, it is enclosed in a cone. The height of the tensegrity, shown by h, is the distance between the top and the base n-gons. The lengths of the bars and the vertical cables are shown by b and L, respectively. The top n-gon is twisted by a particular angle, which is a function of n. To understand the configuration of a TP with $r_h \neq r_o$, consider a truncated pyramid (Figure 4-4.a). The nodes of the base n-gon are numbered from 1 to n in the counter-clockwise direction, and the corresponding nodes on the top n-gon are numbered from $n+1$ to $2n$. A right-hand or dextrorse TP is built if the top n-gon is twisted by $\theta=\frac{\pi}{2}+\frac{\pi}{n}$ counter-clockwise, and then vertical cables are added such that node $n+1$ connects to node 2, n+2 connects to 3, and so on (see Figure 4-4.b). Similarly, a left-hand or sinistrorse TP is obtained if the top n-gon is twisted by $\frac{\pi}{2}+\frac{\pi}{n}$ clockwise and the vertical cables are added between nodes $n+2$ and 1 and so on, according to Figure 4-4.c. The right-hand and left-hand tensegrities are the mirror images of each other and demonstrate similar characteristics. In this thesis, TP refers to a right-hand tensegrity prism. In addition, due to the high rigidity of the bars compared with the cables, it is assumed here that under the external loads when the TP deflects, the bar lengths remain constant but the cable lengths change.

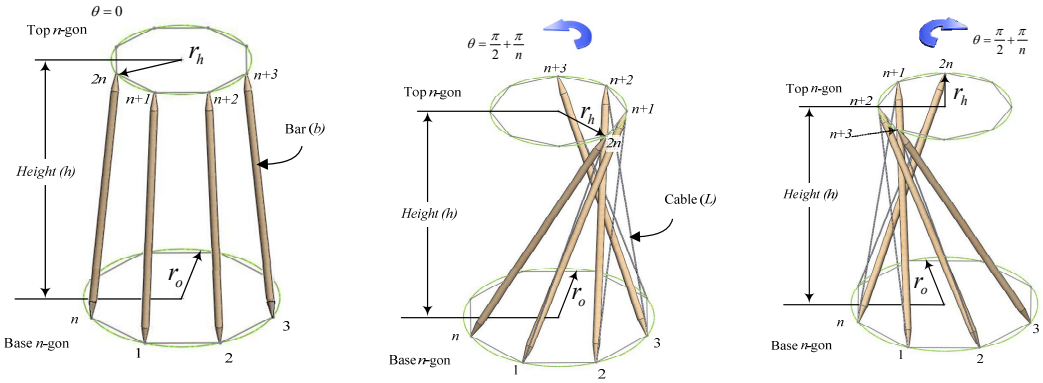

a. b. c.

Figure 4-4. How an n-gon tensegrity prism (n-gon TP) is built a. n-gon truncated pyramid b. Right-hand TP (studied in this chapter) c. Left-hand TP

In the TP shown in Figure 4-4.b, using basic geometry, the height of the structure (h) and the length of the vertical cable (L) can be expressed as functions of the twist angle, θ:

$$h = \sqrt{b^2 - {r_o}^2 - {r_h}^2 + 2r_o r_h \cos(\theta)} \tag{4.6}$$

$$L = \sqrt{b^2 + 2r_o r_h \left(\cos(\theta) - \cos\left(\theta - \frac{2\pi}{n}\right)\right)}\ . \tag{4.7}$$

Therefore, at the tensegrity state where $\theta = \frac{\pi}{2}+\frac{\pi}{n}$, we have

$$h_p = \sqrt{b^2 - {r_o}^2 - {r_h}^2 - 2r_o r_h \sin\left(\frac{\pi}{n}\right)} \tag{4.8}$$

$$L_p = \sqrt{b^2 - 4r_o r_h \sin\left(\frac{\pi}{n}\right)}\,. \tag{4.9}$$

A subscript of "p" indicates in this thesis that the corresponding parameter is for when the structure is a tensegrity.

4.3.1 *Prestress state of an n-gon TP*

An n-gon TP has only one state of prestress ($s = 1$)[23]. If the prestress of the vertical cables is set to τ_p , the cable prestress of the base and top n-gons should be $\frac{r_h}{L_p}\tau_p$ and $\frac{r_o}{L_p}\tau_p$, respectively. The prestress of the bars are compressive and equal to $\frac{-b}{L_p}\tau_p$.

4.3.2 *First-order infinitesimal mechanisms (FOIM) of an n-gon TP*

As a special case of the general cyclic frustum tensegrity discussed in 4.2, an n-gon TP with n bar has $2n + 1$ mechanisms including 6 finite mechanisms and $2n - 5$ FOIMs (see Eq.(4.5)). The six finite mechanisms correspond to the rigid body motions, and the other $2n - 5$ mechanisms are FOIMs. For example, the triangular TP with 3 bars and the square prism with 4 bars have one and three FOIMs, respectively.

Calculating and comparing the FOIMs of several n-gon TPs, showed that most of them are too complex to be used as the displacement vector for a spring. This issue will be discussed later in this section. The only exception is a FOIM with a twisting deformation that exists in all n-gon tensegrity prisms, as will be shown in the following paragraphs.

This twisting FOIM is a deformation of the TP when the top and base n-gons maintain their shapes and rotate in opposite directions about the vertical axis of the tensegrity. Since the lengths of the bars are constant, and the bars are arranged symmetrically, they allow for a rotation with a change in the height. In other words, this deflection consists of an infinitesimal twist of the top n-gon with respect to the bottom one, accompanied by a change in the height of the TP.

To realize that this twisting deflection is a common FOIM for all n-gon TPs, consider the relation between the height change dh and twist angle $d\theta$ found by differentiating Eq.(4.6) and assuming the bar lengths are constant:

$$dh = \frac{-r_o r_h \sin(\theta)}{h}\, d\theta\,. \tag{4.10}$$

Equation (4.10) shows that when the top platform rotates, while maintaining its geometry, the height of the tensegrity will increase or decrease. Now, one can find $\frac{dL}{d\theta}$ from Eq.(4.7) and easily show that it becomes zero at the tensegrity state; i.e., $\theta = \frac{\pi}{2} + \frac{\pi}{n}$. This result implies that if the TP is at the tensegrity state, the twisting motion expressed by Eq.(4.10) does not change any cable lengths. Given that the bar lengths are also assumed constant, and the top and bottom n-gons maintain their geometry, the conclusion is that this twisting motion is a FOIM.

To understand the level of complexity of other FOIMs of an n-gon TP, consider a square TP with four bars (Figure 4-5). The left null space of its equilibrium matrix is spanned by nine vectors, which are the mechanisms of the square TP. By using a mathematical method

explained in [72], the six finite mechanisms which describe the rigid body motions are extracted, and, subsequently, a subspace is obtained spanned by three FOIMs. One of these is the twisting mechanism discussed above. By excluding the twisting FOIM from this subspace, two other FOIMs of the mechanism were found. In these two FOIMs, the top and base n-gons distort such that their nodes do not stay in the initial planes. Figure 4-5 shows one of these two FOIMs in which differential deflections are exaggerated for the sake of illustration. For example, the base nodes (1-4), which are initially located on the corners of a square, distort in a way that diagonal nodes 1 and 3 move away from each other and shift upwards where diagonal nodes 2 and 4 move towards each other and shift downwards. Note that theoretically, such a FOIM can be used to build a variable spring. However, for practical applications, providing an out-of-plane deflection while the nodes on each n-gon move is difficult. Following a similar approach, all FOIMS of the 4-gon were investigated, but for the sake of brevity, the results are not detailed here.

In addition, a TP with more than four bars has more FOIMs which are expected to be similar to the second and third FOIMs of the square TP in having out-of-plane deflection of nodes and distorted top and base n-gons. Due to the simplicity of the twisting FOIM, in the rest of this study, the investigation is focused on the twisting FOIM of a n-gon, which is common to all n-gon TPs.

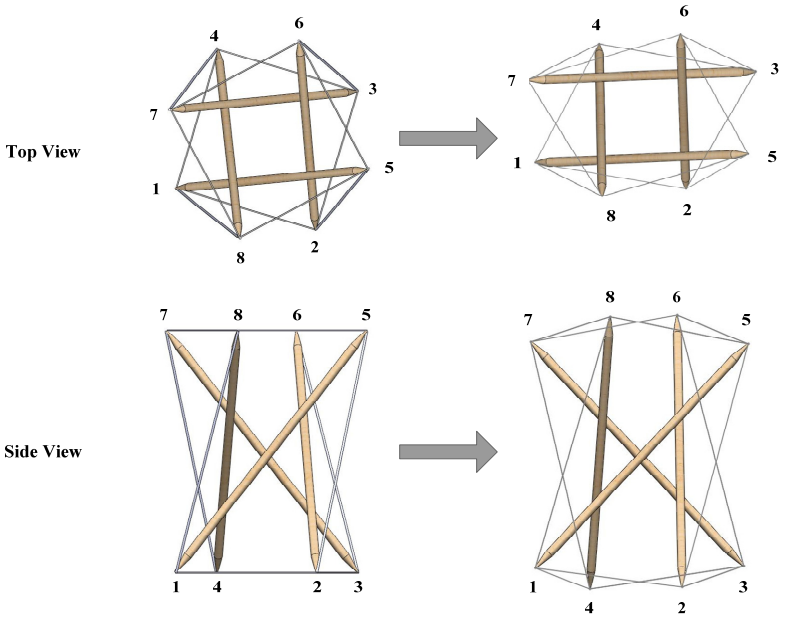

Figure 4-5, Top and side views of the second FOIM of a square TP

4.4 TENSEGRITY PRISM SPRING (TPS)

As explained before, every TP has a FOIM with a twisting motion. The load-displacement relation along this twist is utilized as a spring and hence is called the "tensegrity prism spring" (TPS). Also, remember that the stiffness of this spring is determined solely by the prestress and does not depend on the elastic stiffness of the components in small displacements. Due to the twisting motion of this spring, which preserves the top and bottom n-gons, they can be replaced by two rigid bodies. The top rigid body makes a platform for exerting the load, and the base rigid body provides a base for constraining the

TPS. To constraint the motion of the top platform along the twisting FOIM, the top and base platforms can be constrained by a cylindrical joint that allows rotation and translation along the vertical axis(Figure 4-6 and Figure 4-7).

If a TP is considered as a translational spring, it should be also noted that when a load is applied on the top platform, in addition to the displacement along z, the platform also rotates by β out of the tensegrity state where the angular position θ is $\frac{\pi}{2}+\frac{\pi}{n}$:

$$\beta = \theta - \left(\frac{\pi}{2}+\frac{\pi}{n}\right). \tag{4.11}$$

Note that the structure of a TP where the top and bottom n-gons are replaced by rigid parts is not a "pure tensegrity" anymore. However, due to the restricted motion which is a FOIM, the TP still demonstrates the desired characteristics including stability, being a free-standing structure, and, more importantly, as will be discussed in section 4.6, a fully controllable variable stiffness.

4.4.1 STIFFNESS OF A TRANSLATIONAL TPS

Under a pure axial force along the twist axis (Figure 4-6), the platform moves down to a new equilibrium configuration, and the cable forces change from τ_p to τ. The TPS under this axial force acts as a translational spring. At this new equilibrium, the translational stiffness of the TPS (K_T) is found from

$$K_T = \frac{dF_z}{dh}, \tag{4.12}$$

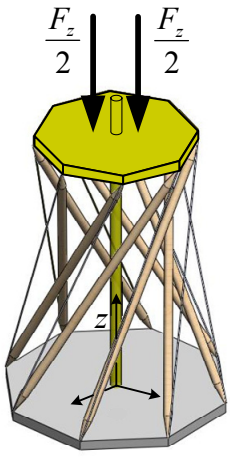

Figure 4-6. Translational TPS

where dF_z and dh are the change in the force applied along the twist axis (z) and the corresponding displacement, respectively. The linear relation between the displacement (dh) and the differential of the cable length (dL) can be determined by projecting the Jacobian matrix of the TP onto the FOIM (J_T):

$$dL = J_T\, dh. \tag{4.13}$$

J_T is a scalar value and can be also found directly as a function of β by using Equations ((**4.6**),(**4.7**),(4.11) ,(**4.13**)) :

$$J_T = \frac{-2h \sin\beta \sin\left(\frac{\pi}{n}\right)}{L \cos\left(\beta + \frac{\pi}{n}\right)}. \tag{4.14}$$

At the tensegrity state where β is zero, J_T becomes zero, confirming the presence of a FOIM. Recall that the platforms and bars are assumed rigid and that by neglecting the friction and gravity forces, the external force (F_z) and the tensions of the n cables are the only working forces. Therefore, the virtual work of the system is

$$\delta W = F_z \delta h - n\tau \delta L\,, \tag{4.15}$$

where δh and δL are virtual displacements, and τ is the tension of each cable. The tension of the cables depends on the stiffness of the material of the cable (k_c), the current length of the cable L, and the natural length of the cable L_N:

$$\tau = k_c(L - L_N)\,. \tag{4.16}$$

Since the system is studied under static equilibrium, the virtual work vanishes, and Eq.(4.15) yields

$$F_z dh = n\tau dL\,. \tag{4.17}$$

Substituting (4.13) into (4.17) and considering that the result holds true for any arbitrary dh , Eq.(4.17) yields

$$F_z = nJ_T\tau\,. \tag{4.18}$$

Note that at the tensegrity state ($\beta = 0$) J_T becomes zero, and Eq.(4.18) verifies that the tensegrity is prestressable; i.e., that nonzero τ corresponds to zero F_z.

Using Eq.(4.14) in (4.18) gives a relation between the external force (F_z) and cable tensions (τ) as a function of β:

$$F_z = \frac{-2nh \sin\beta \sin\left(\frac{\pi}{n}\right)}{L \cos\left(\beta + \frac{\pi}{n}\right)}\,\tau\,. \tag{4.19}$$

The translational stiffness (K_T) is then found from Eqs.(4.12) and (4.18) :

$$K_T = \frac{dF_z}{dh} = \frac{d(nJ_T\tau)}{dh} = n\frac{dJ_T}{dh}\tau + nJ_T\frac{d\tau}{dh}\,. \tag{4.20}$$

In the general case when the external force (F_z) is applied on the top platform, it moves to a new equilibrium configuration, and the Jacobian of the system is not zero any more. In this case, the cable tension can be considered as an original prestress at the tensegrity state τ_p plus a change from the prestress caused by the deformation due to the external loading τ_l:

$$\tau = \tau_p + \tau_l \,. \tag{4.21}$$

Also, using the chain rule in Eq.(4.20) $\left(\frac{d\tau}{dh} = \frac{d\tau}{dL}\,\frac{dL}{dh}\right)$ and remembering that $\frac{d\tau}{dL}$ is the elastic stiffness of the cables (k_c), and $\frac{dL}{dh}$ is the Jacobian J_T, Eq.(4.20) yields

$$K_T = n\frac{dJ_T}{dh}\tau_p + n\frac{dJ_T}{dh}\tau_l + nk_c{J_T}^2 = K_{T_{\tau_p}} + K_{T_{\tau_l}} + K_{T_e} \,. \tag{4.22}$$

Eq.(4.22) shows that the translational stiffness of TPS (K_T) has three components:

1. $K_{T_{\tau_p}}$, termed the "translational prestress stiffness/translational antagonistic stiffness," which is a function of the prestress of the cable (τ_p) and the change of the geometry, represented by ($n\frac{dJ_T}{dh}$).
2. $K_{T_{\tau_l}}$, termed the "translational load stiffness," which is a function of the part of the tension (τ_l) caused by the external load and the change of the geometry, represented by ($n\frac{dJ_T}{dh}$).
3. K_{T_e}, termed the "translational elastic stiffness," which is a function of the elasticity of the cables (k_c) and the geometry represented by the Jacobian (J_T).

$K_{T_{\tau_p}}$, $K_{T_{\tau_l}}$ and K_{T_e} can be expressed in terms of β by using Eq.(4.14):

$$K_{T_{\tau_p}} = n\frac{2\sin\left(\frac{\pi}{n}\right)h^2}{r_o r_h L\cos\left(\beta+\frac{\pi}{n}\right)}\left\{\frac{-2\,r_o r_h \sin\left(\frac{\pi}{n}\right)\sin^2(\beta)}{L^2\cos\left(\beta+\frac{\pi}{n}\right)} + \frac{\cos(\beta)}{\cos\left(\beta+\frac{\pi}{n}\right)} - \frac{r_o r_h\sin(\beta)}{h^2} + \frac{\sin(\beta)\sin\left(\beta+\frac{\pi}{n}\right)}{\cos^2\left(\beta+\frac{\pi}{n}\right)}\right\}\tau_p \,. \tag{4.23}$$

$K_{T_{\tau_l}}$ is identical to $K_{T_{\tau_p}}$ except that τ_p is replaced by τ_l, and finally:

$$K_{T_e} = n\left\{\frac{2h\sin\beta\sin\left(\frac{\pi}{n}\right)}{L\cos\left(\beta+\frac{\pi}{n}\right)}\right\}^2 k_c \,. \tag{4.24}$$

At the tensegrity state, the only nonzero stiffness is coming from the prestress stiffness $K_{T_{\tau_p}}$ and is called K_{T_p}:

$$K_{T_p} = K_{T_{\tau_p}}\Big|_{\beta=0} = n\frac{2\sin\left(\frac{\pi}{n}\right){h_p}^2}{r_o r_h L_p\cos^2\left(\frac{\pi}{n}\right)}\tau_p \,, \tag{4.25}$$

which depends on the number of cables, the dimensions of the prism, and the prestress in the cables. The prestress in the cable can arbitrarily change and hence be controlled by means of the force actuators such as the smart materials embedded into the cables.

Therefore, the translational variable stiffness is obtained as a result of the force control in the cables.

4.4.2 *STIFFNESS OF A ROTATIONAL TPS*

Under a pure moment about the twist axis, the TP forms a variable rotational TPS (Figure 4-7) and works as a torsion spring. Under this moment, the platform twists to a new equilibrium configuration, and the force of the cables changes from τ_p to τ. At this new equilibrium, the rotational stiffness of the TPS (K_R) is found by

$$K_R = \frac{dM_z}{d\beta}. \tag{4.26}$$

To find the stiffness of a rotational TPS in terms of the known parameters such as the tension of the cables and the geometry parameters, the same approach explained for the translational TP spring is applied: first, the rotational Jacobian (J_R) is defined in Eq.(4.27) and expressed in terms of β in Eq.(4.28) by using Eqs.(4.7) and (4.11). Then, using the principle of virtual work a relation between the moment (M_z) and the rotation (β) is found, and, finally, the components of the total rotational stiffness (K_R) are found in Eq.(4.30). These components are the rotational prestress stiffness ($K_{R_{\tau_p}}$), the rotational load stiffness ($K_{R_{\tau_l}}$), and the elastic stiffness (K_{R_e}) which are presented in Eqs.(4.31)-(4.33). Eq.(4.16), which finds the tension of the cable, is also valid here.

$$dL = J_R\, d\beta \tag{4.27}$$

$$J_R = \frac{2r_o r_h \sin\beta \sin\left(\frac{\pi}{n}\right)}{L} \tag{4.28}$$

$$M_z = nJ_R\tau \tag{4.29}$$

$$K_R = n\frac{dJ_R}{d\beta}\tau_p + n\frac{dJ_R}{d\beta}\tau_l + nk_c{J_R}^2 = K_{R_{\tau_p}} + K_{R_{\tau_l}} + K_{R_e} \tag{4.30}$$

$$K_{R_{\tau_p}} = n\frac{2r_o r_h \sin\left(\frac{\pi}{n}\right)}{L}\left\{\cos(\beta) - \frac{2r_o r_h \sin^2(\beta)\sin\left(\frac{\pi}{n}\right)}{L^2}\right\}\tau_p \tag{4.31}$$

$$K_{R_{\tau_l}} = n\frac{2r_o r_h \sin\left(\frac{\pi}{n}\right)}{L}\left\{\cos(\beta) - \frac{2r_o r_h \sin^2(\beta)\sin\left(\frac{\pi}{n}\right)}{L^2}\right\}\tau_l \tag{4.32}$$

$$K_{R_e} = n\left\{\frac{2r_o r_h \sin\beta \sin\left(\frac{\pi}{n}\right)}{L}\right\}^2 k_c \tag{4.33}$$

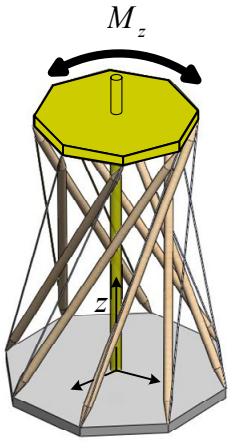

Figure 4-7. Rotational TPS

At the tensegrity state, the rotational Jacobian (J_R), the rotational load stiffness ($K_{R_{\tau_l}}$), and the elastic stiffness (K_{R_e}) vanish and the total stiffness comes from merely the prestress stiffness found from the following equation:

$$K_{R_p} = K_{R_{\tau_p}}\Big|_{\beta=0} = n\frac{2r_o r_h \sin\left(\frac{\pi}{n}\right)}{L_p}\tau_p \,. \tag{4.34}$$

This stiffness depends on the geometry of the TPS and the prestress in the cables. Therefore, with a fixed geometry, this stiffness can change from zero to any desired value limited by the strength of the cable. Therefore, the rotational variable stiffness is created as a result of the force control in the cables.

4.5 CASE STUDY

In order to demonstrate the feasibility of the TPS, the same case study of the engine mount presented in section 3.4 is presented again; however, this time, a TPS is designed and used as the AVS. In addition, the characteristics of the proposed TPS and its dependencies on the design parameters are detailed.

In all vehicles, the engine mounts attach the engine to the chassis and control the bouncing of the engine from low-frequency shock excitations (0-20 Hz) caused by sudden acceleration and braking or riding on bumpy roads. In order to provide this control a stiff mount, that provides low displacement transmissibility, is required. In high frequencies (20-200 Hz), there are vibration excitations caused by the firing pulse and eccentric rotating parts inside the engine. In such frequencies, the engine mounts are supposed to act as vibration isolators [69]. This function can be obtained by a soft mount with low force transmissibility. The challenge is that for an optimum performance the stiffness of the mount should change with the frequency.

A variable spring such as a TPS can address this challenge by providing a variable stiffness by adding a TPS in parallel with a soft mount. The TPS can be actuated by increasing the prestress and can provide additional stiffness when a stiffer mount is desired. The concept of such a system is schematically shown in Figure 4-8.a, and the parameters are

listed in Table 4-3. This variable stiffness mount (VSM) is a square TP in a parallel arrangement with a soft rubber mount. Four piezo actuators are embedded in the four bars that generate the prestress. A bearing between the platform of the TPS and the upper plate of the VSM allows the platform to rotate relative to the upper plate. The stiffness of the soft rubber mount ($0.5x10^5$ N/m) is lower than the stiffness of a regular passive engine mount (PM) ($1.3x10^5$ N/m) designed for a specific engine (Figure 4-8.b). In high frequencies, the cables have no prestress, and, therefore, the stiffness caused by the TPS is zero. In this case, the total stiffness of the VSM is less than half of the total stiffness of the PM (passive engine mount). In the low-frequency range, actuators extend 186 microns to generate 3670 N compression simultaneously in the bars, which corresponds to 2200 N prestress in the cables. This level of prestress generates ($4x10^5$ N/m) prestress stiffness (see Eq.(4.25)), which is three times more than the stiffness of the PM. Consequently, the VSM becomes stiffer as desired in the low-frequency range.

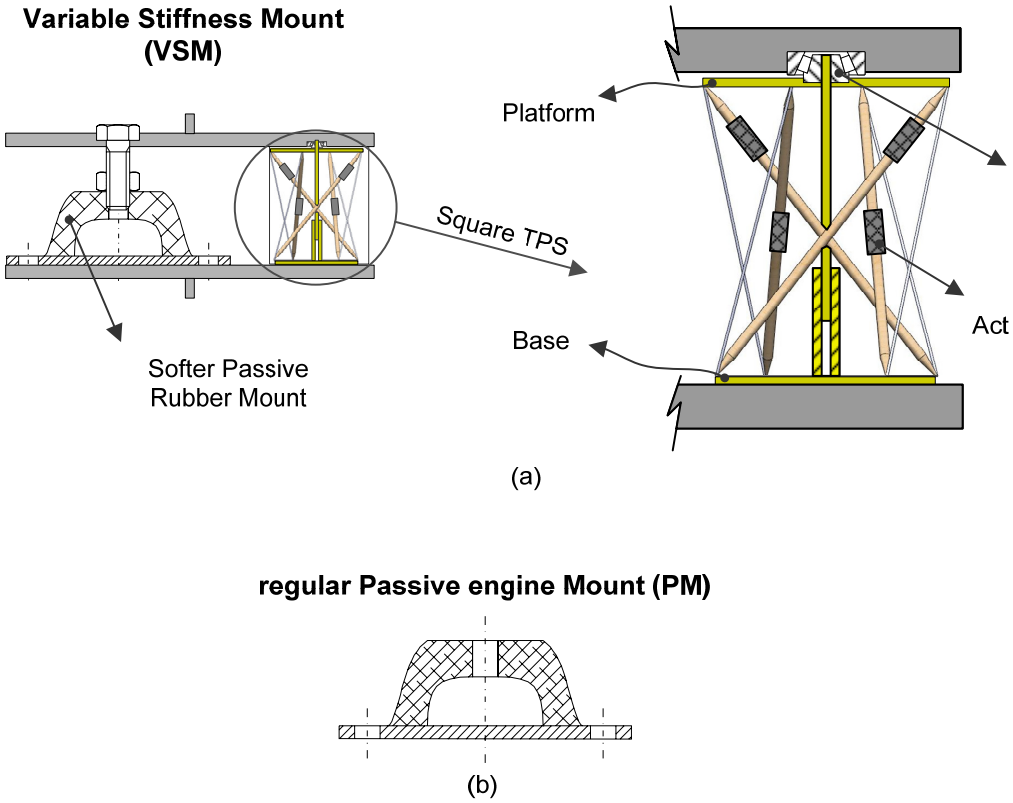

Figure 4-8. a. Variable Stiffness engine Mount(VSM) made with a soft rubber mount and a square TP b. Regular passive engine mount (PM)

Table 4-3. Parameters of the passive engine mount and the proposed variable stiffness TP engine mount

	Specification	Variable	Value	Unit
Engine	Mass	m_e	244	kg
VSM (Variable stiffness TP engine mount)	Number of bars	n	4	-
	Diameter of cables[7]	d	2.38	mm
	Cable breaking strength	τ_{max}	3500	N
	TP height	h_p	50	mm
	Top platform radius	r_h	20	mm
	Base platform radius	r_o	20	mm
	Elastic modulus of cable	E	100	GPa
	Stiffness of softer mount	k_r	0.5x10^5	N/m
	Damping of softer mount	c_r	300	N.s/m
PM (The passive engine mount)	Stiffness of the passive mount	k_R	1.3x10^5	N/m
	Damping of the passive mount	c_R	610	N.s/m

In order to evaluate the performance of the proposed VSM, as explained above, the displacement transmissibility in low frequencies and the force transmissibility in high frequencies of the VSM and a passive mount PM will be compared.

Figure 4-9.a,b shows one-degree-of-freedom vibration models of an engine with three VSMs and three PMs, respectively. Figure 4-10 demonstrates and compares the transmissibilities of three systems: Curve 1 is the transmissibility of the VSM when the prestress is zero so the TPS is not active; Curve 2 is the transmissibility of the VSM while the TPS is always active with 2200 N prestress; and Curve 4 is the transmissibility of the PM. The controlled VSM (Curve 3) begins on Curve 2 and is switched to Curve 1 at the intersection of Curves 1 and 2 (at about 5 Hz) by a control system. As Figure 4-10 reveals, the maximum transmissibility of the controlled VSM has reached to one third of its corresponding PM. This decrease is a large improvement.

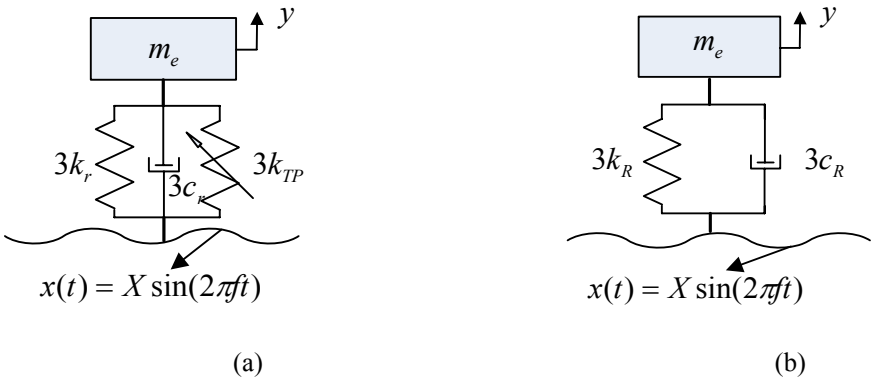

Figure 4-9. a. A one DOF engine vibration model with VSM, b. A one DOF engine vibration model with PM

[7] 77x19 aircraft steel cables, Nominal Diameter 2.38 mm, Min. Breaking Strength 3500 N

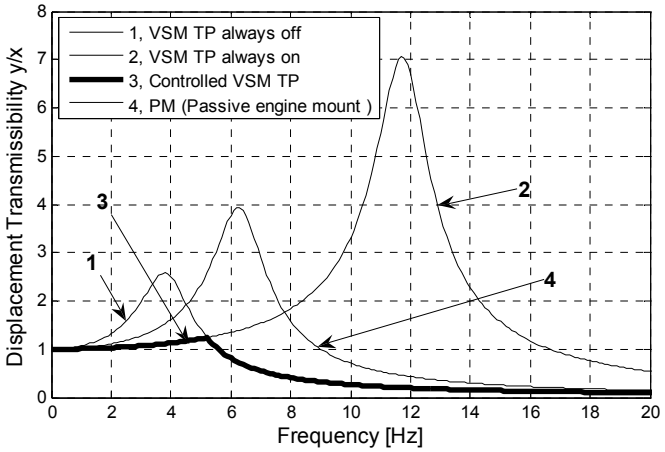

Figure 4-10. Displacement Transmissibility

At the higher frequencies, as explained above, the goal is to minimize the force transmissibility from the engine to the body (chassis). This transmissibility is plotted in Figure 4-11 for the PM and the desired VSM as identified above. This figure suggests that the desired VSM provides an improved isolation at high-frequency ranges. For example, around the idle speed of the engine (600 rpm/20 Hz) 60% lower transmissibility is obtained compared to that of the PM. In terms of vibration isolation, the VSM provides 94 % isolation and the PM provides 86 % isolation. This difference means that the VSM improves the isolation by 10% at idle speed. This is mainly due to the lower stiffness and lower damping of the VSM at this frequency range.

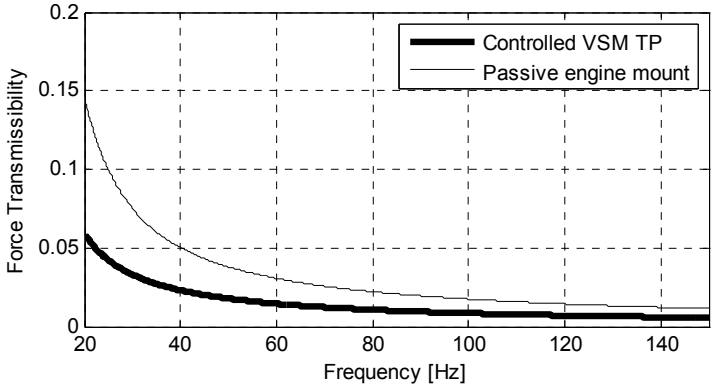

Figure 4-11. Force Transmissibility

As explained above, the variable stiffness characteristics of a TP spring provide a more desirable performance when a VSM is utilized as an engine mount. However, the proposed design is based on the assumption that the stiffness of the TPS is sufficiently linear.

Figure 4-12 and Figure 4-13 show the force-displacement and stiffness graphs of the square TPS used in the VSM for the deflection range of engine mounts. While the average displacement range of the engine mounts is 0.3 millimeters ($\pm$ 0.15 mm) [71], to provide a better insight into the variations of the stiffness, a wider range of 2 mm ($\pm$ 1 mm) of displacement was considered. Figure 4-12 and Figure 4-13 show the force-displacement and stiffness of the square TPS at static equilibrium with a cable prestress of 2200N. Note that the positive displacement and force are along the *z* axis and upward. The stiffness is the

slope of the force-displacement curve in Figure 4-12. The stiffness change for the working range of an engine mount (± 0.15 mm) is less than 1%. This change can be ignored and the spring can be conceived as a linear spring. The stiffness change increases almost quadratically with displacement as shown in Figure 4-13, so for large the displacement, applications, significant changes in the stiffness should be considered. For instance, when the displacement range reaches 2mm, the stiffness change is 20%.

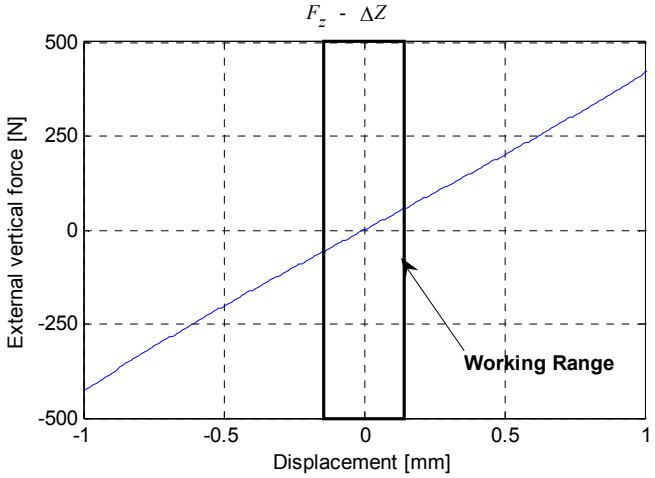

Figure 4-12. Force-Displacement relation of the square TP spring (Prestress 2200 N)

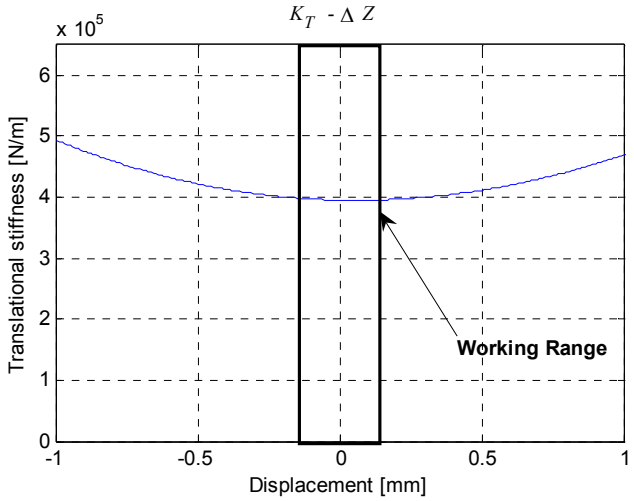

Figure 4-13. Stiffness change with displacement of the square TP spring (Prestress 2200 N)

4.6 DISCUSSION OF THE DESIRED CHARACTERISTICS OF A VARIABLE TPS

Based on the previous case study on the engine mount, the following characteristics are desirable in any variable stiffness for their effectiveness in practical applications:

1. Fast response.
2. High stiffness controllability.
3. Linearity.
4. Sufficient stiffness magnitude.

In the followings sections, these properties are discussed and evaluated for the proposed TPS.

4.6.1 FAST RESPONSE

As Eq.(4.22) shows, the stiffness of a TPS can be varied by changing the prestress (τ_p). Changing the prestress does not change the geometry of the TPS as long as it is in the tensegrity state, because the new prestress still belongs to the null space of the same equilibrium matrix and therefore does not disturb the equilibrium (i.e., the tensegrity state is maintained). As a result, the stiffness control is not associated with any finite displacement. In other words, the displacement of the actuators that control the stiffness is infinitesimal and therefore can be performed very fast. For example, in the case study mentioned in the previous section, the time required for the stiffness change of the square TP, is only for the actuator to develop the desired force. This force can be developed in less than 0.1sec by using a suitable piezo actuator.

In contrast, all other mechanical variable stiffness springs reviewed in Chapter 2 section 2.4, provide variable stiffness based on the geometry change, which is associated with finite displacements of the links and clearly results in a longer response time and higher power consumption.

4.6.2 HIGH STIFFNESS CONTROLLABILITY (R)

The stiffness controllability is defined as the ratio of the controllable (variable) stiffness to the total stiffness. Here, the controllable stiffness is from the prestress. In a translational TPS, for instance, the prestress stiffness is the only controllable part, and therefore the stiffness controllability becomes

$$R = \frac{K_{T_{\tau_p}}}{K_T} = \frac{K_{T_{\tau_p}}}{K_{T_{\tau_p}} + K_{T_{\tau_l}} + K_{T_e}}. \tag{4.35}$$

The magnitude of R varies between zero and one. A ratio of one indicates the best controllability and hence is desired. At the tensegrity state, since the elastic stiffness and the load stiffness are zero, R becomes one. In other words, at the tensegrity state, the stiffness can be changed and controlled from zero to a maximum value determined by the strength of the elements (cables and bars). As a result, TPS has the highest stiffness controllability at the tensegrity state. This result is true for a rotational TPS as well.

4.6.3 LINEARITY

The change of the total stiffness with the displacement is understood as the nonlinearity of the TPS. As was seen in the case study (Figure 4-13), the stiffness of the TPS changes rapidly by a fourth-order polynomial with displacement. Generally, this rapid change occurs because when a TPS deforms under an external load, the elastic stiffness and load stiffness are built up, and, consequently, the total stiffness changes. Therefore, a TPS, in general, is a nonlinear spring. However, the nonlinearity depends on the geometrical parameters such as the height, the platform and base radii. As a result, the nonlinearity can be tailored by using the appropriate geometry according to the corresponding application. For instance, the nonlinearity of the TPS proposed in section 4.5 caused a 1% change in the total stiffness over

its working range (Figure 4-13) and therefore was suitable for the engine mount application.[8]

4.6.4 *SUFFICIENT STIFFNESS MAGNITUDE*

In addition to having complete control over the stiffness (stiffness controllability), it is critical to provide a sufficiently large range of variable stiffness. It was mentioned in section 4.6.2 that theoretically, the range of K_{T_p} is limited by the strength of the cables. Therefore, using stronger cables and bars as well as powerful actuators extends the range of the prestress and, hence, stiffness to any desired value. This result, however, is accompanied by disadvantages such as bigger actuators and higher costs. As an alternative option, changing the geometry of the TPS can be considered as a more affordable method for obtaining the desired range of stiffness. The effects of geometry on the stiffness range of a TPS are determined by Eq.(4.25). In order to study these effects, parameters such as the height and the size of the top and base platforms, the height ratio ($\frac{h_p}{r_o}$), and the platform ratio ($\frac{r_h}{r_o}$) are considered as the main indicators of the geometry. Also, changing the number of the bars (n) and the overall size of the TPS are two other methods that were investigated. The prestress, height and platform ratios can be varied theoretically from zero to infinity, and the number of the bars can be varied from three to infinity. Based on these definitions, the trend of the change in the stiffness range for each parameter while the others were kept constant was observed and is summarized in Table 4-4.

Table 4-4: The effects of different geometrical parameters on the stiffness magnitude of a Translational TPS

	Increase of the prestress $\tau_p \uparrow$	Increase of the height ratio $\frac{h_p}{r_o} \uparrow$	Increase of the platform ratio $\frac{r_h}{r_o} \uparrow$	Increase of the overall Size (scale) $h_p, r_o \,\&\, r_h \uparrow$	Increase of the # of bars $n \uparrow$
Stiffness magnitude of a Translational TP Spring	↑	↑	↓	↓	↓
stiffness magnitude of a Rotational TP Spring	↑	↓	Maximum at $\frac{r_h}{r_o} = \frac{1}{\sin(\frac{\pi}{n})}$ where $h = 0$	↑	↓

It was also seen that the techniques mentioned in Table 4-4 to increase the stiffness magnitude worked against the linearity and caused a more nonlinear stiffness. Therefore, the final design will be a compromise between the magnitude and the linearity, and this table can be used as a guideline for designing a TPS. In the following, the results that can be obtained from the table are discussed. As an example, the TPS introduced in section 4.5 is used by changing the parameters and comparing the effects.

Prestress: Increasing the prestress from zero to the yield strength of the cable increases the stiffness of a TPS. However, since the tension of the cable may increase beyond the prestress due to the external load, the prestress should be set lower than the yield strength. Figure 4-14 compares the stiffness of the TPS of the case study (Table 4-3) with two

[8] . As an estimate, the change in stiffness of one commercial rubber mount designed with tight tolerances on the dynamic stiffness for accurate vibration calculation was measured to be 0.7% in its working range. The stiffness of regular engine mounts is expected to be even more nonlinear.

prestress levels of 2200 N and 1100 N. The stiffness change, as expected, is higher when the prestress is higher. This result may not be easy to see from the figure but changes from .015 N/m to .03 N/m occur when the prestress changes from 1100 N to 2200 N in the given displacement range. This increase in the nonlinearity occurs because the increase in the prestress is obtained by decreasing the natural length of the cables. A shorter cable corresponds to a higher elastic stiffness, which is the root cause for the higher nonlinearity of the TPS.

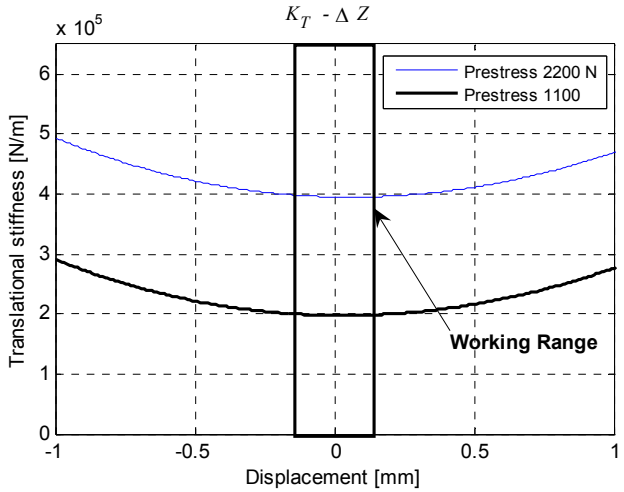

Figure 4-14. Effects of prestress on translational TPS

Height ratio: A taller TPS has higher translational stiffness and lower rotational stiffness. Figure 4-15 compares the example of the case study with a tensegrity twice as tall. The other parameters of the geometry and prestress are the same. Figure 4-15 clearly shows that the magnitude of stiffness increases. This increase however is accompanied by some increase in the nonlinearity which is visible in the figure. This additional increase occurs because in a taller tensegrity, the same translational deflection along the *z* axis corresponds to a larger twisting motion, which generates a larger deviation from the tensegrity state and hence more nonlinearity.

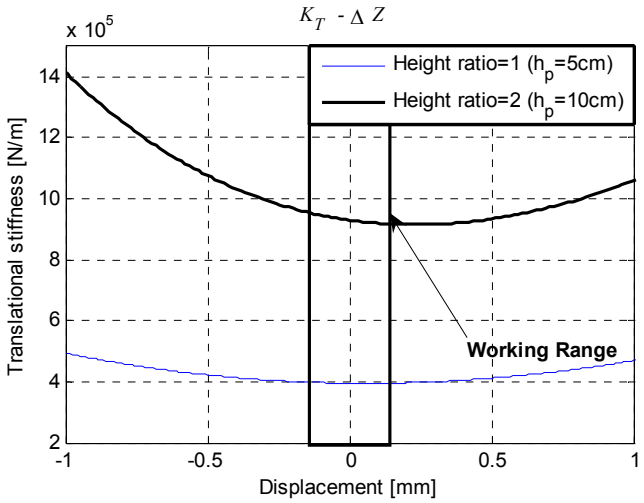

Figure 4-15. Effect of height ratio on translational TPS

Platform ratio: The platform ratio defines the conicity of the TPS. When the platform ratio is zero, the TPS is an upright cone; at a platform ratio of one, the TP becomes a cylinder; and when this ratio is more than one, the geometry of the TPS is a truncated upside-down cone.

By increasing the platform ratio while other geometrical parameters and prestress are constant the length of the cable (L) and the platform radius (r_h) are increased. These changes, according to Eq.(4.23) and Eq.(4.24), decrease all the stiffness components : $K_{T_{\tau_p}}$, $K_{T_{\tau_l}}$ and K_{T_e}. Therefore, the stiffness magnitude of a translational TPS decreases. In contrast, a larger platform ratio, which is accompanied by longer cables, improves the linearity of a translational TPS, as Figure 4-16 reveals.

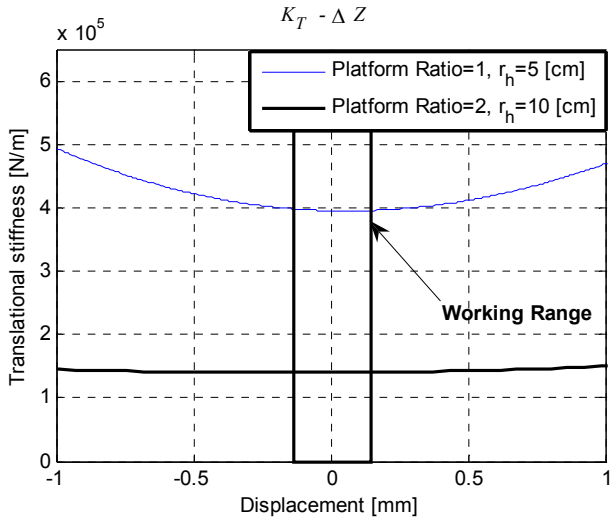

Figure 4-16. Effects of platform ratio on translational TPS

In a rotational TPS, on the other hand, it can be analytically shown every particular height has a platform ratio that maximizes the magnitude of the stiffness. In addition, the overall maximum achievable rotational stiffness is obtained when the height is zero and the platform ratio is $\frac{1}{sin(\frac{\pi}{n})}$.

Overall size of the TPS: Scaling up a TPS while the prestress is kept constant improves the linearity but decreases all the stiffness component in a translational TPS: $K_{T_{\tau_p}}$, $K_{T_{\tau_l}}$ and K_{T_e} expressed by Eq.(4.23) and Eq.(4.24),which , consequently, decreases the magnitude of the translational stiffness. Figure 4-17 compares the TPS of the case study with another one twice as big. In a rotational TPS, this change decreases the linearity but increases the magnitude of the rotational stiffness. The latter result can be seen from Eqs.(4.31)-(**4.33**).

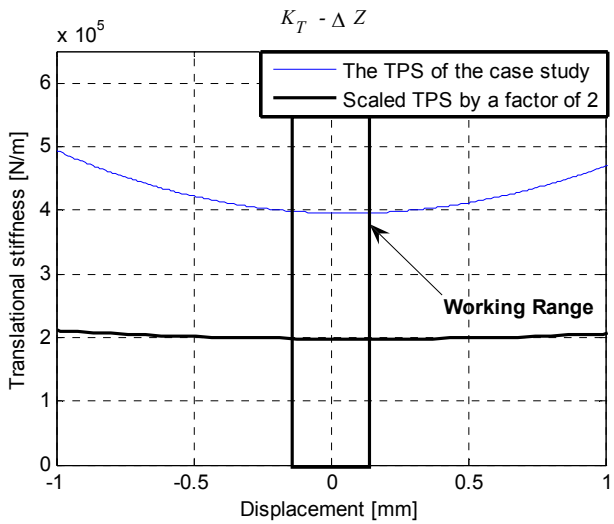

Figure 4-17. Effects of overall size on a translational TPS

Number of the bars: When numbers of bars increases while the prestress, height and sizes of the top and base platforms are kept constant, the relative twist between top and base platforms (θ) of a TPS decreases. As a result, bars and cables will be less inclined respect to the base and top platform and consequently the prestresses of the bars and cables will be less significant in the stiffness of the TPS. Therefore, using n-gons with a higher n without changing the geometry parameters and prestress, decreases the stiffness of the translational and rotational TPS and improves linearity. The numerical examples clearly verified this improvement. In the TPS proposed in the case study, increasing n to 5, as seen in Figure 4-18, results in a drop in the stiffness magnitude but gives a more linear TPS.

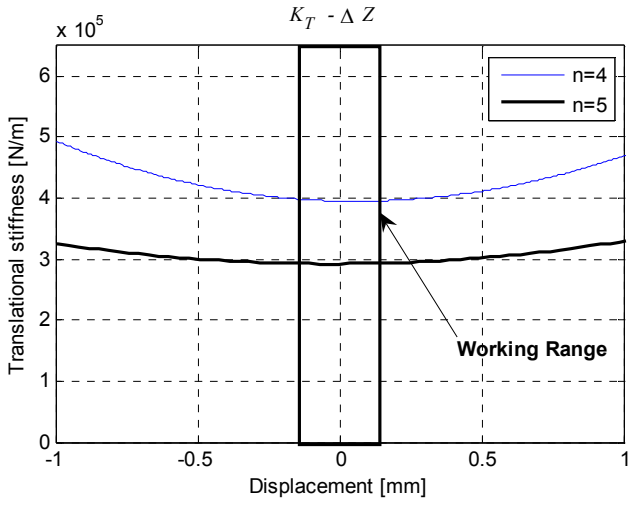

Figure 4-18. Effects of the number of bars on translational TPS

4.7 CONCLUSIONS

It was shown that a subgroup of kinematically and statically indeterminate pin-jointed structures (prestressed and kinematically singular structures) with first-order infinitesimal mechanisms such as tensegrities can be used as variable stiffness springs along their infinitesimal mechanisms. Tensegrity prisms were investigated, and a first-order infinitesimal mechanism was found to be suitable for this purpose. This mechanism was shown to have a twisting motion and hence can be easily constrained and used as a translational or rotational spring. A mathematical model was developed for the stiffness components along this infinitesimal mechanism. It was shown that in the tensegrity state, the stiffness is determined by solely the prestress. Therefore, the stiffness is fully controllable through force control in the members (bar or cables), which can be realized by piezo force actuators. The feasibility of the concept and the characteristics of such a variable spring were demonstrated through a case study of a typical engine mount. A design for the variable stiffness mount was given and compared with the design of a passive mount. A performance comparison based on displacement transmissibility at low frequencies and force transmissibility at high frequencies was presented. This comparison showed that with a simple on-off control at the frequency of 5Hz, the maximum displacement transmissibility at low frequencies dropped by a factor of three. At the idle speed of the engine, 60% lower transmissibility was obtained by using a VSM compared to the PM. This decrease corresponds to a 10% improvement in the vibration isolation. The effects of different geometrical parameters as well as the prestress on the characteristics of such variable stiffness were discussed. It was concluded that the range of stiffness as well as its linearity can be tailored through the geometrical parameters such as the platform ratio, height, and size. Also, it was shown that the linearity and stiffness range usually change in opposite directions, and, hence, an optimization will be necessary according to each particular application.

Chapter 5 PERFORMANCE ANALYSIS OF THE VSM

In previous chapters, the concept of the antagonistic variable stiffness spring (AVS) was presented, and its application in a variable stiffness mount (VSM) was discussed. It was explained why an AVS is a semi-active force-controlled spring and how a VSM performed better than other semi-active vibration mounts in simulation. In order to demonstrate the practicality of the AVS and the VSM and confirm the simulation results, an engine mount is considered as a real industrial application. A VSM was built and configured as an engine mount. In this chapter, the design and the testing process of the VSM are briefly explained, and the experimental results and their analysis are presented.

5.1 DESIGN OF THE VSM

Figure 5-1 shows a schematic illustration of the VSM that was designed and tested. The base (1) is fastened to the vibrating surface and the sprung mass seats on the platform (5) of the VSM. The deadweight is supported by soft rubber mounts (6). The adjustable connecting rod (7) is used to compensate for the static deflection caused by the deadweight in the soft rubber mounts (6) and to make sure the cables (10, 11) are installed normal to the working direction (or that the cables are parallel with the base). The ends of the two cables (10, 11) are fixed on the side plates (2,3). They (10, 11) pass around the cable pins (9) and connect the platform (5) and side plates (2,3). The Piezoelectric actuator (8), which is located between the side plates (2,3), turns the rotating side plate (3) when activated and consequently increases the tension of the cables. The side plate acts also as a lever and leverages the displacement of the actuator by a factor of 3 at the cable connection point. The soft rubber mounts used in the VSM were selected from available industrial rubber mounts. Maintaining the prestress is the main function of the cables (10,11) in a VSM. Doing so can be achieved by using similar elastic material with other forms such as plates. For this reason, the VSM was also tested with thin plates (as shown in Figure 5-2).

A solid model of the designed VSM is shown in Figure 5-3, which has more details than the schematic shown in Figure 5-1. Upper plates (13) prevent the slide of the cables (10,11) or plates (12) on pins (9). The vertical guide system (14) is designed to confine the platform motion along the vertical direction. However, the wide arrangement of the cables (10,11) or plate (12) on the platform (5) and side plates(2,3) guarantees the vertical motion of the platform. As a result, the vertical guide system (14) was not used during the experiments (see Figure 5-4), to avoid possible friction and the rattle-damping effect of the ball bearings in the high-frequency range experiments. The horizontal guide system(15) was devised to

provide equal prestress in cable (10) and cable (11) and, similarly, equal prestress in the plates. The horizontal guide system (15) also provides a mechanism for adjusting the prestress manually, measuring the prestress (16) and adjusting the cable/plate lengths.

The core of this VSM is a set of cables/plates which are prestressed and use a force actuator (a pizeo actuator in our design) to change the stiffness. The force change in the cables/plates is accompanied by small displacements due to the cable elongations. For details on the theoretical background of the design, see 0Chapter 3.

The actual prototype is shown in Figure 5-4. The prototype has an adjustable design to facilitate the testing process. For example, the length and arrangement of the cables as well as the number of the soft rubber mounts can be changed. these features, however, increased the overall size of the VSM (22 x 21 x 14 [cm^3]). If the VSM was to be designed for specific applications, its size could be smaller and in the range of the available hydraulic engine mounts.

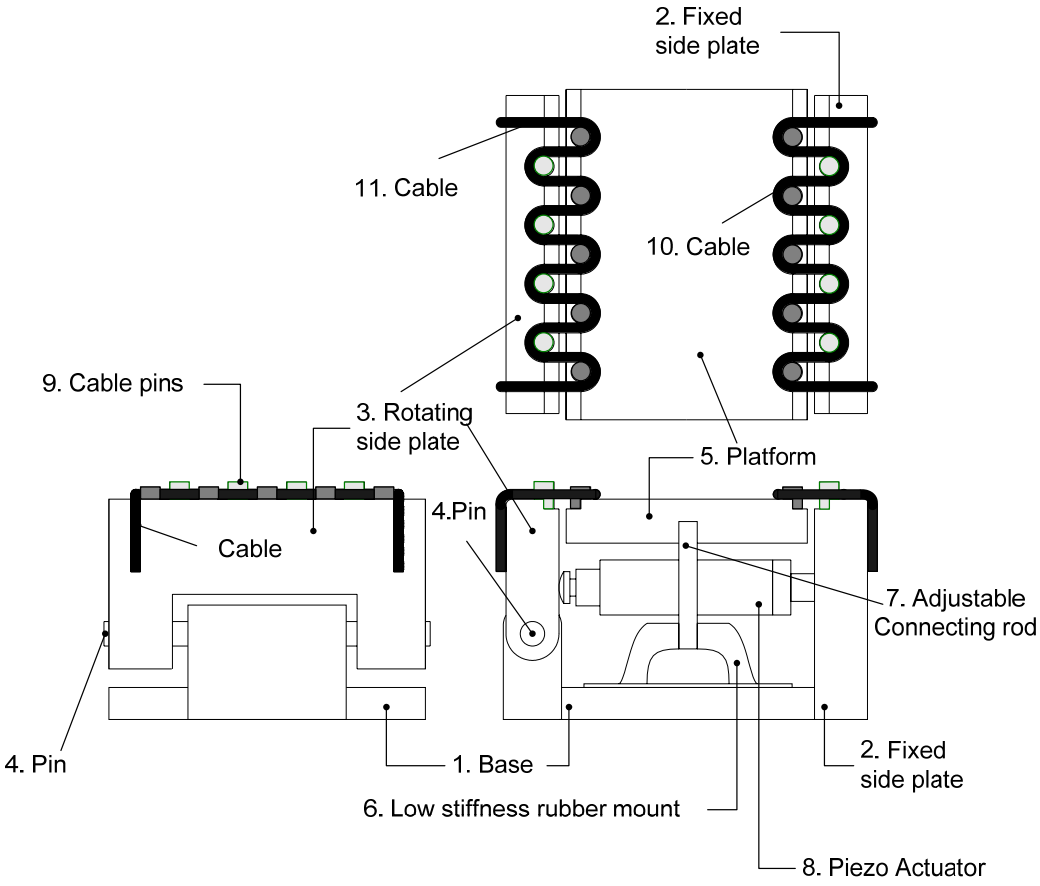

Figure 5-1 Components of the designed and built antagonistic variable stiffness mount (VSM) that uses cable

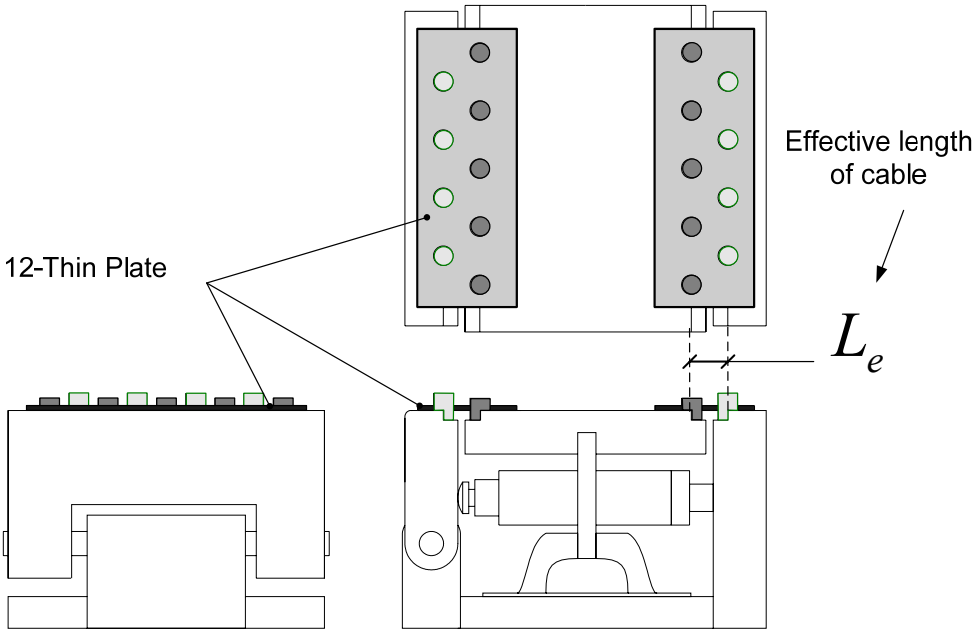

Figure 5-2. VSM that uses Plate

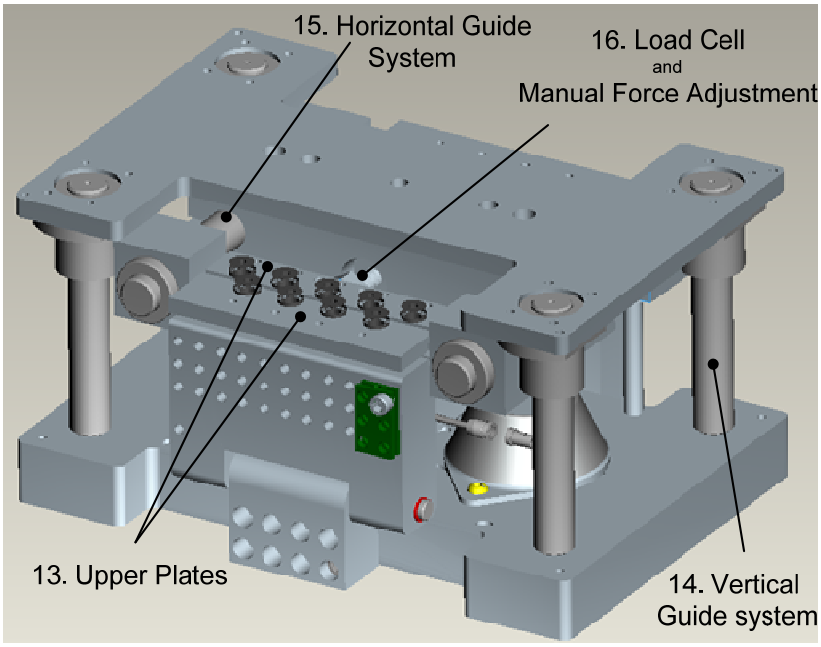

Figure 5-3 .Solid model of the VSM

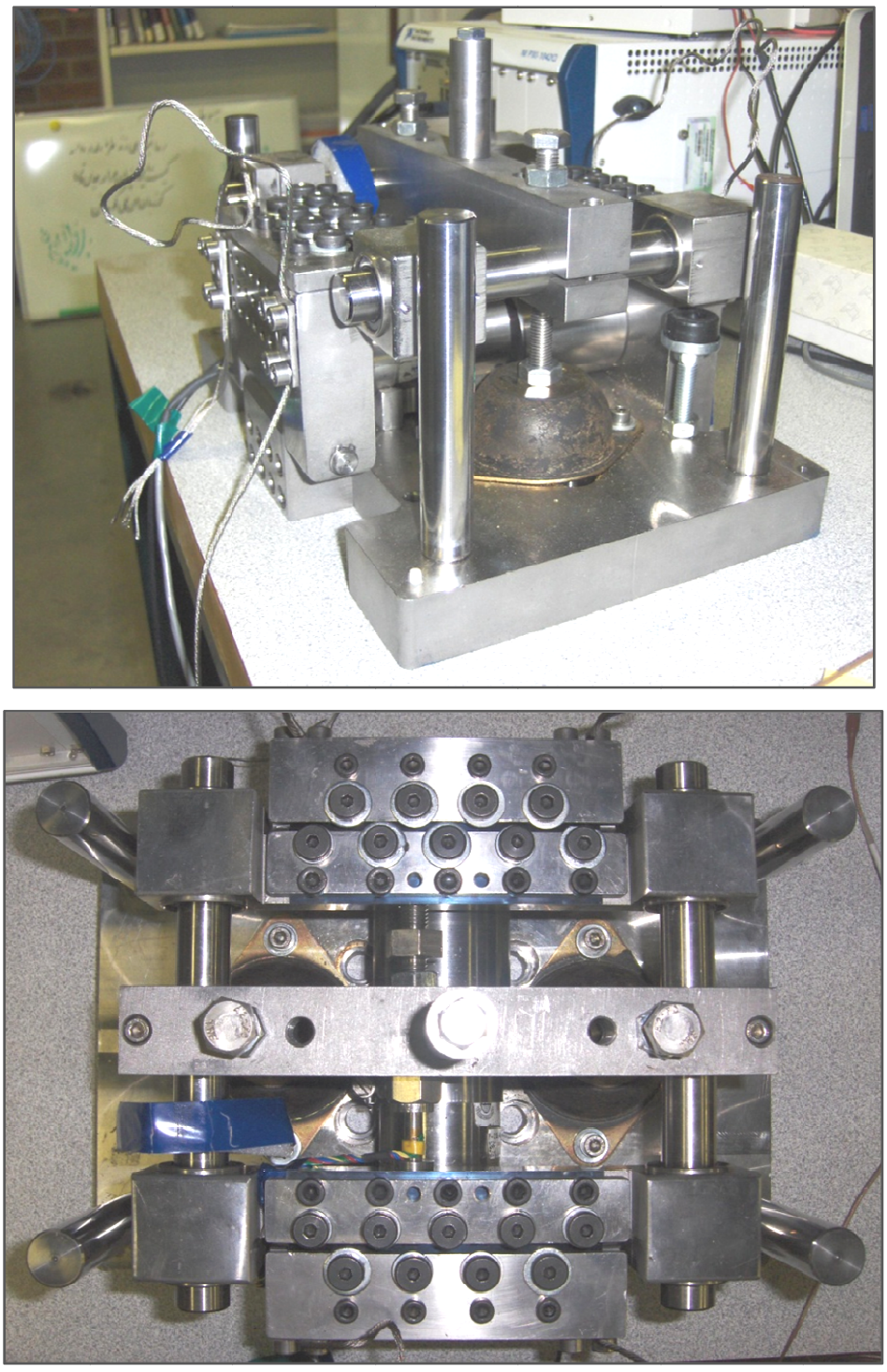

Figure 5-4. The fabricated VSM

5.2 COMPONENTS OF THE VSM

The key components of the fabricated VSM (Figure 5-4) are explained in this section. The characteristics of these components are summarized in Table 5-1 and then more details are provided on each one.

Table 5-1. Characteristics of key components used in the designed and built VSM

Tag # on Figure 5-1, Figure 5-2	Name	Type	Property
10,11	Cable	7x49 Wire rope - Galvanized steel	Nominal Diameter: 1.98 mm / Min Breaking Strength: 2500 N, Measured Elasticity E=79.8 GPa effective length of the cable ( ): 17 mm
12	Plate	High Carbon Spring Steel, 1095 Blue Tempered	Width: 115 mm, Thickness: 0.15 mm effective length of the plate ( ): 17 mm
8	Piezo Actuator	High voltage and High stroke Piezo actuator (P-235.4 PI Co.)	Maximum Displacement: 60 Maximum compresional force:30 kN Input Voltage (0-1000 V) fed by fast response amplifier (PI E-508.OE)
6	Rubber mounts	Novibra M50-A industrial rubber mounts	Static stiffness: 52 N/mm Dynamic stiffness: 85 N/mm Damping: 120 N.s/m

5.2.1 CABLES

Wire ropes (Figure 5-5.a), also known as aircraft cables, were used as cables. Wire ropes are inexpensive. They are also much more flexible (with low bending stiffness) than a single wire (Figure 5-5.b) with the same strength. In the design of the VSM presented in section 3.4 (summarized in Table 3-1), the effective length of the cables (20 mm) is relatively short compared to their diameter (2 mm). As a result, using a single wire that is 2 mm in diameter and has a large bending stiffness creates additional and considerable stiffness along the working direction. Using wire ropes with large numbers of strands decreases this undesired stiffness significantly, compared to the prestress and elastic stiffness. The cable used in the VSM was a 7x49 wire rope made of 343 wires grouped in 49 strands. The specifications of this cable are presented in Table 5-2.

As Table 5-2 shows, the outer diameter of a wire rope (here 2.4 mm) is slightly larger than the diameter of a single wire with the same strength (nominal diameter, here 1.98 mm).

Figure 5-5. a. Wire rope b. Cross section of a 7x49 wire rope

Table 5-2. Cable specification

Outer Diameter	Nominal Diameter		Construction Figure 5-5	Min Breaking Strength	Material
mm	in	mm		N	
2.4	5/64	1.98	7x49 (343 wires)	2500	Galvanized steel

The modulus of elasticity of a wire rope varies from between 60 - 180 GPa depending on its construction and manufacturing process. For example, wire ropes with a lower number of wires and also wire ropes that have been prestressed during manufacturing have higher elasticity [95]. It is interesting to note that the elasticity of wire ropes can be as low as one-

third of the elasticity of steel. This property is a significant advantage for wire ropes when used in a VSM. The low elasticity of the cable desirably provides higher linearity in a VSM. New and unused wire ropes demonstrate even lower elasticity during the first load cycles of their useful life. The elasticity of the cable used in the VSM (Table 5-2) was found to be 79.8 GPa. This was found from the load-Strain/Displacement diagram of the cable pulled under an axial load shown in Figure 5-6. This diagram was found by pulling the cable from 0 to 1 kN. In order to find the hysteretic characteristics of the cable in its working range, the force was periodically decreased to 0.4 kN and increased to 1 kN. One of the hysteretic cycles is shown in Figure 5-7. This hysteretic effect is caused by the friction force between the wires. The area under the hysteretic graph indicates the energy dissipation in each cycle. It will be seen in section 5.4.3 that this hysteresis affects the stiffness of the VSM when the base platform's relative displacement is small. Figure 5-6 also shows the stiffening of new and unused wire ropes. As the displacement and strain kept increasing, the rate of this increasing reduced and stopped in less than 100 cycles.

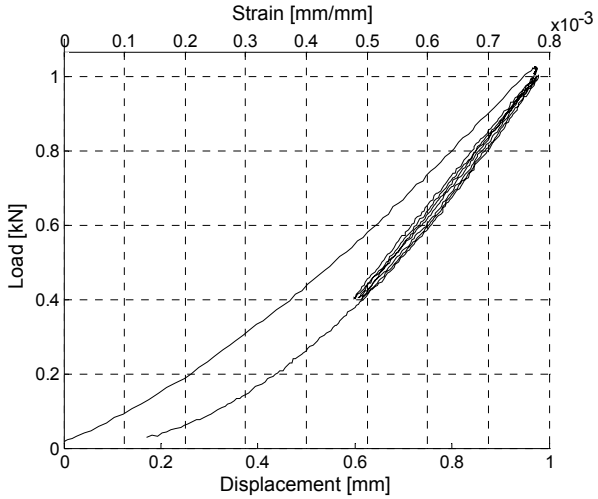

Figure 5-6. Load – Strain and Load-displacement of the cable (Table 5-2) used in VSM

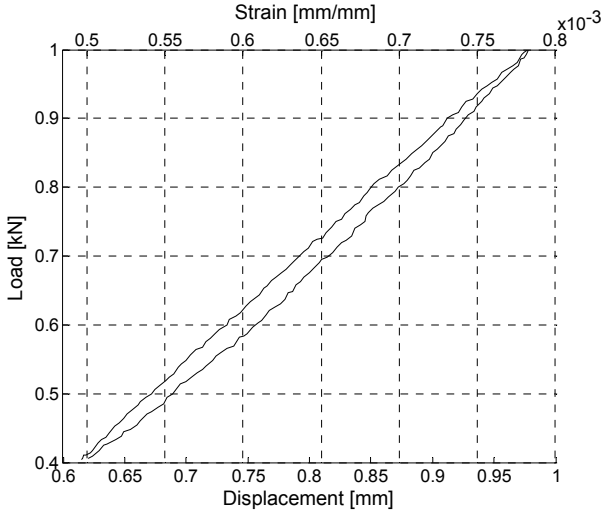

Figure 5-7. Hysteretic effect caused by the internal friction of the wires

5.2.2 PLATES

One technique to avoid the extra stiffness along the working direction of a VSM is using stranded cables. The use of cables was explained in section 5.2.1. Another technique is using thin plates with the same strength of the single wire. The bending stiffness of the thin plate along the working direction of a VSM is insignificant.

The specifications of the thin plates used in the VSM are presented in Table 5-3.

Table 5-3. Plate specification

Width	Thickness		Material
mm	in	mm	
115	0.006	0.15	High Carbon Spring Steel, 1095 Blue Tempered

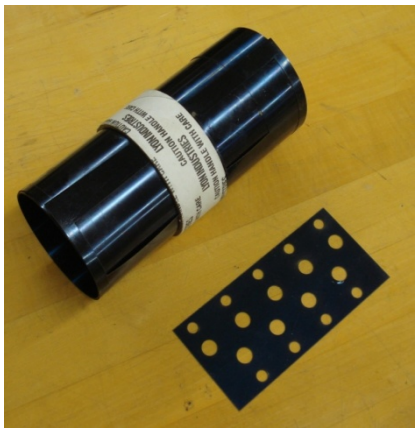

Figure 5-8. Thin plate used in the VSM

5.2.3 *ACTUATOR*

In order to generate prestress in the cables or plate promptly, a high-voltage and high-stroke piezo actuator (8 in Figure 5-1) was used (P-235.4 PI Co.) The implemented piezo actuator can apply up to 30 kN compression and in an unloaded condition has 60 μm stroke. By applying a 0-1000 V input to the piezo actuator, its head is extended roughly proportional to the applied voltage and pushes the rotating side plate (3 in Figure 5-1) and pulls the cables. The side plate acts as a lever and leverages the displacement of the actuator by a factor of 3 at the cable connection point.

Although piezo actuators look like the regular actuators common in mechanical engineering applications (e.g., hydraulic or pneumatic actuators), they work differently. Hydraulic or pneumatic actuators, within their nominal stroke, can exert a nominal force. The maximum force capacity of piezo actuators, on the other hand. is always coupled with the displacement. For example, the piezo actuator used in this prototype (P-235.4), at 1000 V when restrained between infinitely rigid walls (zero displacement), can exert 30 kN. However, in order to get more displacement, the maximum force of the actuator must be decreased. For example, in order to achieve the maximum displacement (60 μm) at 1000 V, the selected actuator should be unloaded.

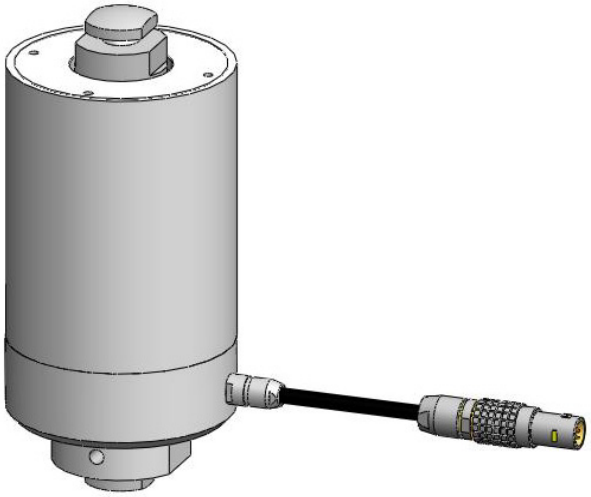

Figure 5-9. Piezo Actuator (Courtesy Physik Instrumente (PI) GmbH & Co.)

The relation between the displacement and the maximum generated force at a certain actuation voltage is linear. Curves 1 and 2 in Figure 5-10 present the relation between the displacement and the generated force of the selected actuator at 1000 V and 500 V, respectively. The dotted line (Curve 3) is the stiffness of the external object pushed by the actuator. The intersection of these curves gives the maximum load that the actuator can apply and the corresponding displacement. For example, the selected actuator, pushing an object with 250x10^6 N/m at 1000 V, applies 10 kN force and moves its contact point with the object by 40 μm.

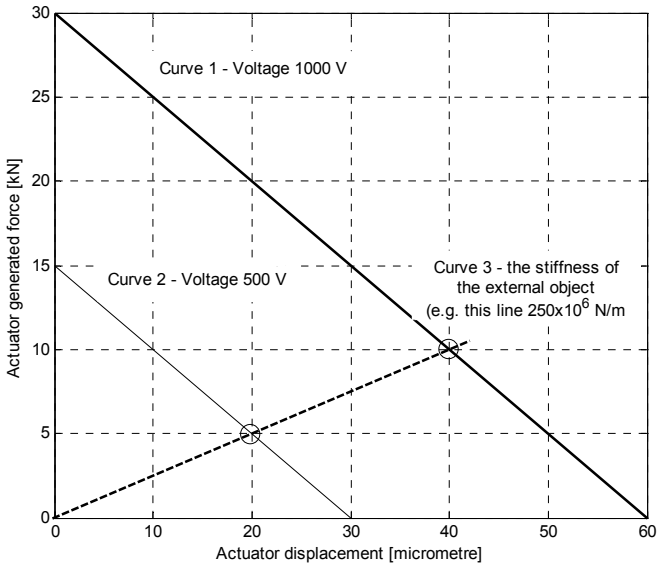

Figure 5-10. Force-displacement characteristics of the piezo actuator

By considering the above-mentioned characteristics of the piezo actuators and the elasticity of the side plate, the rotating plate, and the cables, an actuator (P-235.4, Figure 5-9), was selected with a safety factor of 2.

5.2.4 *AMPLIFIER*

In order to activate the piezo actuator reliably and quickly, a high-voltage (0-1000 V) amplifier (PI E-508.OE) was used. This amplifier is a high-current amplifier, especially designed for switching applications and can output a peak current of 400 mA for 5 ms. The amplifier was controlled directly by an analog signal made by the control system. Figure 5-11 shows the frequency response of this amplifier when used with the selected actuator P-235.4 with a capacitance of 2400 ηF. As this figure shows, this amplifier can activate the actuator with a 1000 V input signal in about 0.2 s (a frequency of 5 Hz).

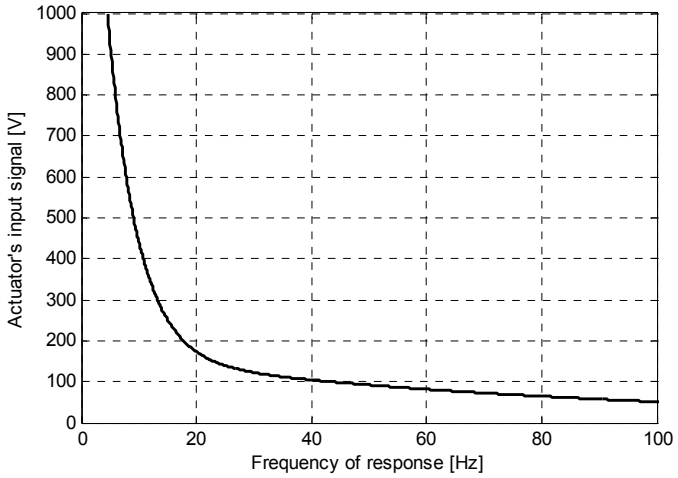

Figure 5-11. Frequency response of the amplifier for the selected actuator

5.2.5 *RUBBER MOUNT*

Soft rubber mounts (6 in Figure 5-1) were used to support the weight of the mass and to provide low damping and stiffness for the VSM. Novibra M50-A, an industrial rubber mount, was used as a soft rubber mount in the VSM (Figure 5-13.a). This rubber mount allows high deflection. It has a compact size and tight tolerances on dynamic stiffness. The static and dynamic stiffness of each rubber mount is 52 N/mm and 85 N/mm, respectively. The damping is 120 N.s/m.

Figure 5-12. Rubber mount

5.3 THE CONFIGURATIONS OF THE VSM AND PASSIVE MOUNT

In order to compare the performance of the VSM with a passive equivalent mount, two configurations, as shown in Figure 5-13, are used. In Figure 5-13a, two rubber mounts are used with the AVS being switched off. This configuration represents a passive mount. As a result, based on the information provided in Table 5-1, the dynamic stiffness (K_r) and

damping (C_r) of this passive mount becomes 1.7x10^5 N/m and 240 N.s/m, respectively. The configuration of the VSM is shown in Figure 5-13.b. Four rubber mounts are used to make the low stiffness (k_r) and low damping (c_r) of the VSM. As a result of the new arrangement of rubber mounts, the stiffness (k_r) and damping (c_r) are half of K_r and C_r in the previous configuration, which simulates the equivalent passive mount. The AVS is switched on at certain times to increase the overall stiffness.

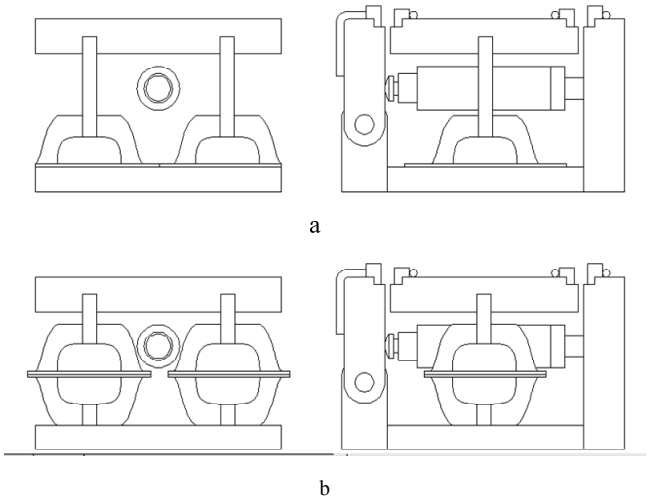

Figure 5-13. Arrangement of the rubber mounts for a. representing the passive mount (without using the AVS) b. VSM

5.4 MODELING AND PARAMETER IDENTIFICATION

Two mathematical models are developed for the proposed VSM: one for the VSM that uses cables (VSM-C) and another one for the VSM that uses plates (VSM-P). These models will be used to predict the performance of the VSM and are necessary for control and/or design improvements.[9] The models of the VSM-C and VSM-P are developed based on their static and dynamic characteristics found from experiments.

A dynamic testing machine (Figure 5-14) was used for static and dynamic stiffness measurement of the the VSM-C and VSM-P. This servo-hydraulic machine could reliably produce quasi-static displacements and required sinusoidal signals in frequencies lower than 15 Hz at the base. The platform was connected to the fixed top griper. The relative displacement between the base and platform, the force at the platform, and the prestress of the VSM-C and VSM-P were collected.

[9] . In the rest of the thesis, the VSM tested with cables is called VSM-C, and the VSM tested with plates is called VSM-P. The term VSM will refer to both of them.

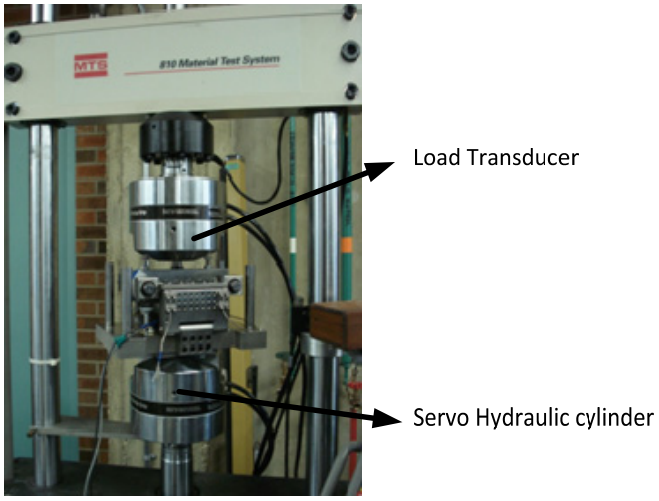

Figure 5-14. Set-up on the Dynamic Testing machine

5.4.1 STATIC STIFFNESS TEST

The common range of displacement for machinery and building vibration is between 0.02 m to 2mm peak to peak, which happens at frequencies between 10 Hz to 100 Hz [63]. Therefore, the maximum working range of the VSM as a vibration mount would be 2 mm peak to peak (or ±1 mm). The maximum working range is shown by two vertical lines in the force–displacement figures (Figure 5-15 and Figure 5-16). The VSM, as an engine mount, however, requires a smaller working range: ±0.3 mm [71]. In the static stiffness test, the VSM-C and VSM-P were displaced ±4 mm and ±1.5 mm, which are more than the maximum working range, to provide a better insight into the stiffness variations when the VSM deflects and settles at new equilibrium positions.

5.4.1.1 Static Stiffness of the VSM with Cable (VSM-C)

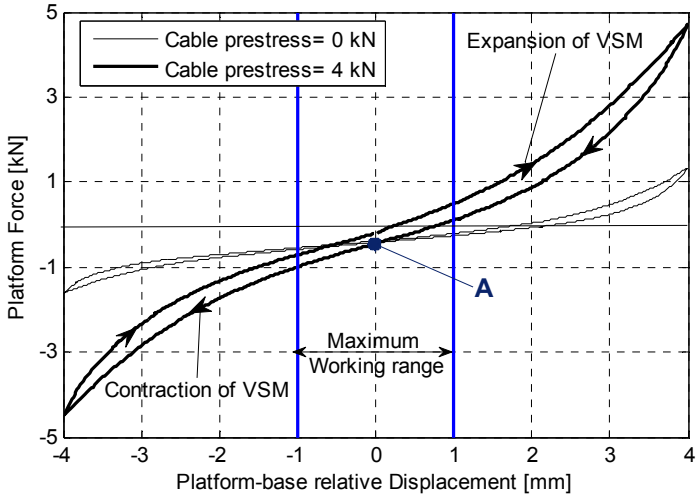

Figure 5-15. Static test of the VSM with cable (VSM-C)

In order to study the static stiffness of the VSM-C, the relation between the applied force to the platform and the resulting relative displacement between the platform and the base were measured (Figure 5-15). Before applying the external load to the platform, a

deadweight of 0.54 kN was applied. This deadweight mimicked the weight of the isolated mass. In this experiment, the deadweight was the portion of the weight of the engine carried by one engine mount. For this reason, the curves begin at point **A**. At this point, the cables become horizontal and normal to the displacement direction as seen in Figure 5-1. Then, the base was displaced ± 4 mm in a quasi-static way while the cable prestress force was set to zero in one test and 4 kN in another one. By introducing the displacement, the cable force started increasing. For example, with 4 kN prestress set at zero displacement, the cable force reached 9 kN when the base displacement was at 4mm.

At a high prestress (4 kN), a hysteretic effect is caused by the friction between the cable strands. When the prestress is zero, the hysteresis is negligible in the working range. In contrast, when the prestress is 4 kN, this effect becomes significant. The hysteretic effect, as will be seen in the dynamic stiffness tests, significantly changes the dynamic stiffness of the VSM. This researcher was not initially aware of this hysteretic effect. The hystersis, as will be shown in section 5.5.1.1, works in favor of the isolation by providing more damping at high prestress and increasing the effective dynamic stiffness.

The static stiffness of the VSM is the slope of the tangent line to the curves in Figure 5-15 at point A. By this definition, the static stiffness of the VSM with zero prestress becomes 160 N/mm, which increases to 510 N/mm with a prestress of 4 kN. In summary, according to the quasi-static test on the VSM (shown in Figure 5-15) the AVS, when activated, increases the stiffness of the VSM by a factor of three.

5.4.1.2 Static Stiffness of the VSM-P

Similar to the quasi-static test on the VSM-C, the VSM-P was quasi-statically tested, and the relation between the force and platform-base relative displacement was found (Figure 5-16). The VSM-P was tested within a smaller range of displacement ($\pm 1.5\, mm$) than the VSM-C. Beyond this range, the plates slipped under the upper plates (Items 13 in Figure 5-3). This range is still more than the maximum working range of the VSM ($\pm 1\, mm$). The slippage happened since the plates had a higher elasticity ($200\, GPa$) than the cables ($78{,}9\, GPa$). In fact with equal displacement in the VSM-C and VSM-P, the force generated in the plates of the VSM-P is higher than the force generated in the cables of the VSM-C. As a result, the plates are pulled out of their grips more easily than cables and this difference eliminates the range of displacement in the VSM-P. To increase the displacement range of the VSM-P, the bolts on the upper plates (Item 13 in Figure 5-3) should be tightened to the side plates (Items 2 and 3 in Figure 5-3) with higher torques. This tightening increases the friction between the plate and the contacting surfaces and prevents the plate from slipping out of its grips.

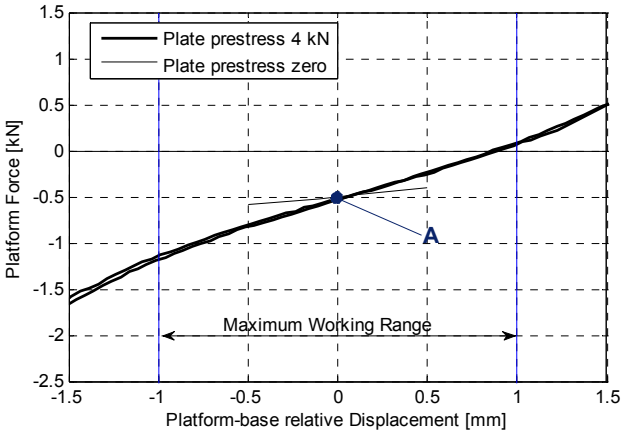

Figure 5-16. Static test of the VSM with Plate (VSM-P)

The hysteretic effect, which was quite significant in the VSM-C, was not seen in the VSM-P as expected. The loading and unloading curves followed the same path in both the contraction and expansion of the VSM-P. The static stiffness of the VSM-P with zero prestress was found to be 170 N/mm and at high prestress (4kN) became 570 N/mm. The static stiffness was quite similar to that of the VSM-C. Similarly, a 3 times increment in the static stiffness happened when the VSM-P was activated with a high prestress (4 kN). Unlike the similarity of the static stiffness between the VSM-C and VSM-P, the dynamic stiffness of these two mounts behaved differently. This result is explained in the following sections.

5.4.2 DYNAMIC STIFFNESS TEST

A dynamic testing machine (Figure 5-14) was used to determine the dynamic stiffness and the phase response of the VSM. First, the base was moved upward in order to resemble a constant deadweight (W_o) of 0.54 kN. At this load, the cables of the VSM are horizontal. Then, the servo-hydraulic cylinder produced a sinusoidal signal ($x = X_o \sin(2\pi f)$) with a constant amplitude (X_o) and constant frequency (f). At the same time, the load produced at the platform was measured. This force was the initial preload, W_o, (0.54 kN) plus an oscillating force, which was the response of the VSM to the base excitation. This oscillating force was determined by the elasticity of the rubber mount, the prestress stiffness of the VSM (when prestress existed), the damping of the rubber mounts, and the friction of the cable strands. The oscillating force was approximated with a sinusoidal wave form ($F_o \sin(2\pi f + \varphi)$) with the same frequency as the displacement (x) but with a phase difference (φ). The dynamic stiffness (k_D) was then found as

$$k_D = \frac{F_o}{X_o}. \qquad 5.1)$$

The dynamic stiffness (k_D) and the phase response (φ) of the VSM were found for a small excitation amplitude ($\pm$ 0.1 mm) and a large excitation amplitude ($\pm$ 1 mm) for a frequency range of 1 Hz to 14 Hz.

5.4.2.1 Dynamic stiffness of VSM-C

The dynamic stiffness of an inactive VSM-C (zero prestress) for the frequency range of 1-14 Hz is shown in Figure 5-17, which shows that the dynamic stiffness at the fixed excitation amplitude does not change with the frequency of the excitation in the given range. However, the dynamic stiffness is sensitive to the excitation amplitude and drops as the amplitude of

excitation increases. This result will be shown to be caused by the nonlinear behavior of the cable. This trend is better seen in the active VSM-C with high prestress in Figure 5-18.

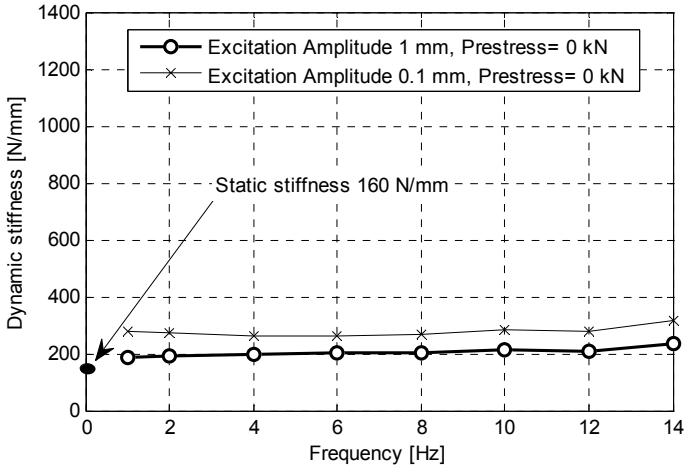

Figure 5-17. Dynamic Stiffness of the inactive VSM-C Prestress equals zero, tested in different excitation frequencies

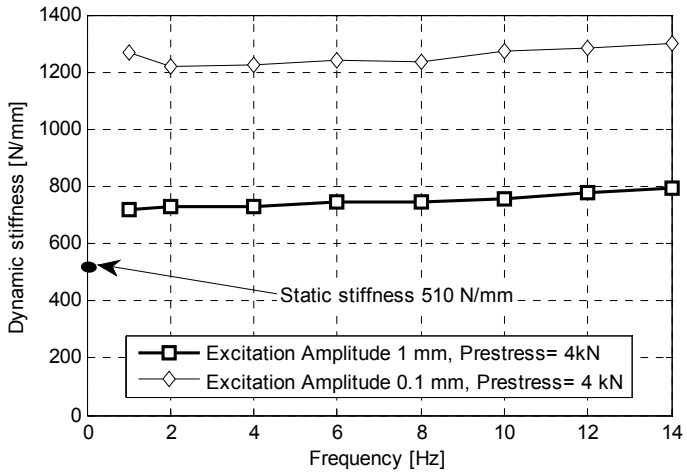

Figure 5-18. Dynamic Stiffness of the active VSM-C , Prestress equals 4 kN, tested in different excitation frequencies

As Figure 5-18 reveals, the dynamic stiffness of an active VSM is almost independent of the frequency. As well, the dynamic stiffness is always larger than its corresponding static stiffness and decreases as the amplitude of the excitation increases. The static stiffness of the active VSM was found in the previous section to be 510 N/mm. The dynamic stiffness, found from Figure 5-18, at a small excitation amplitude ($\pm$ 0.1 mm) is about 750 N/mm and at a large excitation amplitude ($\pm$ 1 mm) is about 1250 N/mm.

The dependency of the dynamic stiffness on the excitation amplitude originates from the internal friction between the cable strands. In order to explain this effect, the quasi-static test of the active VSM presented is presented in the range of the large excitation amplitude ($\pm$ 1 mm) in Figure 5-19. As was explained earlier in this section, the dynamic stiffness was found to be almost independent of the excitation frequency. Therefore, the quasi static test results (Figure 5-15 and Figure 5-19) for the test done at a low-frequency are valid for

higher frequencies, as well. The hysteresis loop for a typical loading cycle is shown by the dashed lines (Figure 5-19). Points B_1 and B_2 (or C_1, C_2) correspond to the maximum/minimum forces and associated displacements in each cycle. Therefore, the dynamic stiffness is determined by the slope of the lines passing through B_1 and B_2 (or C_1, C_2). Note that the slopes of such lines are generally larger than the loading/unloading curves. As a result, the dynamic stiffness of the active VSM with an excitation amplitude of 1 mm is the slope of line B_1B_2, and, consequently, the dynamic stiffness of the active VSM with an excitation amplitude of 0.1 mm is the slope of line C_1C_2 , which is larger than the slope of B_1B_2. This difference graphically explains why the dynamic stiffness increases with a decrease in displacement.

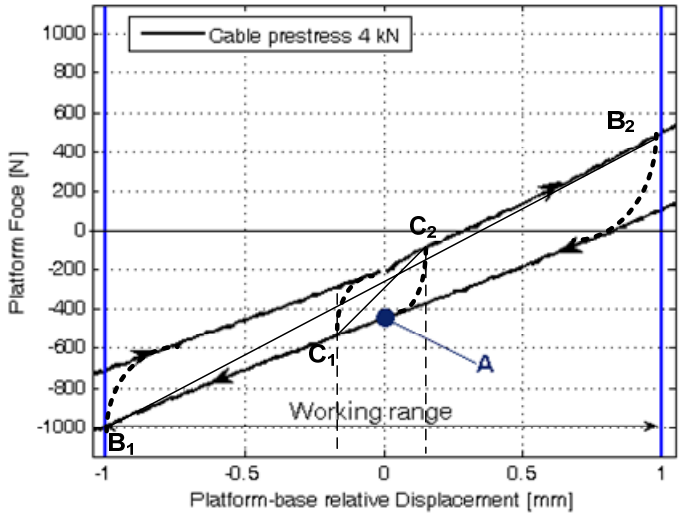

Figure 5-19. How the hysteresis in a VSM-C affects on its dynamic stiffness

Figure 5-17 and Figure 5-18 show that the dynamic stiffness at the fixed excitation amplitude does not change with the frequency of the excitation in the given range. In other words, in this frequency range, the dynamic stiffness is independent of the velocity of excitation. This fact shows that the viscous damping in the dynamic stiffness is negligible. The insignificant effect of the viscous damping on the dynamic stiffness is also shown by the small values of the phase angle (Figure 5-20). The four curves show the phase shift (φ) between the excitation displacement (x) and the approximated sinusoidal force measured at the platform (F) for the inactive and active VSM-C (Figure 5-17 and Figure 5-18). As Figure 5-20 shows, the phase difference is in the range of 0 to 10° for most of the tests. In comparison, in hydromounts in which the viscous damping is the major factor for the dynamic stiffness, the phase shift is about 50° [71].

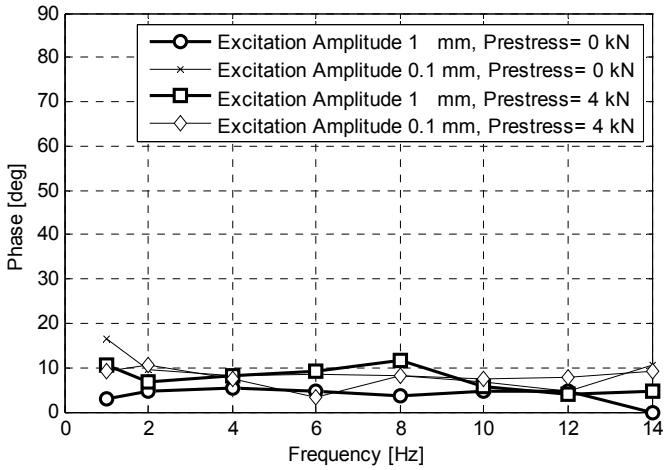

Figure 5-20. Phase response of the inactive and the active VSM-C in different excitation frequencies

5.4.2.2 Dynamic stiffness of VSM-P

Figure 5-21 and Figure 5-22 demonstrate the dynamic stiffness of an inactive and active VSM-P, respectively. The dynamic stiffness of a VSM-P, in contrast to the dynamic stiffness of a VSM-C, is independent from the excitation displacement amplitude. This result was expected since no hystersis was noticed in the static stiffness test (see Figure 5-16), and, as a result, the effect of the wire friction is negligible in a VSM-P. The dynamic stiffness of a VSM-P, similar to that of a VSM-C, is independent from the excitation frequency and slightly larger than its corresponding static stiffness. The dynamic stiffness of the inactive and active VSM-P was found to be 200 N/mm and 600 N/mm, respectively, while they had a static stiffness of 170 N/mm and 570 $/mm$.

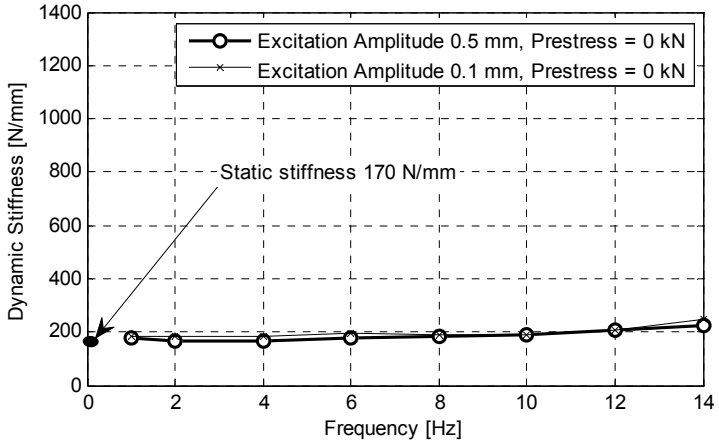

Figure 5-21. Dynamic stiffness of the inactive VSM-P, prestress equals zero, tested in different excitation frequencies

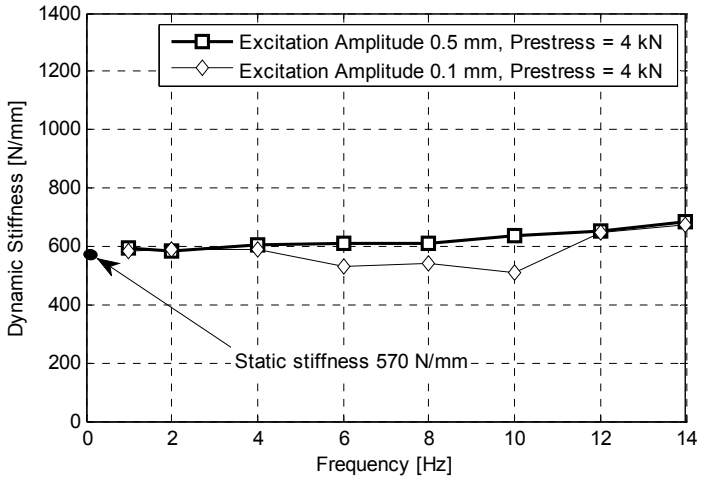

Figure 5-22. Dynamic stiffness of the active VSM-P, prestress equals 4 kN, tested in different excitation frequencies

The excitation displacement and the force measured at the platform had very small phase difference that can be neglected (Figure 5-23). This result indicates that the VSM-P acts as a pure stiffness spring and does not have a viscous damping component.

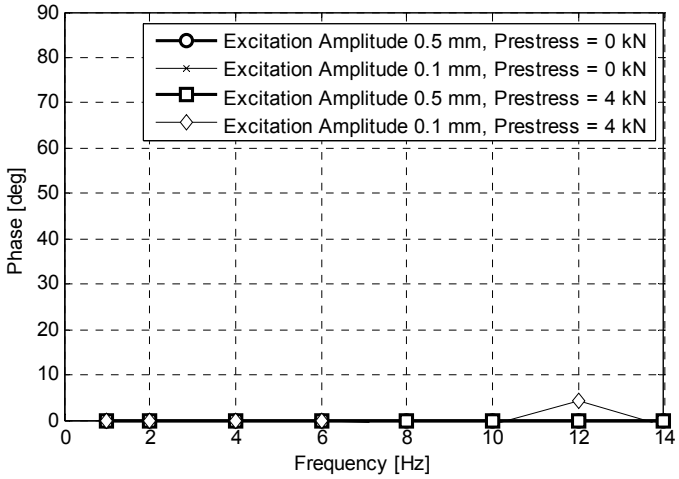

Figure 5-23. Phase response of the inactive and the active VSM-P in different excitation frequencies

5.4.3 Dynamic model of the VSM

The VSM-P was modeled as a linear spring and damper in which the stiffness originates from the stiffness of the soft rubber mount and prestress of the plate. It was attempted to model the VSM-C similarly, as a linear spring and damper in which the stiffness originates from the stiffness of the soft rubber mount and the prestress of the cable. However, it was found that such a model could not accurately predict the performance of the VSM-C, mainly because the friction between the strands of the cable introduced a significant nonlinearity in the high prestress range. In addition, since this friction was not a constant term, it could not be modeled as coulomb damping. Finally, a simple empirical model was developed based on the force-displacement relation of the VSM-C in dynamic stiffness tests.

5.4.3.1 Dynamic model of VSM-C

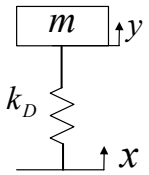

Figure 5-24. Model of the VSM used for predicting the transmissibility of the VSM-C

The dynamic stiffness of the VSM-C was shown to be a function of the relative displacement of the base and platform $(x - y)$. As the test results showed, the friction between the cable strands introduced a hysteresis into the force displacement relation of the VSM that affected the dynamic stiffness (k_D). First, it was tried to model this effect as a simple coulomb friction, which could not predict the performance accurately mainly because the friction was not constant, and nonlinearly depends on the relative displacement of the base and platform of the mount $(x - y)$.

The proposed model (Figure 5-24) of a VSM is a single spring. Its stiffness is found by interpolating the dynamic stiffness test results. Therefore, this experimental model is based on four dynamic stiffness values found in four different relative displacements (Table 5-4). This experimental model was capable of describing the displacement transmissibility of the VSM.

Table 5-4 shows the test results for the dynamic stiffness of the VSM versus the different relative displacements between 0.2 mm to 2 mm. Based on these data, a third-order polynomial Interpolation was used to describe the dynamic stiffness between 0.2 – 2 mm. The dynamic stiffness for displacements lower than 0.2 mm and higher than 2 mm was approximated by extrapolation.

Table 5-4. Dynamic stiffness values of the active VSM-C in different displacements

$x - y$ [mm]	k_D [N/mm]
0.2	1400
0.5	1038
1	862
2	823

5.4.3.2 Dynamic model of VSM-P

In section 3.4, nonlinear equations of motions were used to find the displacement transmissibility at each frequency. However, the test results of the VSM-P showed that a linear model of the model discussed in section 2.7, represented again in Figure 5-12, can predict the harmonic test results of the VSM-P very accurately mainly because enough stiffness linearity was included in the design of the VSM, and the elasticity of the cable did not affect the stiffness noticeably. In addition, the friction effects that provide nonlinear characteristics in the VSM-C do not exist here. In this linear model, the total damping of the VSM-P (c_r) originates from the soft rubber mount. The total stiffness of the VSM-P is the summation of the stiffness of the soft rubber mount (k_r) and the prestress stiffness (k_p). c_r and k_r are found by knowing the configuration of the VSM-P (Figure 5-13.b) and the stiffness and damping of each rubber mount (Table 5-1). k_p is equal to $2\tau_p/L_e$, in which τ_p is the total prestress in the plate, and L_e is the effective length of the plate. In the experiments in which

the VSM-P was inactive, τ_p was zero, and when the VSM-P was active, τ_p was 4 kN. L_e was 17 mm (see Table 5-1).

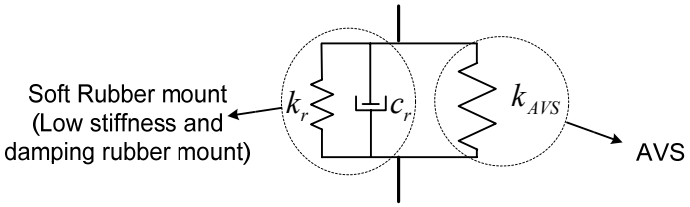

Figure 5-25. Model of the VSM-P used for predicting the transmissibility of the VSM-P

5.5 PERFORMANCE TESTS

The performance of a mount, such as the proposed VSM, is measured according to four expected tasks [94]:

1. Deadweight support.
2. Vibration displacement control: control the bounce of the mass near the resonance.
3. Vibration isolation: isolating the mass from the excitation source.
4. Motion control: limiting the displacement of the mass caused by the shock excitations.

As a semi-active mount, The VSM is expected to react quickly to a change in the operating condition and to adapt the stiffness value to achieve best performance. Therefore, the response time of the VSM, in addition to the four abovementioned criteria, needs to be measured.

The VSM supports the deadweight by using passive mounts, and, hence, it was excluded from the performance tests. The displacement transmissibility test was performed to evaluate the ability of the VSM in vibration-control and vibration isolation (Items 2 and 3). A shock test was designed to determine the VSM's performance for sudden movements of the base (Item 4). The last test was done to demonstrate how quickly the control system of the semi-active VSM can detect an excessive vibration and take the appropriate action. The details of these tests and the results are presented in the following section.

5.5.1 DISPLACEMENT TRANSMISSIBILITY TEST (HARMONIC TEST)

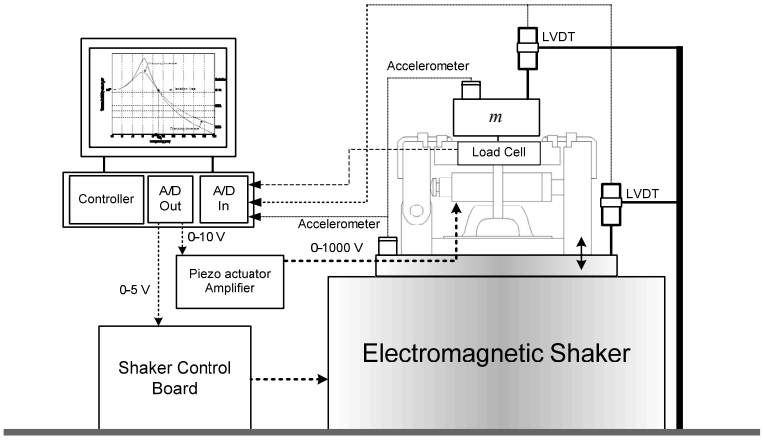

Figure 5-26. Shaker table set-up

An electromagnetic shaker table and the set-up shown in Figure 5-26 were used to determine the displacement transmissibility of the VSM. Its base was excited by a sinusoidal displacement with frequencies from 1.5 Hz to 100 Hz while a mass of 54 Kg was on the platform. The displacement of the platform and base were measured by using two sets of LVDTs and accelerometers. The maximum velocity of the base was kept constant, so that the product of the frequency of the base excitation (f) and its amplitude (X) remained at 2 mmHz. As a result, at low-frequency (2 Hz), the corresponding amplitude of the excitation was 1 mm, whereas at high-frequency (100 Hz), the amplitude was selected to be 0.01 mm.

The VSM-C and VSM-P with the configurations shown in Figure 5-13.a and their equivalent passive mount (Figure 5-13.b) were tested for their displacement transmissibilities. The VSM-C and VSM-P were tested twice: in the inactive mode (with no prestress) and in the active mode (with a prestress of 4 kN). The transmissibility curves of these tests are shown in Figure 5-27 and Figure 5-29.

5.5.1.1 Displacement transmissibility of VSM-C

The transmissibility curves of these tests are shown in Figure 5-27. The transmissibility curve of the passive mount shows the natural frequency to be at 10 Hz. This natural frequency complies with the dynamic stiffness of this configuration shown in Figure 5-17 (200 N/mm for large amplitude). The natural frequency of the inactive mount, found from its corresponding transmissibility curve, is 8 Hz. This frequency (8 Hz) is smaller than the natural frequency of the passive mount (10 Hz). This result was expected as the stiffness (k_r) and viscous (c_r) damping of the inactive mount were half of those of the equivalent passive mount. Lower stiffness and damping is desired for a VSM in the high-frequency range as they offer better isolation. This difference clearly can be seen by comparing the transmissibility curves of the passive mount and the inactive VSM in Figure 5-27.

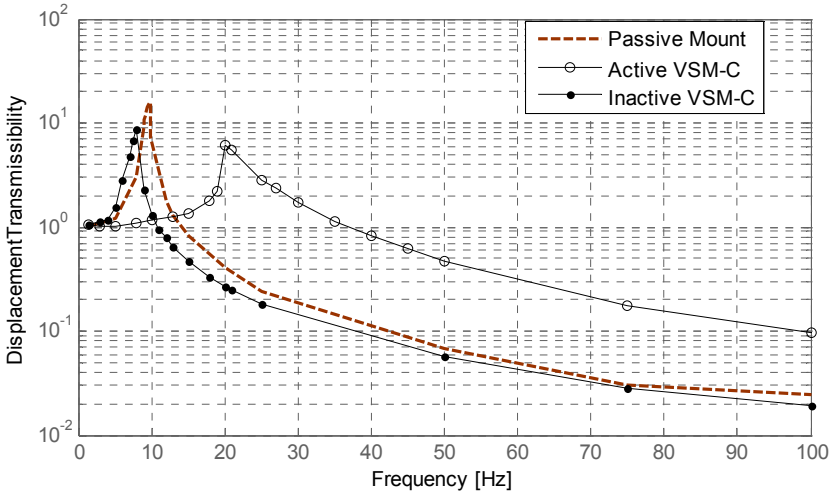

Figure 5-27. Measured displacement transmissibility of the VSM-C in different configurations

Figure 5-27 shows the displacement transmissibility of the active VSM-C. The active VSM-C offers a natural frequency around 20 Hz. It is notable that this transmissibility curve does not look like the regular transmissibility curves found for a mount with linear damping and stiffness. The regular transmissibility curves are more symmetric about the natural frequency. As Figure 5-27 reveals, the transmissibility of an active VSM-C has a sharp

increase near the natural frequency. This effect could be due to the hysteresis of the internal friction in the cables, which is dependent on the displacement and hence grows at large displacements around the natural frequency.

The model shown in Figure 5-24 was numerically simulated, and its transmissibility is compared with the test results and shown in Figure 5-28, which shows that the model predicts the natural frequency and accurately describes the experimental results for the frequencies lower than the natural frequency. The ability of the model (Figure 5-24) to describe the performance at frequencies lower the natural frequency is very useful as the VSM-C needs to be active at only a part of this frequency range, as will be explained in section 5.6. This simple model, however, cannot predict the exact transmissibility at the natural frequency and does not match accurately at the high-frequency with the experimental results, mainly because the model is purposely based on the data for relative displacements between 0.2 - 2 mm. This range is the working range of the model when the VSM-C is active at high prestress. At the resonance frequency, the relative displacements are more than 2 mm and at higher frequencies are lower than 0.2 mm. However, at the resonance and high frequencies, the VSM-C is inactive and the model is not needed.

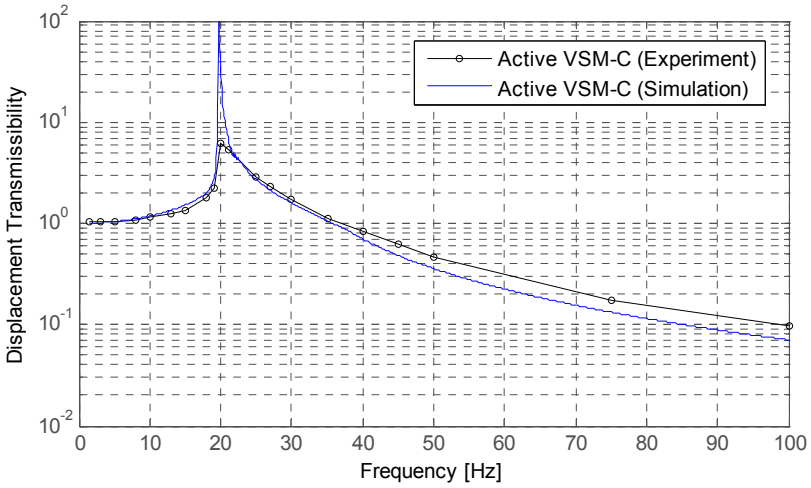

Figure 5-28. Comparison between measured and simulated displacement transmissibility of the VSM-C at high prestress

5.5.1.2 Displacement transmissibility of the VSM-P

The displacement transmissibility of VSM-P in active and inactive modes is shown in Figure 5-29. As was expected, the transmissibility curves of the inactive VSM-P in Figure 5-29 and the inactive VSM-C in Figure 5-27 are almost identical, because in both the VSM-P and VSM-C, when working in the inactive mode, only the rubber mounts are engaged. The transmissibility curve of an active VSM-P in Figure 5-29, however, is quite different from its counterpart (the transmissibility curve of an active VSM-C in Figure 5-28). The active VSM-P has a natural frequency around 18 Hz, which is at least 3 Hz smaller than the natural frequency of the VSM-C. These differences were expected as the VSM-P had lower dynamic stiffness (see section 5.4.2), and the nonlinear effects of the wires' friction, seen previously in the active VSM-C (Figure 5-18), did not exist in the active VSM-P.

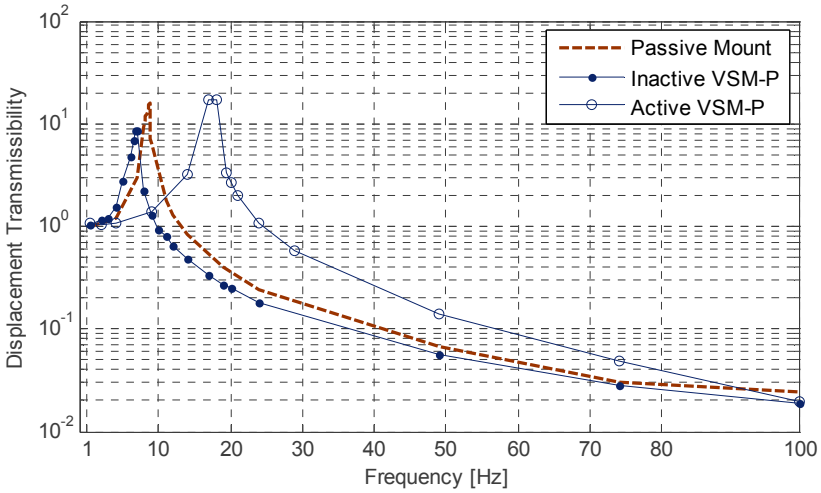

Figure 5-29. Measured displacement transmissibility of VSM-P in different configurations

The previously found dynamic stiffness of the active VSM-P (about 620 N/mm in Figure 5-22) predicted a natural frequency of around 17 Hz if the VSM-P was considered as a linear system. This predicted frequency is very close to the natural frequency found here (18 Hz). In addition, the shape of the transmissibility curve of the active VSM-P shown in Figure 5-29 is similar to the transmissibility curve of a linear mount with constant stiffness and damping. These facts led to the simple linear model for the VSM-P explained before in 5.4.3.2 (Figure 5-25). Figure 5-30 compares the simulation results from this model and the experimental results from the active VSM-P. Clearly, the model accurately predicts the experimental results. The simplicity of the model of an active VSM-P (Figure 5-25) is an advantage over the model of the active VSM-C (Figure 5-24), which needed information from a dynamic stiffness test.

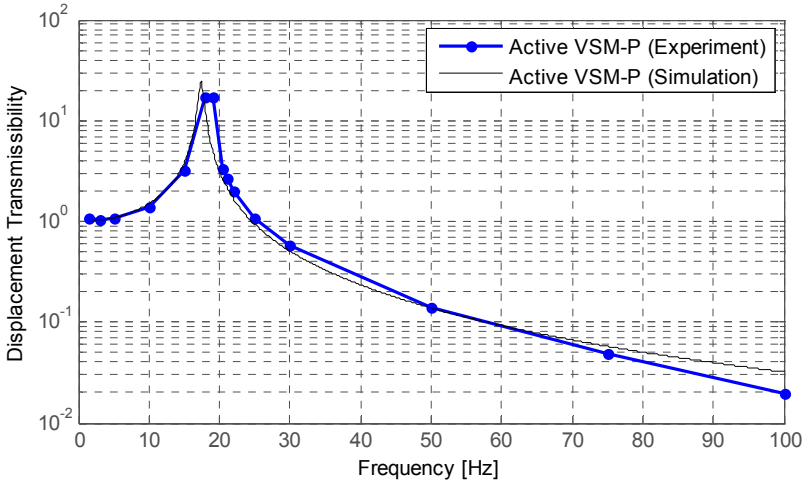

Figure 5-30. Comparison between measured and simulated displacement transmissibility of VSM-P at high prestress level

5.5.2 SHOCK TEST

An electromagnetic shaker table setup was used in order to perform the shock test on the VSM. The experimental results presented here belong to the shock test on the VSM-C. A step

function of 2 V was fed into the shaker table input, and a shock displacement wave as shown in Figure 5-31 was created with a maximum displacement of 3.4 mm. The displacement of the platform was measured by using LVDTs; first when the VSM-C was inactive (with a passive mount) and second, when it was active (with a cable prestress of 4 kN). The displacement of the base and platform displacements of VSM-C for the two tests is shown in Figure 5-31. As was explained in section 5.3, the first test resembles test for the passive engine mount. Therefore, Figure 5-31 compares the performance of the active VSM-C with its equivalent passive mount. As this figure shows, the active VSM-C has a better performance in response to shock, as the smaller maximum relative displacement (less than half) indicates. In Figure 5-32, the relative displacements are plotted for the two above mentioned tests. In this figure, the settling time of the VSM-C is 0.2 sec whereas in the passive mount, this time is about 0.7 s.

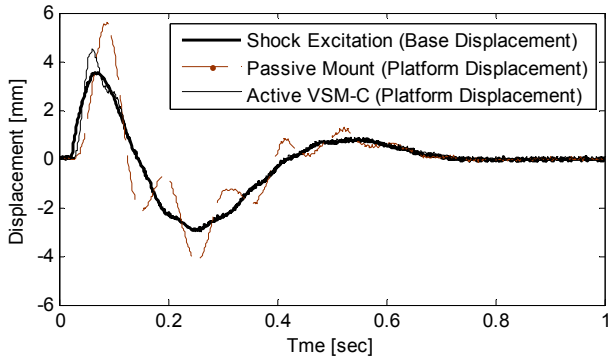

Figure 5-31. Shock excitation at the base of the VSM-C and the resulted platform displacements

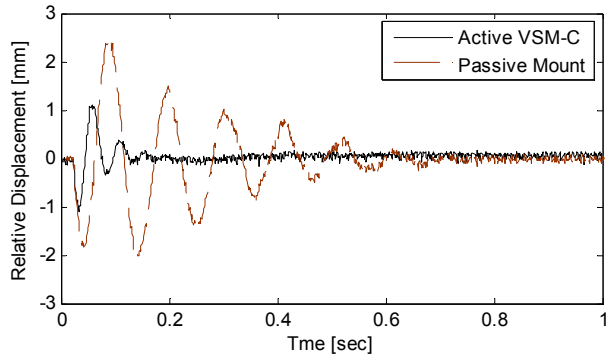

Figure 5-32. Relative displacements of the passive mount and VSM-C caused by a shock

5.5.3 VSM RESPONSE TIME MEASUREMENT

This test evaluates how quickly and effectively the VSM acts in a real situation. This test measures the response time of the whole system including the mechanical and control units. In particular, the following items affect the whole system's response time:

- Sensing and data processing.
- Piezoelectric actuator and its amplifier.
- Mechanical system dynamics.

The VSM-C with configuration shown in Figure 5-13.a and the shaker test setup (Figure 5-26) were used. LVDTs were used as the displacement sensor. The shaker table was first excited with a frequency smaller than the natural frequency of the VSM-C while VSM-C is not active. Then the frequency of the shaker table was suddenly shifted to the natural frequency of the VSM-C. At resonance, the platform's amplitude kept increasing. The control system should detect such an excessive vibration and control it by activating the VSM-C.

In order to overcome the backlash between mechanical parts at a low prestress, an initial prestress of 1400 N was put into the cables by using a tensioner bolt while the piezo actuator was inactive. The natural frequency of this VSM-C with 1400 N prestress was measured to be about 14 Hz. Activating the actuator increased the prestress to 2250 N.

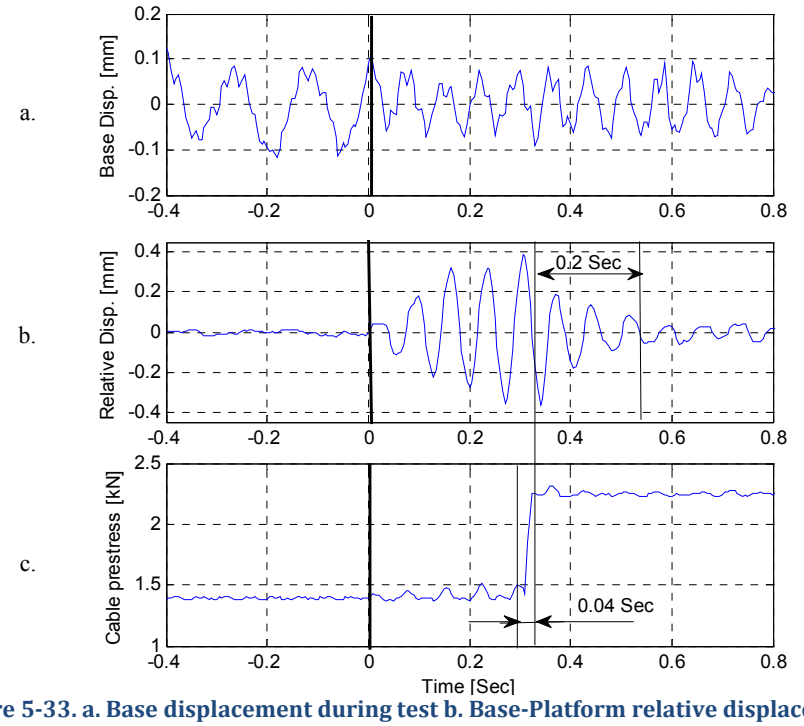

Figure 5-33. a. Base displacement during test b. Base-Platform relative displacement c. Cable force in the VSM-C

Figure 5-33.a shows the displacement of the base made by the shaker table; Figure 5-33.b the relative displacement of the base vs. platform, and Figure 5-33.c shows the prestress of the cables. Initially, the base was excited at 7 Hz with an amplitude of of 0.1 mm. At time zero, the frequency was switched to 14 Hz without changing the base's vibration amplitude. By switching the frequency to 14 Hz, which is the natural frequency of the VSM-C with 1400 N prestress, the relative base-platform displacement, as shown in Figure 5-33.b, was increased by about ten times to 0.4 mm. The control system monitored the base amplitude around the natural frequency (12-16 Hz). This amplitude was found by using the RMS of the base displacement signal read by the LVDT. In order to approximate the amplitude reliably by using RMS, about 2 periods of the displacement signal were used. Two periods of a 14 Hz sinusoidal signal take 0.14 s. If this amplitude exceeded more than a certain threshold, a signal was sent to the amplifier of the piezoelectric actuator to activate it. As can be seen in Figure 5-33c, it takes about 0.3 s before the actuator force increases. In about 0.04 second, the prestress increases to the high level. This short time is the response time of the actuator and the mechanical system, which provide the prestress in the cables. After the prestress

increases, the prestress stiffness of the VSM-C increase and result in a new steady state response for the relative amplitude equal to 0.015 mm. Before the steady state, a transient phase that last about 0.2 s occurs. This time depends on the deadweight and the dynamic parameters of the VSM-C such, as stiffness and damping.

In summary, the control system takes about 0.3 s to detect the excessive vibration and activate the actuator, and the VSM-C takes another 0.2 s to isolate the platform from the base excitation. As a result, in about 0.5 s, the excessive relative displacement is built up, detected, and suppressed.

5.6 CONTROL CRITERION FOR THE SEMI-ACTIVE VSM

In the previous sections, the VSM and its dual characteristics in the active and inactive states (with and without prestress) were presented and discussed. It was also briefly mentioned that the VSM is required to be active at low frequencies and inactive at high frequencies and that this requirement is the overall control criterion for this device. In this section, this criterion is further described, and the performance improvements are elaborated.

5.6.1 CONTROL CRITERION FOR THE SEMI-ACTIVE VSM-C

The transmissibility curves of Figure 5-27 are reproduced here in Figure 5-34. The transmissibilities of the VSM-C in the active and inactive modes intersect at 10 Hz. The control system of the VSM-C turns on the piezo actuator at frequencies lower than 10 Hz and turns it off at frequencies higher than 10 Hz. As a result, the actual transmissibility of the controlled VSM-C or the “Semi-active VSM-C” in Figure 5-34, first follows the ”Active VSM-C” curve up to 10 Hz and then, by switching to high prestress, follows the ”Inactive VSM-C” curve. As Figure 5-34 reveals, the semi-active VSM-C, at low frequencies (less than 10 Hz), controls the platform bounce much better than the passive mount. For example, the transmissibility of the semi-active VSM-C at 10Hz is 1.11, which is about fifteen times smaller than that of the passive mount (i.e., 15.19). The semi-active VSM-C also provides better isolation at the high-frequency range. For instance, at 20 Hz, which corresponds to an engine speed of 600 rpm, the semi-active VSM-C provides 73% isolation. This result means that the VSM-C improves the isolation by 22% when substituted for the passive mount. In terms of the reduction of the vibration, the semi-active VSM-C improves the isolation by 3.6 dB at 20, when compared with the passive mount. At higher frequencies, the passive mount is already quite efficient in isolating the vibration, as shown by its low transmissibility. Therefore, improvements at frequencies higher than 30-40Hz cannot be significant. The VSM-C in such frequencies offer the same isolation (or slightly better) as seen in Figure 5-34. For instance, at 50 Hz the passive mount provided 93% isolation and the semi-active VSM-C provided 94.5% which was 1.5% further isolation.

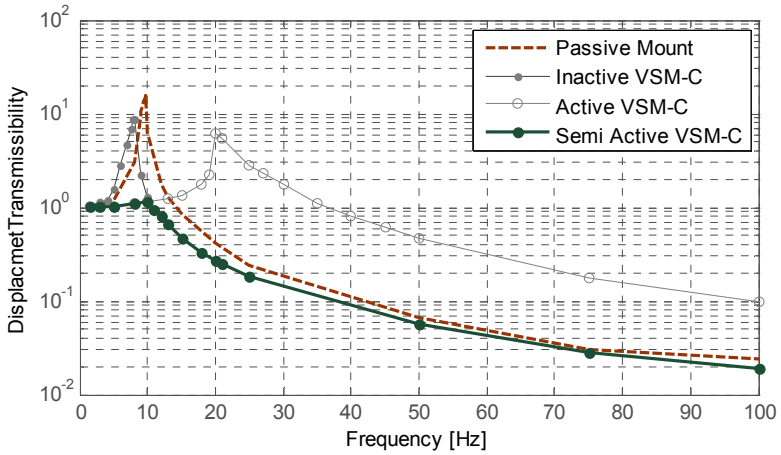

Figure 5-34. The control criterion of the semi-active VSM-C

5.6.2 *Control criterion for the semi-active VSM-P*

The semi-active VSM-P, similar to the semi-active VSM-C, is activated by the control system only at low frequencies. The transmissibility curves of the VSM-P, in the active and inactive states, intersect at about 10 Hz. Therefore, in order to obtain the lowest transmissibility, the VSM-P is activated at frequencies lower than the intersection frequency (10 Hz) and remains inactive at frequencies higher than 10 Hz. The transmissibility curve of the controlled VSM-P, or the "semi-active VSM-P", is also shown in Figure 5-35, which shows that the semi-active VSM-P controls the platform bounce at low frequencies very effectively. For example, the transmissibility of the semi-active VSM-P at 10 Hz is 1.38, which is about one-eleventh of the measured transmissibility (15.19) of the passive mount at the same frequency (10 Hz). In addition, this semi-active VSM-P provides better isolation at the high-frequency range than the passive mount. At high frequencies, the semi-active VSM-C and the semi-active VSM-P follow the same curve. As a result, the improvement previously seen in the semi-active VSM-C, is also achieved by the semi-active VSM-P.

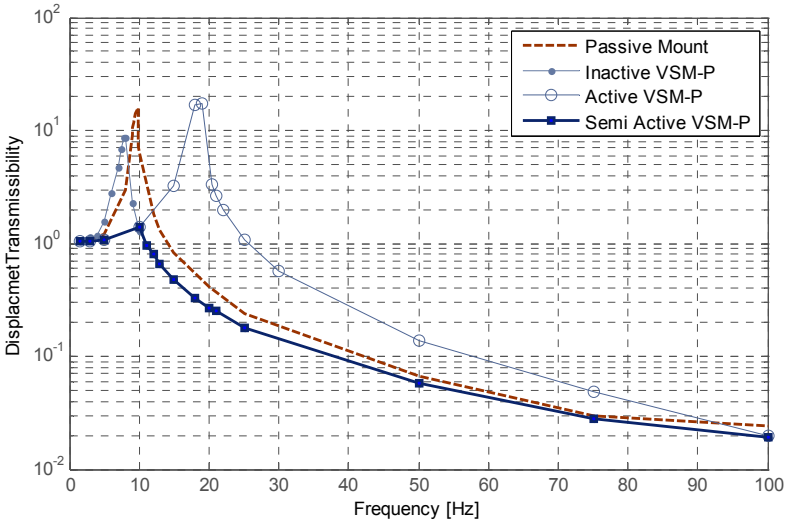

Figure 5-35. How the Semi-active VSM-P works and its comparison with an equivalent passive mount

5.6.3 *Semi-active VSM-C versus semi-active VSM-P*

Figure 5-36 shows the curves of Figure 5-34 and Figure 5-35 together. Figure 5-36 shows, in the lower-frequency range, the semi-active VSM-C provides slightly better vibration displacement control than the semi-active VSM-P. For example, the transmissibility of the semi-active VSM-C at 10 Hz is 1.11 which is smaller than the transmissibility of the semi-active VSM-P (1.38). This small difference is caused by the friction of the cable's wires, which was seen as hysteresis and resulted in a higher dynamic stiffness. As a result, the friction and the hysteresis in the VSM-C works in favor of the semi-active VSM-C and improves its performance.

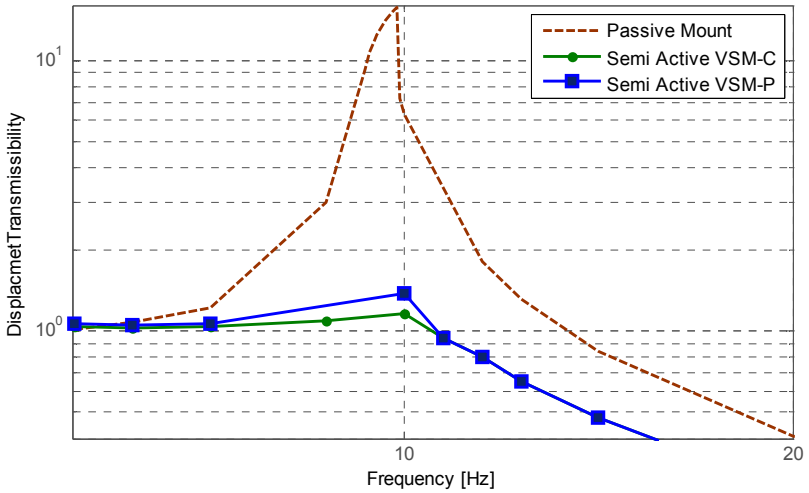

Figure 5-36. Transmissibility comparison between semi-active VSM-C and semi-active VSM-P

5.7 Summary

The proposed VSM consists of a soft rubber mount installed in parallel with an AVS (Antagonistic Variable stiffness Spring). The soft rubber mount supports the deadweight while the AVS provides additional stiffness when activated by a simple On-off control system. The AVS is a kinematically singular prestressable mechanism with first-order infinitesimal mechanism. Wire cables (cable) and thin plates (plate) were used to carry the prestress and create the variable stiffness. The stiffness of the AVS is controlled by the level of prestress in the cables or plates.

A VSM with an adjustable design was fabricated and tested for performance evaluation. The performance was measured based on the four criteria (1) how much it controls the displacement near the resonance, (2) how well it isolates the vibration in high frequencies, (3) how well it controls the motion caused by shock, and (4) how fast it reacts to control the vibration. For this evaluation, static and dynamic stiffness tests as well as a shock test were performed on the VSM. The response time of the controlled VSM was also measured. The comparison was performed with an equivalent passive mount.

Chapter 6 SUMMARY, CONCLUSIONS AND RECOMMENDATIONS

In this thesis, kinematically singular pre-stressed mechanisms have been used to develop practical semi-active variable stiffness springs for vibration isolation. These new springs, called AVSs, provide a wide ranges of stiffness change in a reasonable size. The stiffness of an AVS can be changed much faster than that of other available mechanical variable stiffness springs since it relies on prestress change and minimal motions in the links. The AVS, when used in parallel with a soft rubber mount, makes a mount/isolator called a VSM. The theoretical and experimental results showed that a VSM performs significantly better than a regular passive mount.

This chapter presents a brief summary of the results and discussions on how the developed AVS meets the desired characteristics of a general variable stiffness spring. Its possible applications are also presented in this chapter as well as some suggestions for future research.

6.1 SUMMARY

Kinematically singular prestressed mechanisms along their singular directions (FOIM) are stiffened only by prestress. In other words, the elasticity of the links of these mechanisms does not contribute to the stiffness along a FOIM. This unique characteristic was used in this research in order to develop a variable stiffness spring (AVS) and a variable stiffness mount/isolator (VSM). This research demonstrates that kinematically singular mechanisms have possible applications even though singularity is usually preconceived as a problem. As a result, singular configurations are usually avoided, and the useful applications of singularities are not explored thoroughly in the literature.

An AVS as a prestressable mechanism maintains prestress. The prestress of the links in an AVS create a stiffness which is called prestress stiffness. The stiffness of an AVS can be controlled and changed very quickly by changing the prestresses of the links. Any kinematically singular and prestressed mechanisms can be considered for making an AVS. In this thesis, however, two types of prestressed mechanisms were chosen for making an AVS: cable-driven mechanisms and tensegrities.

Cable-driven mechanisms were used as the first development platform for the AVS. Cable-driven mechanisms in general are prestressed mechanisms but not generally

kinematically singular. The stiffness model of cable-driven mechanisms and the stability conditions on each stiffness component were studied. Two main criteria for an AVS as an effective solution for vibration-control were determined: (1) The prestress stiffness should be dominant in the total stiffness of the AVS, and (2) the range of the stiffness change should be significant. It was shown that in kinematically singular configurations of the mechanism, both criteria can be met. In such configurations, the overall stiffness is merely prestress stiffness and hence fully controllable.

Tensegrities were used as the second platform for developing an AVS. Tensegrities are known as prestressable and kinematically singular pin-jointed structures/mechanisms. Tensegrity prisms were investigated and one of their FOIMs was found suitable for making an AVS. This FOIM is a simple twisting motion. A tensegrity prism can be easily constrained along this FOIM and used as a translational or rotational spring. A mathematical model was developed for the stiffness components along this FOIM. It was shown that in the tensegrity state, the stiffness is merely determined by the prestress. Therefore, the AVS made with tensegrity is fully controllable through force control in the members (bars or cables), which can be realized by using piezo force actuators.

To elaborate on the feasibility of making an AVS for vibration applications, two similar case studies were presented. The first case study compared the performance of a VSM developed by using cable-driven mechanisms with the performance of a commercial passive mount by using numerical simulations of a nonlinear model. The second case study compared the performance of the same passive engine mount with the performance of a VSM that was developed with tensegrity. It was shown that under feasible conditions, both VSMs performed better than a passive engine mount in both low-frequency and high-frequency excitations. This result was obtained for the price of a small amount of power used to stretch the cables and set the prestress in them. The effects of different geometrical parameters as well as the prestress on the characteristics of the VSM with tensegrity were discussed. It was concluded that the range of stiffness as well as its linearity can be tailored through the geometrical parameters. Also, it was shown that the linearity and stiffness range usually changed in opposite directions, and, hence, an optimization would be be necessary for each particular application.

A VSM with an adjustable design was fabricated and tested for performance evaluation. The performance was measured based on four criteria: (1) how much it controls the displacement near resonance, (2) how well it isolates the vibration in high frequencies, (3) how well it controls the motion caused by shock, and (4) how fast it reacts to control the vibration. For this evaluation, static and dynamic stiffness tests as well as a shock test were performed on the VSM. The response time of the controlled VSM was also measured. The comparison was performed with an equivalent passive mount.

6.2 DISCUSSION

As this thesis showed, the AVS and VSM demonstrate the potential for a range of vibration applications, but also have some limitations. In this section, this potential and these limitations are discussed.

6.2.1 CHARACTERISTICS OF THE AVS

It was explained that an AVS, in order to be used as an effective semi-active variable stiffness spring, needs to have the four desired characteristics of a general variable stiffness spring discussed in Chapter 2, section 2.5:

- Fast response.
- High stiffness controllability.
- Linearity.
- Sufficient stiffness magnitude.

Based on the simulation and experimental results for the VSM, these characteristics are assessed in the developed AVS in the following paragraphs.

- **Fast response**

AVS is a fast-response mechanical variable stiffness spring as it relies on prestress change, which is associated with minimal motions in the links. The available mechanical variable stiffness springs, in contrast, provide variable stiffness based on the geometry change, which is associated with finite displacements of the links and clearly results in a long response time and high power consumption.

- **High stiffness controllability**

The stiffness controllability (R) was defined as the ratio of the controllable (variable) stiffness to the total stiffness. In an AVS, the prestress stiffness is the controllable stiffness and also the only source of stiffness. As a result, an AVS has the highest stiffness controllability ($R = 1$). This property means that the stiffness of an AVS can be controlled by the prestress level from zero to any desired value limited only by the strength of the links.

The stiffness controllability of the developed VSM was designed to be high but could not achieve the maximum of 1 because of the constant stiffness of the soft rubber mount that exists all the time. The soft rubber mount supports the dead weight of the isolated mass. If the VSM is intended to work normal to gravity, the soft rubber mount can be eliminated and the highest stiffness controllability can be achieved. The stiffness of the tested VSM could be changed from 85 N/mm to 600 N/m. As a result, the stiffness controllability of the tested VSM was 0.87.

- **Linearity**

The AVS is a nonlinear spring; however, the nonlinearity can be tailored for each application. The change of the total stiffness with the displacement is understood as the nonlinearity of an AVS. The stiffness of an AVS changes with the displacement. Generally, this change occurs because when an AVS deforms to another static equilibrium under the external load, the other sources of stiffness such as elastic stiffness shows up since the mechanism is not at a singular position anymore. Consequently, the total stiffness at the new equilibrium changes. Therefore, an AVS, in general, is a nonlinear spring. However, the nonlinearity depends on the geometrical parameters of an AVS. It was shown in this thesis that the nonlinearity can be tailored by using an appropriate geometry for each application. For instance, the nonlinearity of the AVS proposed in Chapter 4 caused a 1% change in the total stiffness over its working range. This range of nonlinearity is suitable for some applications such as engine mounts. As another example, consider the force-displacement curve of the VSM-P shown in Figure 5-16. In the working range, the relation between the

measured force and the displacement can be considered as a linear relation. It was shown that a linear stiffness assumption for a VSM could correctly predict the experimental results (see Figure 5-30).

- **Sufficient stiffness magnitude**

AVS can produce a large stiffness magnitude. In contrast to the common notion of prestress stiffness, the tested VSM with regular wire cables and a feasible prestress (4 kN) produced a large prestress stiffness. For example, the VSM-P produces 600 N/mm, which is three times higher than the stiffness of a regular engine mount (200 N/mm).

6.2.2 CHARACTERISTICS OF THE VSM

The four desired characteristics discussed above are the general characteristics of an AVS. An AVS, when used in parallel with a soft rubber mount forms a semi-active variable stiffness mount/isolator called a VSM. As a result, a VSM inherits the desired characteristics, mentioned in the previous section, from its AVS. In addition, a VSM demonstrates several additional potential characteristics in vibration applications. These characteristics are summarized in the followings paragraphs.

- **Better vibration displacement control at resonance**

  One of the main advantages of the semi-active VSM is its ability to provide better vibration displacement control at resonance. As an example, the maximum displacement of the semi-active VSM was measured to be more than ten times less than that of the passive mount (see Figure 5-34, Figure 5-35).
- **Better vibration isolation in high frequencies**

  As a result of having lower stiffness and damping at high frequencies, a VSM provides better isolation at high frequencies(Figure 5-34 and Figure 5-35). For instance, at 20 Hz, which corresponds to an engine speed of 600 rpm, the semi-active VSM provides 73% isolation. This results means that the VSM at 20 Hz improves the isolation by 22% when substituted for a passive mount. In terms of reduction of vibration, the VSM improves the isolation by 3.6 dB at 20 Hz, when compared with the passive mount. Note that at higher frequencies, the passive mount is already quite efficient in isolating the vibration as its low transmissibility demonstrates. Therefore, improvements at frequencies higher than 30-40Hz are not as significant as improvements at low frequencies. The VSM at such frequencies offers the same isolation (or slightly better), as seen in Figure 5-35. For instance, at 50 Hz, the passive mount provided 93% isolation, whereas the VSM-C provided 94.5% isolation, or 1.5% more isolation.
- **Better motion control under shock**

  The semi-active VSM limited the relative motion caused by the shock. It also suppressed the vibration caused by shock faster than the passive mount (Figure 5-32).
- **Fast dynamics**

  The fast dynamics of the VSM is inherited from the fast response of its AVS, as was explained above. The semi-active VSM had a response time of half a second in the tested prototype. Increasing the prestress of the cable/plate can be achieved quickly since only small stretches of the cables/plates are required. For example in the experiments explained in Chapter 5, the required stretch was less than half a millimeter (see Figure 5-33).

- **Uncomplicated on-off control**

  As shown in the dynamics test, a simple ON-OFF controller can provide the desired response. During the design process, PID controllers were also evaluated for their ability to gradually control the prestress level to reach a high response without experiencing an over shoot. The improvement was found to be negligible.

- **Low energy consumption**

  Similar to all semi-active solutions, the semi-active VSM has low energy consumption. The energy is used only to activate the semi-active VSM by stretching the cables/plates. In the built prototype, this energy was 0.11 J for making a prestress of 4 kN. Maintaining the high prestress level in the active mode theoretically does not consume energy. However, a small drift of energy may occur while the high prestress level is maintained in the cables/plates.

6.2.3 LIMITATIONS

The development of the AVS concept is based on small displacement along infinitesimal mechanism. Most of applications in vibration-control deals with small displacements less than a millimeter. The effectiveness of such an AVS for vibration application was shown by simulation and experimental results. In order to use an AVS in large displacement applications, the nonlinearity effects due to large displacements need to be studied, and possible solutions for the linearity improvements be provided.

The fabricated VSM was devised as a general vibration mount. In order to demonstrate the fast dynamics of the AVS, a fast response piezo actuator was used. As was shown in section 5.5.3, the prestress level of the VSM was increased by 1 kN in 0.04 s. This short response time clearly demonstrated the fast response of the VSM. However, for an engine mount application, considered as a case study in this thesis, the piezo actuator is unnecessarily fast and expensive. Using a piezo actuator also introduced several new challenges for the manufacturing process. The stroke of the selected piezo actuator was 60 micrometers. The manufacturing tolerances and backlashes between the moving parts, which were also in the micrometer range, reduced the effective stroke of the piezo actuator. As a result, the actuator could not provide the high prestress of 4 kN. In order to achieve the high level of prestress, a turning bolt was implemented to stretch the cables.

6.3 POSSIBLE APPLICATIONS AND FUTURE WORKS

In this thesis, the AVS and VSM were explored as semi-active engine mounts for a vibration-control application. However, AVSs and VSMs could be used for a variety of demanding vibration applications with dual vibration characteristics. As another application, AVSs and VSMs might be useful for seismic-control applications where a VSM could act as a variable stiffness base for a structure or a building. Several mechanical solutions are available for preventing earthquake damage, all based on geometry change. They provide a stiff base in normal condition which then quickly turns into a soft base when earthquake waves hit. A VSM can provide these characteristics faster than the available solutions. The challenge will be devising a mechanical switch that keeps the prestress on the VSM in normal conditions and releases the prestress when an earthquake strikes.

It was shown in this thesis that the stiffness of an AVS and a VSM can be changed very quickly at a low energy cost. As a result, AVSs and VSMs can also be used as active elements in vibration applications. As a fast-response variable stiffness spring, An AVS can be

implemented in robotics for grasping applications where the stiffness of the gripper needs to be adjusted according to the compliance of the object.

This thesis studied tensegrities as kinematically singular prestressed mechanisms. The infinitesimal mechanisms (FOIMs) of tensegrities were of particular interest in this work. Researchers in Structural Engineering also study tensegrities and their FOIMS. However, in Structural Engineering, tensegrities are used for different purposes such as light or deployable structures. This thesis used FOIMs to make an AVS, whereas in Structural Engineering, FOIMs are avoided as they might decrease the stiffness of the structure. Reinforcing of the tensegrity by adding additional links, is one way to eliminate the FOIMs and increase the stiffness of the tensegrity. However, this technique increases the weight of the structure and is not desired for several applications such as deployable and space structures, in which light weight is advantageous. The stiffening property of the prestress along the FOIMS and the study of the geometrical parameters of tensegrities explained in this thesis can be extended for developing light deployable structures. Such optimum structures can be stiffened effectively by the state of the prestress without eliminating the FOIMs.

The fabricated VSM was devised as a general vibration mount but tested only as an engine mount. The fabricated VSM can be used to explore different case studies. It can also be used to study the nonlinear hysteresis effect caused by frictions in the wire-cables.

The current piezo-actuation system provides an unnecessarily fast response for a wide range of mechanical vibration-control systems. For example, in the response test of the VSM set as an engine mount (Figure 5-33), the piezo-actuation time (0.04 s) was less than one tenth of the total time needed for detecting and controlling the excessive vibration (0.5 s), while, for an engine mount application, a longer actuation-time is still acceptable. As a result, for systems with slow dynamics, piezo-actuation is too fast, while other actuators such as hydraulic or pneumatic ones are expected to provide the required force in a reasonable time at lower cost. In addition, hydraulic and pneumatic pressure are available in some vehicles. For these reasons, making a VSM as a new engine mount in the size of common engine mounts with hydraulic or pneumatic actuators can be pursued as one possible line of future research.

The current study looked at applications with small displacements. In order to use AVS in large displacement applications, the nonlinearity effects due to large displacements need to be studied and possible solutions for the linearity improvement need to be provided. As was shown in Chapter 4, the linearity of the AVS using tensegrity is more flexible than the linearity of the AVS using cable-driven mechanisms. As a result, the tensegrity-based AVS has more potential to be used for larger displacement applications.

Piezo-actuators, when used in an AVS or VSM to increase the prestress, first need to overcome the backlashes and manufacturing tolerances of the joints. The piezo-actuators' stroke and joints' tolerances are both in the range of several micrometers. As a result, a part of the useful stroke of the piezo actuator is consumed, and the theoretical maximum prestress level cannot be reached in the links of the AVS. Eliminating the joints of the AVS by using the idea of the compliant mechanisms is another research avenue that can lead to designing a backlash-free AVS. The author started working on this idea during his visit to the Structural Group at the University of Cambridge. Using a complaint mechanism will facilitate the effective use of piezo actuation.

Chapter 7 REFERENCES

1. Walsh, P., Lamancusa, J., 1992, "A variable stiffness vibration absorber for minimization of transient vibrations," *Journal of Sound and Vibration*, **158**(2), pp. 195–211.

2. Sun, J., Jolly, M., Norris, M., 1995, "Passive, adaptive and active tuned vibration absorbers—a survey," 50th anniversary of the design engineering division, A Special Combined Issue of the *Journal of Mechanical Design* and the *Journal of Vibration and Acoustics*, **117**(3B), pp. 234–242.

3.Jalili, N., 2002, "A comparative study and analysis of semi-active vibration-control systems," *Journal of Vibration and Acoustics*, **124**(4), pp. 593–605.

4.Chakarov, D., 2004, "*Study* of the antagonistic stiffness of parallel manipulators with actuation redundancy," Mechanism and Machine Theory, **39**(6), pp. 583-601.

5.Lee, S. H., Lee, J. H., Yi, B., Kim, S. H., Kwak, Y., 2005, "Optimization and experimental verification for the antagonistic stiffness in redundantly actuated mechanisms: A five-bar example," *Mechatronics*, **15**(2), pp. 213-238.

6.Simaan, N., Shoham, M., 2003, "Geometric interpretation of the derivatives of parallel robots' Jacobian matrix with application to stiffness control," *Journal of Mechanical Design, Transactions of the ASME*, **125**(1), pp. 33-42.

7.Kim BH, Yi BJ, Oh SR, Suh IH, 2003, "Independent finger and independent joint-based compliance control of multifingered robot hands," *IEEE Transactions on Robotics and Automation*, **19**(2), pp. 185-199.

8.Brennan MJ, 2006 ,"Some recent developments in adaptive tuned vibration absorbers/neutralizers," *Shock and Vibration*, **13**(4-5), pp. 531-543.

9.Azadi, M., Behzadipour, S., Faulkner, G., 2009, "Antagonistic Variable Stiffness Elements," *Mechanism and Machine Theory*, **44**(9), pp. 1746-1758.

10.Azadi, M., Behzadipour, S., Faulkner, G., "A Variable Spring Using a Tensegrity Prism," Accepted for publication at *ASME Journal of Mechanisms and Robotics*, April 2010.

11.Harris. C. M., 1996, *Shock and vibration handbook 4th edition,* McGraw-Hill, New York.

12.Behzadipour, S., Khajepour, A., 2006, "Stiffness of Cable-based Parallel Manipulators with Application to the Stability Analysis," ASME *Journal of Mechanical Design*, **128**(1), pp. 303-310.

13.Azadi, M., Behzadipour, S., 2007, "A Planar Cable-driven Mechanism as a New Variable Stiffness Element," Proceeding of SAE 2007 Noise and Vibration Conference, SAE Paper No. 2007-01-2421.

14. Azadi, M., Behzadipour, S., 2008, "An Application of Parallel Singularity in Variable Stiffness Elements," Proceeding of ASME International Design Engineering Technical Conferences, Paper No. DETC2008-49414.

15. Azadi, M., Behzadipour, S., 2007, "Variable antagonistic stiffness element using tensegrity structure," Proceeding of ASME International Mechanical Engineering Congress, Paper No. IMECE2007-42475.

16. Azadi, M., Behzadipour, S., Faulkner, G., 2009, "Variable Stiffness Tensegrity Prism Spring," Proceeding of 2009 ASME International Design Engineering Technical Conferences, Paper No. DETC2009-87407.

17. Azadi, M., Behzadipour, S., Guest, S. D., 2010, "A New Variable Stiffness Spring Using A Prestressed mechanism," Proceeding of 2010 ASME International Design Engineering Technical Conferences, Paper No. DETC2010-28496.

18. Azadi, M., Behzadipour, S., Faulkner, G., 2010, " Performance analysis of a semi-active mount made by a new variable stiffness spring," submitted for publication in *Journal of Sound and Vibration*.

19. Azadi, M., Behzadipour, S., Faulkner, G., 2010, "Variable Stiffness Spring using Tensegrity Prisms," U.S. Provisional Patent Application Serial No. 61/352,474.

20. Calladine, C.R., Pellegrino, S., 1991, "First-order Infinitesimal Mechanisms," *International Journal of Solids and Structures*, **27**(4), pp. 505-515.

21. El-Khasawneh B. S., and Ferreira P. M., 1999, "Computation of Stiffness and Stiffness Bounds for Parallel Link Manipulators," *International Journal of Machine Tools and Manufacturing*, **39**, pp. 321–342.

22. Salisbury j.K., 1980, "Active Stiffness Control of a manipulator in Cartesian Coordinate," In Proceeding of the 19th IEEE Conference on Decision and Control, pp. 87-89.

23. Murakami H., 2001, "Static and Dynamic Analysis of Tensegrity Structures Part 2. Quasi-Static Analysis," *International Journal of Solids and Structures*, **38**, pp. 3615-3629

24. Guest, S, 2006, "The stiffness of prestressed frameworks: A unifying approach," *International Journal of Solids and Structures*, **43**(3-4), pp. 842-854.

25. Cho, W., Tesar, D., Freeman, R.A, 1989, "The dynamic and stiffness modeling of general robotic mechanism systems with antagonistic actuation," Proceedings. 1989 IEEE International Conference on Robotics and Automation (Cat. n89CH2750-8), **3**, pp. 1380-7.

26. Choi, H.R., Chung, W.K., Youm, Y., 1994, "Stiffness analysis and control of redundant mechanisms," Proceedings - IEEE International Conference on Robotics and Automation, **1**, pp. 689-695.

27. Svinin M. M., Hosoe S., Uchyiama M., 2001, "On the Stiffness and Stability of Gough-Stewart Platforms," IEEE International Conference on Robotics and Automation, pp. 3268–3273.

28. Kawamura S., Choe W., Tanak S., Pandian S. R., 1995, "Development of an Ultrahigh Speed Robot Falcon Using Wire Driven Systems," IEEE International Conference on Robotics and Automation, pp. 215–220,.

29. Guest, S., 2006, "The stiffness of prestressed frameworks: A unifying approach," *International Journal of Solids and Structures*, **43**(3-4), pp. 842-854.

30. Narasimhan. S, Nagarajaiah. S, March 2005, "A STFT semiactive controller for base isolated buildings with variable stiffness isolation systems," *Engineering Structures*, **27**(4), pp. 514-523.

31.Hiller, M., Fang, S., Mielczarek, S., Verhoeven, R., Franitza, D., 2005, “Design, analysis and realization of tendon-based parallel manipulators,” *Journal of Mechanism and Machine Theory*, **40**(4), pp. 429-445.

32.Svinin, M.M., Hosoe, S., Uchiyama, M., Luo, Z.W., 2002, "On the stiffness and stiffness control of redundant mechanisms,” Proceedings-IEEE International Conference on Robotics and Automation, **3**, pp. 2393-2399.

33.Svinin, M. M., Ueda, K., Uchiyama, M., 2000, “On the Stability Condition of a Class of Parallel manipulators,” IEEE International Conference on Robotics and Automation, pp. 2386–2391.

34.Motro, R., 2003, *Tensegrity : structural systems for the future*, Kogan Page Science, London.

35.K. Snelson, 1965, Continuous tension, discontinuous compression structures, US Patent 3169611, 1965.

36.Heartney. E., 2009, *Kenneth Snelson: forces made visible*, Lenox, MA : Hard Press Editions ; Manchester, VT : In association with Hudson Hills Press.

37.Fuller, R.B., 1975, *Synergetics Explorations in the Geometry of Thinking*, Collier McMillan Publishers, London.

38.Fuller, R.B., 1962, *Tensile-integrity structures*, US Patent 3063521.

39.Furuya, H., 1992, "Concept of Deployable Tensegrity Structures in Space Applications," *International Journal of Space Structures*, **7**(2), pp. 143-151.

40.Wang, B. B., 2004, *Free-Standing Tension Structures From Tensegrity Systems to Cable-Strut Systems*, Taylor & Francis, New York.

41.Kenner, H., 2003, *Geodesic Math and How to Use It,* University of California Press, pp. 8-10.

42.Snelson, K., 2010, http://www.kennethsnelson.net.

43.Chu, R., 1988, “Tensegrity,” Journal of Synergetics, **2**(1).

44.Pugh, A., 1976, *An Introduction to Tensegrity Systems*, University of California Press Berkely.

45.Connelly, R., Back, A., 1998, “Mathematics and tensegrity,” American Scientist, **86**(2), pp. 142-151.

46.Motro, R., Najari, S., Jouanna, P., 1986, “Tensegrity systems, from design to realization,” The First International Conference on Lightweight Structures in Architecture, **1**, pp. 690-697, 1986.

47.Albus, J., Bostelman, R., Dagalakis, N., 1993, "The Nist Robocrane,” *Journal of Robtic Systems*, **10**, pp. 709–724.

48.Landsberger, S. E., Sheridan, T. B., 1993, "A Minimal Linkage: The Tension Compression Parallel Link Manipulator,” In Proceedings of IMACS/SICE International Symposium on Robotics, Mechatronics and Manufacturing Systems, pp. 81–88.

49.Kawamura S., Choe W., Tanak S., Pandian S. R., 1995, "Development of an Ultrahigh Speed Robot Falcon Using Wire Driven Systems,” In IEEE International Conference on Robotics and Automation, pp 215–220.

50.Baker, A., Crane III, C. D., 2006, “Analysis of three degree of freedom 6×6 tensegrity platform,” Proceedings of the ASME Design Engineering Technical Conference2006, DETC2006.

51.Tran, T., Crane, C.D., III, Duffy, J., 2002, “The reverse displacement analysis of a tensegrity based parallel mechanism,” *Robotics, Manufacturing, Automation and Control*. **14**, Proceedings of the Fifth Biannual World Automation Congress, pp. 637-43.

52.Kebiche, K., Kazi-Aoual, M.N., Motro, R., 1999, "Geometrical non-linear analysis of tensegrity systems" *Engineering Structures*, **21**(9), pp. 864-876.

53.Argyris. J.H, Scharpf. D.W., 1972, "Large Deflection Analysis of Prestressed Networks," *Journal of the Structural Division*, **98**(3), pp. 633-654.

54.Connelly, R., Whiteley, W., 1996, "Second-order rigidity and prestress stability for tensegrity frameworks," *SIAM Journal on Discrete Mathematics*, **9**(3), pp. 453–491.

55.Connelly, R., Terrell, M., "Globally rigid symmetric tensegrities," *Structural Topology*, v 21, pp 59–78, 1995.

56.Murakami, H., 2001, "Static and dynamic analyses of tensegrity structures. Part 1. Nonlinear equations of motion," *International Journal of Solids and Structures*, **38**(20), pp. 3599-3613.

57.Murakami, H. Nishimura, Y., 2001, "Static and dynamic characterization of regular truncated icosahedral and dodecahedral tensegrity modules," *International Journal of Solids and Structures*, **38**(50-51) , pp. 9359-938.

58.Skelton. R. E., 2009, *Tensegrity systems*, Dordrecht, New York , Springer.

59.Paul. C., Valero-Cuevas. F.J., Lipson. H., 2006, "Design and control of tensegrity robots for locomotion," *IEEE Transactions on Robotics*, **22**(5), pp. 944-57.

60.Yin, J. P., Duffy, J., Crane III. C. D., 2002, "An analysis for the design of self-deployable tensegrity and reinforced tensegrity prisms with elastic ties," *International Journal of Robotics and Automation*, **17**(1), pp. 38-45.

61.Arsenault. M., Gosselin, C.M., Nov. 2005, "Kinematic, static, and dynamic analysis of a planar one-degree-of-freedom tensegrity mechanism," *Transactions of the ASME. Journal of Mechanical Design*, **127**(6), pp. 1152-60.

62.Oppenheim, I.J., Williams, W.O., 2001, "Vibration of an elastic tensegrity structure," *European Journal of Mechanics, A/Solids*, **20**(6), pp. 1023-31.

63.Inman, D. J., 2001, *Engineering vibration,* Englewood Cliffs, N.J. : Prentice Hall.

64.Symans, M.D., Constantinou, M.C., Jun 1999, "Semi-active control systems for seismic protection of structures a state-of-the-art review," *Engineering Structures*, **21**(6), pp. 469-487.

65.Liu. Y., Matsuhisa. Hi, Utsuno. H., June 2008, "Semi-active vibration isolation system with variable stiffness and damping control," *Journal of Sound and Vibration*, **313**(1-2), pp. 16-28.

66.Jalili, N., 2002, "A comparative study and analysis of semi-active vibration-control systems," *Journal of Vibration and Acoustics*, **124**(4), pp. 593-605.

67.Sun, J.Q., Jolly, M.R., Norris, M.A., 1995, "Passive, adaptive and active tuned vibration absorbers—a survey," 50th anniversary of the design engineering division, A Special Combined Issue of the *Journal of Mechanical Design* and the *Journal of Vibration and Acoustics*, **117**(3B), pp 234–242.

68.Verhoeven, R., 2004, *Analysis of the Workspace of Tendon-based Stewart Platforms*, PhD thesis, University of Duisburg-Essen.

69.Yu, Y., Peelamedu, S. M., Naganathan, N. G., Dukkipati R.V., 2001, "Automotive Vehicle Engine Mounting Systems: A Survey," Transactions of the ASME, *Journal of Dynamic System, Measurement, and Control*, **123**(2), pp. 186–194.

70.Choi, S.B, Song, H.J., Lee, H.H, Lim, S.C., Kim, J.H., Choi, H.J., 2003, "Vibration-control of a passenger vehicle featuring magnetorheological engine mounts," *International Journal of Vehicle Design*, **33**(1-3), pp. 2-16.

71.Kim, G., Singh, R., 1995, ‘‘Study of Passive and Adaptive Hydraulic Engine Mount Systems with Emphasis on Non-Linear Characteristics,’’ *Journal of Sound and Vibration*, **179**(3), pp. 427–453.

72.Pelegrino, S., Calladine, C. R., 1986, “Matrix Analysis of statically and kinematically indeterminate frameworks,” *International Journal of Solids and Structures*, **22**(4), pp. 409-428.

73.Kuznetsov, E.N., 1991, ”Systems With Infinitesimal Mobility: Part II—Compound and Higher-Order Infinitesimal Mechanisms,” *Journal of Applied Mechanics*, **58**(2), pp. 520-526.

74.Tarnai, 1989, “Higher-order infinitesimal mechanisms,” *Acta technica*, **102**(3), pp. 363-363.

75.Tarnai, T., 2001, *Infinitesimal and finite mechanisms,* Chapter 7 in *Deployable Structures* (Editor: S. Pellegrino), Springer, New York, pp. 113-142.

76.Tarnai, T., 1980, “Simultaneous static and kinematic indeterminacy of space trusses with cyclic symmetry,” *International Journal of Solids and Structures*, **16**(4), pp. 347-359.

77.Nishimura, Y.,Murakami, H., 2001, “Initial shape-finding and modal analyses of cyclic frustum tensegrity modules,” *Computer Methods in Applied Mechanics and Engineering*, **190**(43-44), pp. 5795-5818.

78.Murakami, H., Nishimura, Y., 2001,” Initial shape finding and modal analyses of cyclic right-cylindrical tensegrity modules,” *Computers and structures*, **79**(9), pp. 891-917.

79.Chen, S.F., Kao, I., 2000, “Conservative Congruence Transformation for Joint and Cartesian Stiffness Matrices of Robotic Hands and Fingers,” *International Journal of Robotics Research*, **19**(9), pp. 835-847.

80.Yi, B.j., Freeman, R.A., 1992, “Synthesis of actively adjustable springs by antagonistic redundant actuation” *Journal of Dynamic Systems Measurement and Control*-Transactions of the ASME, **114**(3), pp. 454-461.

81.Yi, B.j., Freeman, R.A., 1993, “Geometric analysis of antagonistic stiffness in redundancy actuated parallel mechanisms,” *Journal of Robotic Systems,* **10**(5), pp. 581-603.

82.Oppenheim, I.J., Williams, W.O., 2001, “Vibration and damping in three-bar tensegrity structure,” *Journal of Aerospace Engineering*, **14**(3), pp. 85-91.

83.Loram, I.D., Lakie. M., 2002, “Direct measurement of human ankle stiffness during quiet standing: the intrinsic mechanical stiffness is insufficient for stability,” *Journal of Physiology-London,* **545**(3), pp. 1041-1053.

84.Shadmehr, R., Arbib, M.A., 1992, “A mathematical analysis of the force-stiffness characteristics of muscles in control of a single joint system.,” *Biological Cybernetics*., **66**(6), pp. 463-77.

85.Stokes, I.A.F., Gardner-Morse, M., 2003, “Spinal stiffness increases with axial load: another stabilizing consequence of muscle action,” *Journal of Electromyography and Kinesiology,* **13**(4), pp. 397-402.

86.Liang, C., Rogers, C. A., 1997, “Design of Shape Memory Alloy Springs with Applications in Vibration-control,” *Journal of Intelligent Material Systems and Structures*, **8**, pp. 314-322.

87.Williams, K., Chiu, G., Bernhard, R., 2002, “Adaptive Passive Absorbers Using Shape-memory Alloys,” *Journal of Sound and Vibration*, **249**(5), pp. 835-848.

88.Rustighi, E., Bernan, M.J., Mace, B.R., 2005, “A Shape Memory Alloy Adaptive Tuned Vibration Absorber Design and Implementation,” *Smart Materials and Structures*, **14**, pp. 19-28.

89.Williams, K., Chiu, G., Bernhard, R. , 2005, "Dynamic modeling of a shape memory alloy adaptive tuned vibration absorber," *Journal of Sound and Vibration*, **280**, pp. 211-234.

90.Ginder, J.M., Schlotter, W.F., Nichols, M.E., 2001, "Magnetorheological Elastomers in Tunable Vibration Absorbers," Proceedings of SPIE, **4331**, pp. 103-110.

91.Gong, X.L., Zhang, X.Z., Zhang, P.Q., 2005, "Fabrication and characterization of isotropic magnetorheological elastomers," *Polymer Testing*, **24**(5), pp. 669-676.

92.Shen, Y., Golnaraghi, M.F., Heppler, G.R., 2004, "Experimental research and modeling of magnetorheological elastomers," *Journal of Intelligent Materials and Structures*, **15**, pp. 27-35.

93.Davis, C. L., Lesieutre, G. A., 2000, "An actively tuned solid-state vibration absorber using capacitive shunting of piezoelectric stiffness," *Journal of Sound and Vibration*, **234**(3), pp. 601-617.

94.Shangguan, W.B., May 2009, "Engine mounts and powertrain mounting systems: A review," *International Journal of Vehicle Design*, **49**(4), pp. 237-258.

95.American Steel & Wire Co., 1946, *American tiger brand wire rope engineering handbook*, American steel & wire company, United States Steel, Chicago.

APPENDIX A

The dynamic equations of a quarter car model with an VSM shown in Figure 3-8.a are summarized as:

$$m_e\ddot{y} = \frac{-2nk_{cable}(y-x)}{\sqrt{L_e{}^2+(y-x)^2}}\left(\sqrt{L_e{}^2+(y-x)^2}+L_d-L_o\right)-k_r(y-x)-c_r(\dot{y}-\dot{x})$$

$$m_s\ddot{x} = -m_e\ddot{y}-2(k_{sf}+k_{sr})(x-x_o)-2(c_{sf}+c_{sr})(\dot{x}-\dot{x}_o)$$

where k_{cable} is the elastic stiffness of each cable, m_e is the mass of the engine, n is the number of the cables, and L_0 is the natural length of each cable. Assuming d as the equivalent diameter of the cable, the elastic stiffness coefficient can be written as:

$$k_{cable} = \frac{E\pi d^2}{4L_o}$$

Therefore, the following relation exists between the natural length of the cable and the pretension τ_0:

$$L_o = \frac{L_e+L_d}{1+\frac{4\tau_o}{E\pi d^2}}$$

APPENDIX B VARIABLE STIFFNESS MOUNT'S DRAWINGS

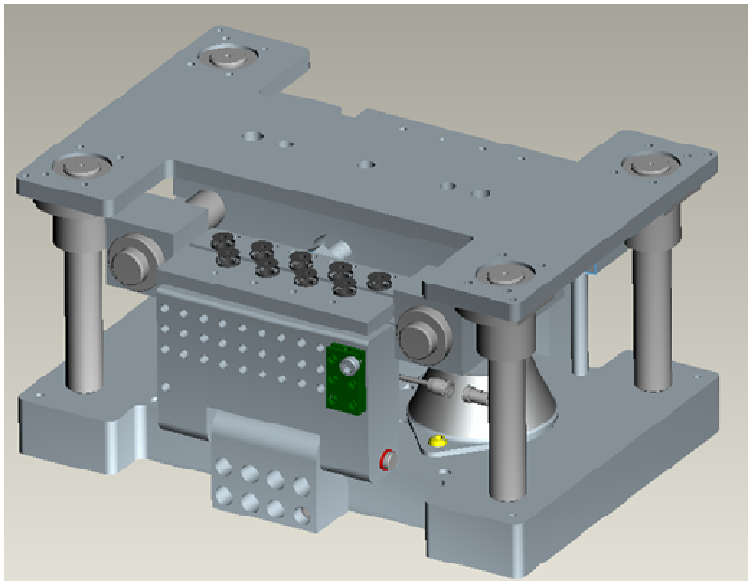

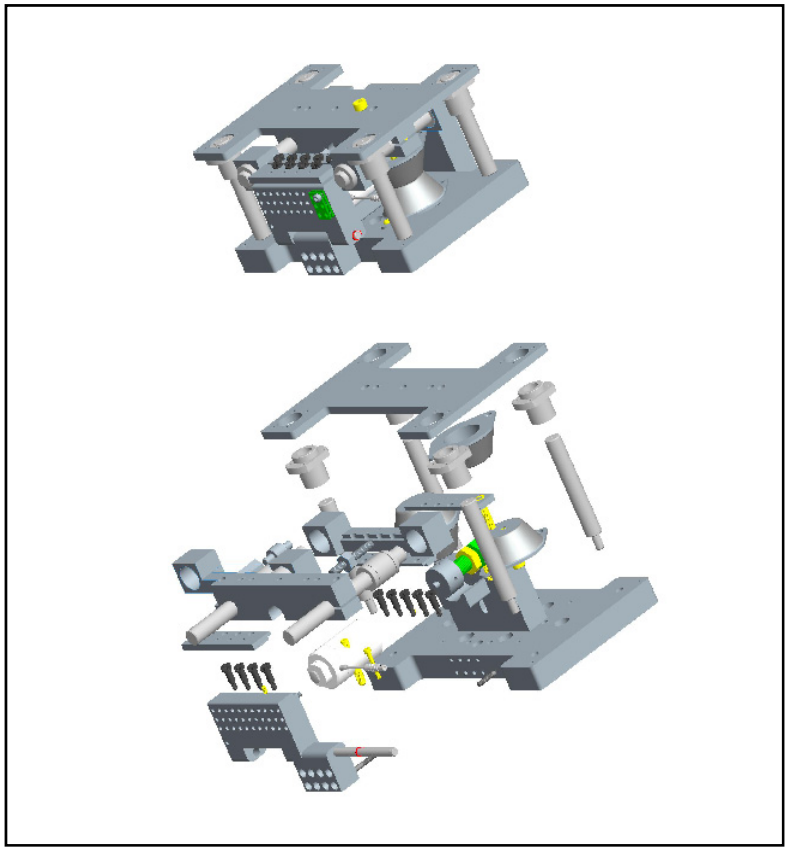

Appendix B

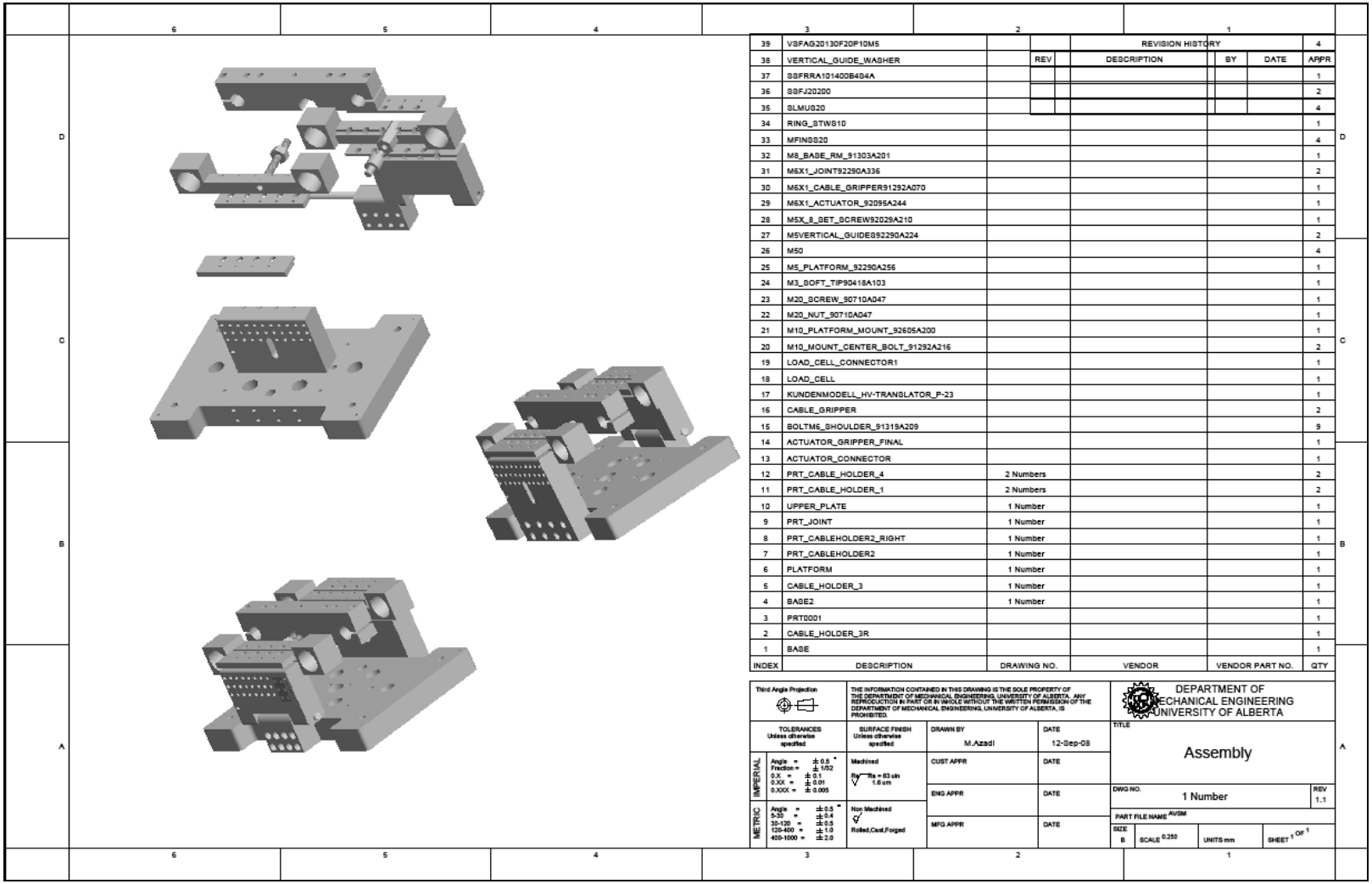

INDEX	DESCRIPTION	DRAWING NO.	VENDOR	VENDOR PART NO.	QTY
39	VBFAG20130F20P10M5				4
38	VERTICAL_GUIDE_WASHER				1
37	SSFRRA101400B4B4A				2
36	SSFJ20200				4
35	SLMUS20				1
34	RING_STWS10				4
33	MFINSS20				1
32	MS_BASE_RM_91303A201				2
31	M6X1_JOINT92290A336				1
30	M6X1_CABLE_GRIPPER91292A070				1
29	M6X1_ACTUATOR_92095A244				1
28	M5X_8_SET_SCREW9202SA210				2
27	M5VERTICAL_GUIDES92290A224				4
26	M50				1
25	M5_PLATFORM_92290A256				1
24	M3_SOFT_TIP90418A103				1
23	M20_SCREW_90710A047				1
22	M20_NUT_90710A047				1
21	M10_PLATFORM_MOUNT_92605A200				2
20	M10_MOUNT_CENTER_BOLT_91292A216				1
19	LOAD_CELL_CONNECTOR1				1
18	LOAD_CELL				1
17	KUNDENMODELL_HV-TRANSLATOR_P-23				2
16	CABLE_GRIPPER				9
15	BOLTM6_SHOULDER_91319A209				1
14	ACTUATOR_GRIPPER_FINAL				1
13	ACTUATOR_CONNECTOR				2
12	PRT_CABLE_HOLDER_4	2 Numbers			2
11	PRT_CABLE_HOLDER_1	2 Numbers			1
10	UPPER_PLATE	1 Number			1
9	PRT_JOINT	1 Number			1
8	PRT_CABLEHOLDER2_RIGHT	1 Number			1
7	PRT_CABLEHOLDER2	1 Number			1
6	PLATFORM	1 Number			1
5	CABLE_HOLDER_3	1 Number			1
4	BASE2	1 Number			1
3	PRT0001				1
2	CABLE_HOLDER_3R				1
1	BASE				1

REVISION HISTORY				
REV	DESCRIPTION	BY	DATE	APPR

Third Angle Projection

DEPARTMENT OF MECHANICAL ENGINEERING
UNIVERSITY OF ALBERTA

TOLERANCES Unless otherwise specified

IMPERIAL: Angle = ± 0.5°; Fraction = ± 1/32; .X = ± 0.1; .XX = ± 0.01; .XXX = ± 0.005

METRIC: 0-30 = ± 0.5°; 30-120 = ± 0.4; 120-400 = ± 0.5; 400-1000 = ± 1.0; 1000-2000 = ± 2.0

SURFACE FINISH Unless otherwise specified

Machined: Ra = 63 uin / 1.6 um

Non Machined: Rolled,Cast,Forged

DRAWN BY	M.Azadi	DATE 12-Sep-08
CUST APPR		DATE
ENG APPR		DATE
MFG APPR		DATE

TITLE: Assembly

DWG NO. 1 Number | REV 1.1

PART FILE NAME AVSM

SIZE B | SCALE 0.250 | UNITS mm | SHEET 1 OF 1

Appendix B

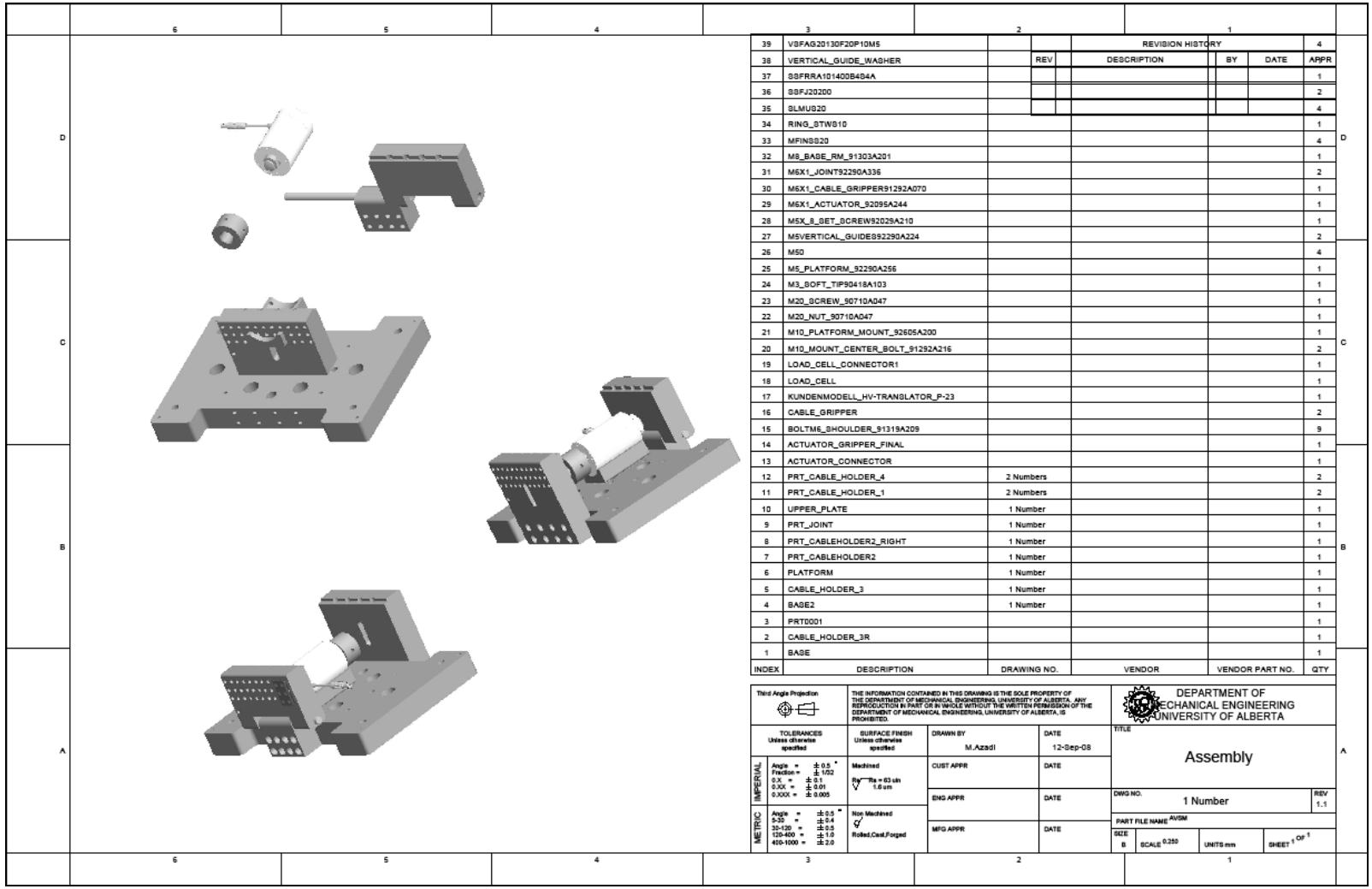

INDEX	DESCRIPTION	DRAWING NO.	VENDOR	VENDOR PART NO.	QTY
39	VSFAG20130F20P10M5				4
38	VERTICAL_GUIDE_WASHER				4
37	SSFRRA101400B4B4A				1
36	SSFJ20200				2
35	SLMUS20				4
34	RING_STWS10				1
33	MFINSS20				4
32	M8_BASE_RM_91303A201				1
31	M6X1_JOINT92290A336				2
30	M6X1_CABLE_GRIPPER91292A070				1
29	M6X1_ACTUATOR_92095A244				1
28	M5X_8_SET_SCREW92025A210				1
27	M5VERTICAL_GUIDES92290A224				2
26	M50				4
25	M5_PLATFORM_92290A256				1
24	M3_SOFT_TIP90418A103				1
23	M20_SCREW_90710A047				1
22	M20_NUT_90710A047				1
21	M10_PLATFORM_MOUNT_92605A200				1
20	M10_MOUNT_CENTER_BOLT_91292A216				2
19	LOAD_CELL_CONNECTOR1				1
18	LOAD_CELL				1
17	KUNDENMODELL_HV-TRANSLATOR_P-23				1
16	CABLE_GRIPPER				2
15	BOLTM6_SHOULDER_91319A209				9
14	ACTUATOR_GRIPPER_FINAL				1
13	ACTUATOR_CONNECTOR				1
12	PRT_CABLE_HOLDER_4	2 Numbers			2
11	PRT_CABLE_HOLDER_1	2 Numbers			2
10	UPPER_PLATE	1 Number			1
9	PRT_JOINT	1 Number			1
8	PRT_CABLEHOLDER2_RIGHT	1 Number			1
7	PRT_CABLEHOLDER2	1 Number			1
6	PLATFORM	1 Number			1
5	CABLE_HOLDER_3	1 Number			1
4	BASE2	1 Number			1
3	PRT0001				1
2	CABLE_HOLDER_3R				1
1	BASE				1

REVISION HISTORY			
REV	DESCRIPTION	BY	DATE	APPR
				1
				2
				4

Third Angle Projection

DEPARTMENT OF MECHANICAL ENGINEERING
UNIVERSITY OF ALBERTA

TOLERANCES Unless otherwise specified
IMPERIAL: Angle = ± 0.5°; Fraction = ± 1/32; 0.X = ± 0.1; 0.XX = ± 0.01; 0.XXX = ± 0.005
METRIC: Angle = ± 0.5°; 0-30 = ± 0.4; 30-120 = ± 0.5; 120-400 = ± 1.0; 400-1000 = ± 2.0

SURFACE FINISH Unless otherwise specified
Machined Ra 1.6 um
Non Machined
Rolled,Cast,Forged

DRAWN BY: M.Azadi
DATE: 12-Sep-08
CUST APPR
ENG APPR
MFG APPR

TITLE: Assembly
DWG NO.: 1 Number
REV: 1.1
PART FILE NAME: AVSM
SIZE: B
SCALE: 0.250
UNITS: mm
SHEET 1 OF 1

Appendix B

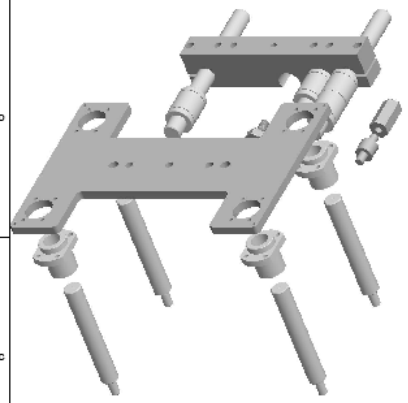

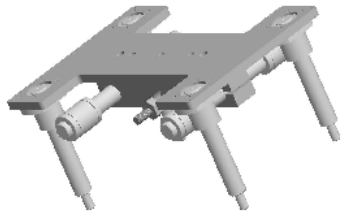

INDEX	DESCRIPTION	DRAWING NO.	VENDOR	VENDOR PART NO.	QTY
39	VSFAG20130F20P10M5				4
38	VERTICAL_GUIDE_WASHER				4
37	SSFRRA101400B4B4A				1
36	SSFJ20200				2
35	SLMUS20				4
34	RING_STW810				1
33	MFINSS20				4
32	M8_BASE_RM_91303A201				1
31	M6X1_JOINT92290A336				2
30	M6X1_CABLE_GRIPPER91292A070				1
29	M6X1_ACTUATOR_92095A244				1
28	M5X_8_SET_SCREW92025A210				1
27	M5VERTICAL_GUIDES92290A224				2
26	M50				4
25	M5_PLATFORM_92290A256				1
24	M3_SOFT_TIP90418A103				1
23	M20_SCREW_90710A047				1
22	M20_NUT_90710A047				1
21	M10_PLATFORM_MOUNT_92605A200				1
20	M10_MOUNT_CENTER_BOLT_91292A216				2
19	LOAD_CELL_CONNECTOR1				1
18	LOAD_CELL				1
17	KUNDENMODELL_HV-TRANSLATOR_P-23				1
16	CABLE_GRIPPER				2
15	BOLTM6_SHOULDER_91319A209				9
14	ACTUATOR_GRIPPER_FINAL				1
13	ACTUATOR_CONNECTOR				1
12	PRT_CABLE_HOLDER_4	2 Numbers			2
11	PRT_CABLE_HOLDER_1	2 Numbers			2
10	UPPER_PLATE	1 Number			1
9	PRT_JOINT	1 Number			1
8	PRT_CABLEHOLDER2_RIGHT	1 Number			1
7	PRT_CABLEHOLDER2	1 Number			1
6	PLATFORM	1 Number			1
5	CABLE_HOLDER_3	1 Number			1
4	BASE2	1 Number			1
3	PRT0001				1
2	CABLE_HOLDER_3R				1
1	BASE				1

REVISION HISTORY

REV	DESCRIPTION	BY	DATE	APPR
				1
				2
				4

Third Angle Projection

DEPARTMENT OF MECHANICAL ENGINEERING
UNIVERSITY OF ALBERTA

TOLERANCES Unless otherwise specified

IMPERIAL
Angle = ± 0.5 °
Fraction = ± 1/32
0.X = ± 0.1
0.XX = ± 0.01
0.XXX = ± 0.005

METRIC
Angle = ± 0.5 °
5-30 = ± 0.4
30-120 = ± 0.5
120-400 = ± 1.0
400-1000 = ± 2.0

SURFACE FINISH Unless otherwise specified
Machined
Ra Ra = 63 uin
1.6 um
Non Machined
Rolled,Cast,Forged

DRAWN BY: M.Azadi
DATE: 12-Sep-08
CUST APPR
DATE
ENG APPR
DATE
MFG APPR
DATE

TITLE: Assembly
DWG NO.: 1 Number
REV: 1.1
PART FILE NAME: AVSM
SIZE: B
SCALE: 0.250
UNITS: mm
SHEET 1 OF 1

Appendix B

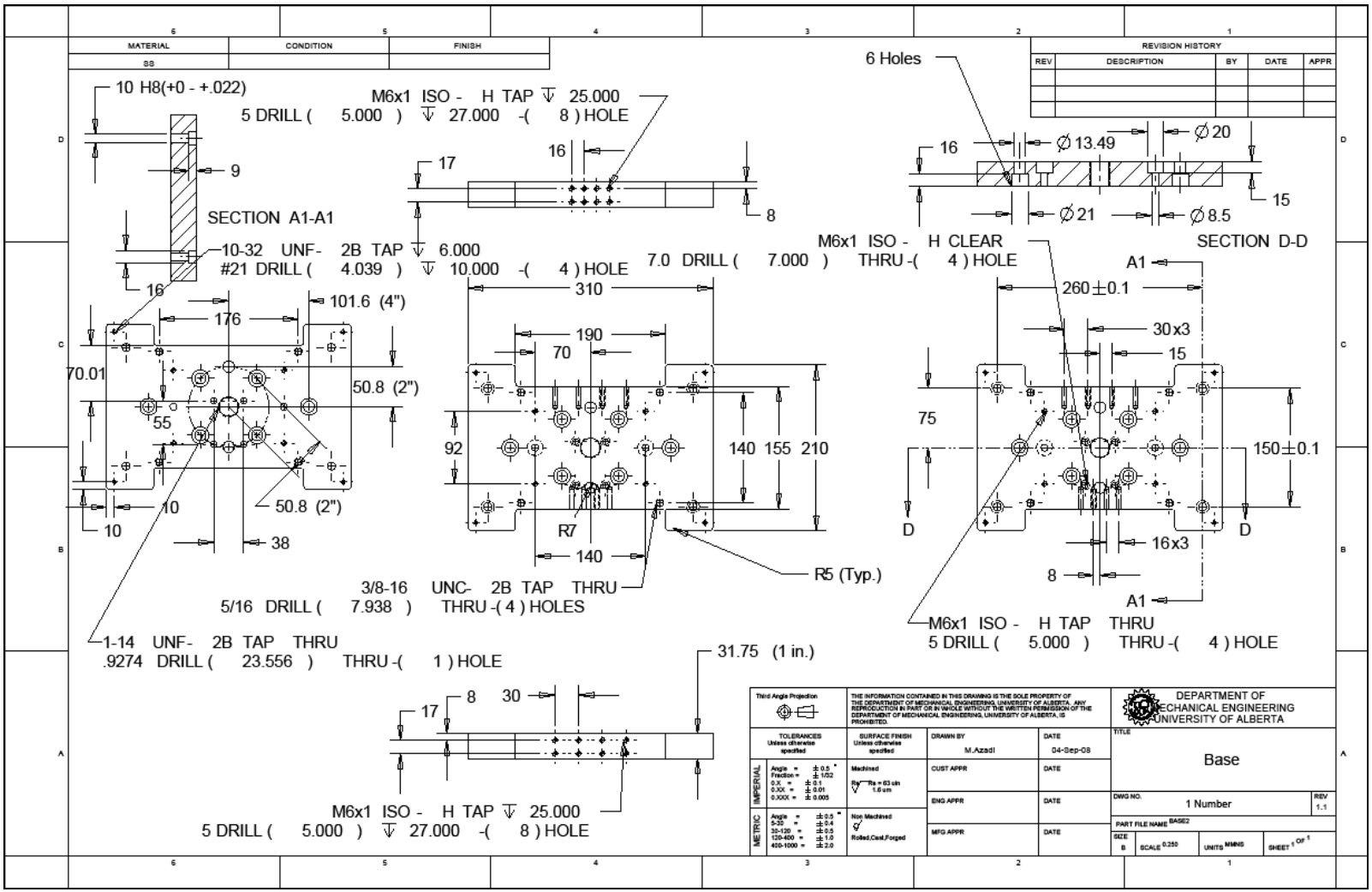
MATERIAL
SS
CONDITION
FINISH
REVISION HISTORY
REV
DESCRIPTION
BY
DATE
APPR
10 H8(+0 - +.022)
9
SECTION A1-A1
M6x1 ISO - H TAP ↧ 25.000
5 DRILL (5.000) ↧ 27.000 -(8) HOLE
17
16
8
10-32 UNF- 2B TAP ↧ 6.000
#21 DRILL (4.039) ↧ 10.000 -(4) HOLE
16
101.6 (4")
176
70.01
50.8 (2")
55
10
10
50.8 (2")
38
7.0 DRILL (7.000) THRU -(4) HOLE
310
190
70
92
140 155 210
R7
140
R5 (Typ.)
3/8-16 UNC- 2B TAP THRU
5/16 DRILL (7.938) THRU -(4) HOLES
1-14 UNF- 2B TAP THRU
.9274 DRILL (23.556) THRU -(1) HOLE
31.75 (1 in.)
17
8
30
M6x1 ISO - H TAP ↧ 25.000
5 DRILL (5.000) ↧ 27.000 -(8) HOLE
6 Holes
16
Ø13.49
Ø20
Ø21
Ø8.5
15
SECTION D-D
M6x1 ISO - H CLEAR
THRU -(4) HOLE
A1
260±0.1
30x3
15
75
150±0.1
D
D
16x3
8
A1
M6x1 ISO - H TAP THRU
5 DRILL (5.000) THRU -(4) HOLE
Third Angle Projection
THE INFORMATION CONTAINED IN THIS DRAWING IS THE SOLE PROPERTY OF THE DEPARTMENT OF MECHANICAL ENGINEERING, UNIVERSITY OF ALBERTA. ANY REPRODUCTION IN PART OR IN WHOLE WITHOUT THE WRITTEN PERMISSION OF THE DEPARTMENT OF MECHANICAL ENGINEERING, UNIVERSITY OF ALBERTA, IS PROHIBITED.
DEPARTMENT OF MECHANICAL ENGINEERING
UNIVERSITY OF ALBERTA
TOLERANCES
Unless otherwise specified
SURFACE FINISH
Unless otherwise specified
DRAWN BY
M.Azadi
DATE
04-Sep-08
CUST APPR
ENG APPR
MFG APPR
IMPERIAL
METRIC
Machined
Non Machined
Rolled,Cast,Forged
TITLE
Base
DWG NO.
1 Number
REV
1.1
PART FILE NAME
BASE2
SIZE
B
SCALE
0.250
UNITS
MMNS
SHEET
1 OF 1

Appendix B

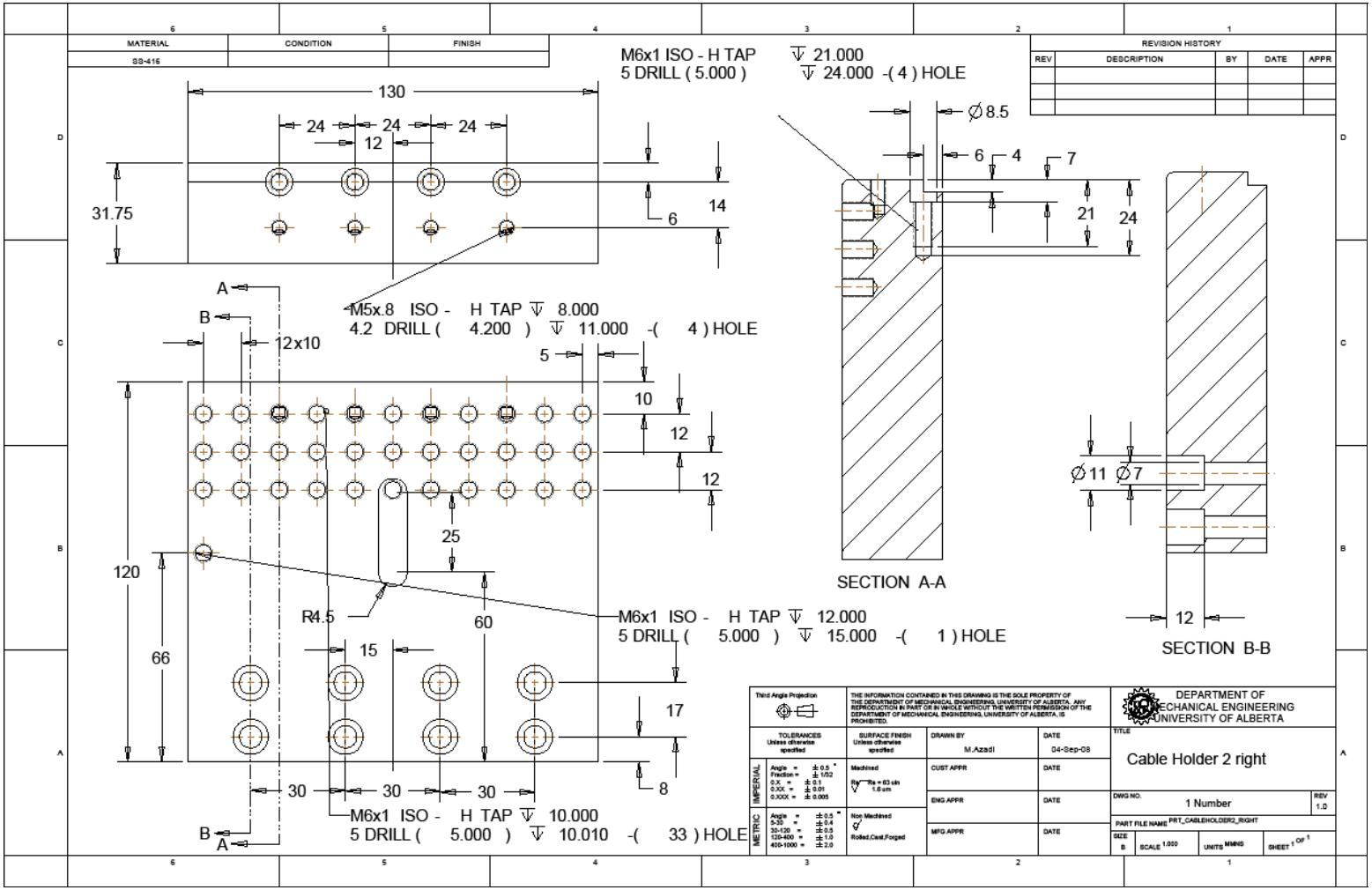
MATERIAL
SS-415
CONDITION
FINISH
REVISION HISTORY
REV
DESCRIPTION
BY
DATE
APPR
M6x1 ISO - H TAP ↧ 21.000
5 DRILL (5.000) ↧ 24.000 -(4) HOLE
130
24
24
24
12
31.75
6
14
M5x.8 ISO - H TAP ↧ 8.000
4.2 DRILL (4.200) ↧ 11.000 -(4) HOLE
A
B
12x10
5
10
12
12
25
120
66
R4.5
60
15
M6x1 ISO - H TAP ↧ 12.000
5 DRILL (5.000) ↧ 15.000 -(1) HOLE
17
8
30
30
30
M6x1 ISO - H TAP ↧ 10.000
5 DRILL (5.000) ↧ 10.010 -(33) HOLE
B
A
Ø8.5
6
4
7
21
24
SECTION A-A
Ø11
Ø7
12
SECTION B-B
Third Angle Projection
THE INFORMATION CONTAINED IN THIS DRAWING IS THE SOLE PROPERTY OF THE DEPARTMENT OF MECHANICAL ENGINEERING, UNIVERSITY OF ALBERTA. ANY REPRODUCTION IN PART OR IN WHOLE WITHOUT THE WRITTEN PERMISSION OF THE DEPARTMENT OF MECHANICAL ENGINEERING, UNIVERSITY OF ALBERTA, IS PROHIBITED.
DEPARTMENT OF MECHANICAL ENGINEERING UNIVERSITY OF ALBERTA
TOLERANCES Unless otherwise specified
SURFACE FINISH Unless otherwise specified
DRAWN BY M.Azadi
DATE 04-Sep-08
IMPERIAL
METRIC
Machined
Non Machined
Rolled,Cast,Forged
CUST APPR
ENG APPR
MFG APPR
DATE
TITLE
Cable Holder 2 right
DWG NO. 1 Number
REV 1.0
PART FILE NAME PRT_CABLEHOLDER2_RIGHT
SIZE B
SCALE 1.000
UNITS MMNS
SHEET 1 OF 1

Appendix B

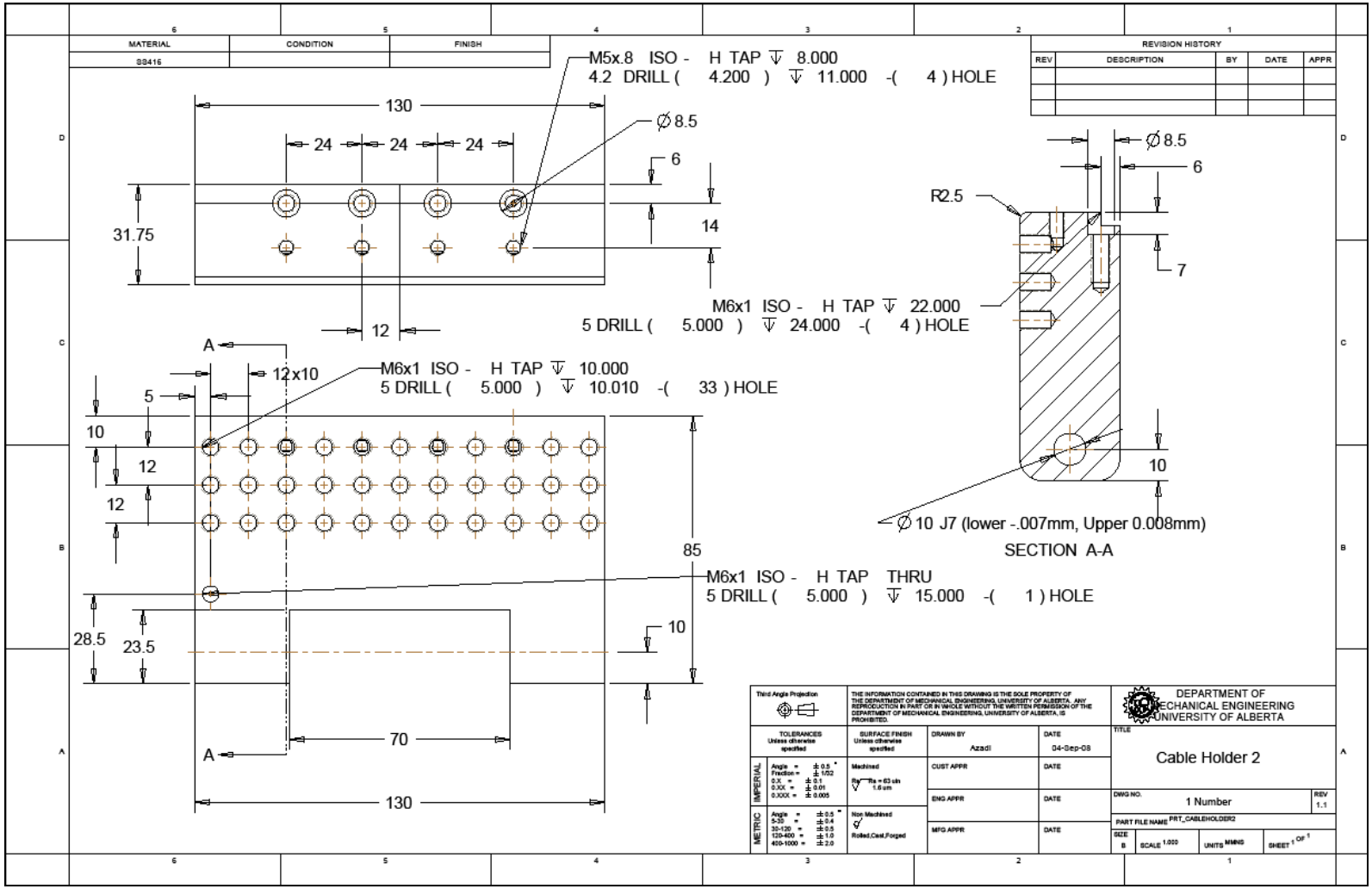
MATERIAL
SS416
CONDITION
FINISH
REVISION HISTORY
REV
DESCRIPTION
BY
DATE
APPR
M5x.8 ISO - H TAP ↧ 8.000
4.2 DRILL (4.200) ↧ 11.000 -(4) HOLE
130
24
24
24
Ø8.5
6
14
31.75
12
M6x1 ISO - H TAP ↧ 22.000
5 DRILL (5.000) ↧ 24.000 -(4) HOLE
R2.5
Ø8.5
6
7
10
Ø10 J7 (lower -.007mm, Upper 0.008mm)
SECTION A-A
A
12x10
M6x1 ISO - H TAP ↧ 10.000
5 DRILL (5.000) ↧ 10.010 -(33) HOLE
5
10
12
12
85
M6x1 ISO - H TAP THRU
5 DRILL (5.000) ↧ 15.000 -(1) HOLE
28.5
23.5
10
70
130
Third Angle Projection
THE INFORMATION CONTAINED IN THIS DRAWING IS THE SOLE PROPERTY OF THE DEPARTMENT OF MECHANICAL ENGINEERING, UNIVERSITY OF ALBERTA. ANY REPRODUCTION IN PART OR IN WHOLE WITHOUT THE WRITTEN PERMISSION OF THE DEPARTMENT OF MECHANICAL ENGINEERING, UNIVERSITY OF ALBERTA, IS PROHIBITED.
DEPARTMENT OF MECHANICAL ENGINEERING
UNIVERSITY OF ALBERTA
TOLERANCES
Unless otherwise specified
SURFACE FINISH
Unless otherwise specified
DRAWN BY
Azadi
DATE
04-Sep-08
CUST APPR
ENG APPR
MFG APPR
IMPERIAL
METRIC
Machined
Non Machined
Rolled,Cast,Forged
TITLE
Cable Holder 2
DWG NO.
1 Number
REV
1.1
PART FILE NAME PRT_CABLEHOLDER2
SIZE
B
SCALE 1.000
UNITS MMNS
SHEET 1 OF 1

Appendix B

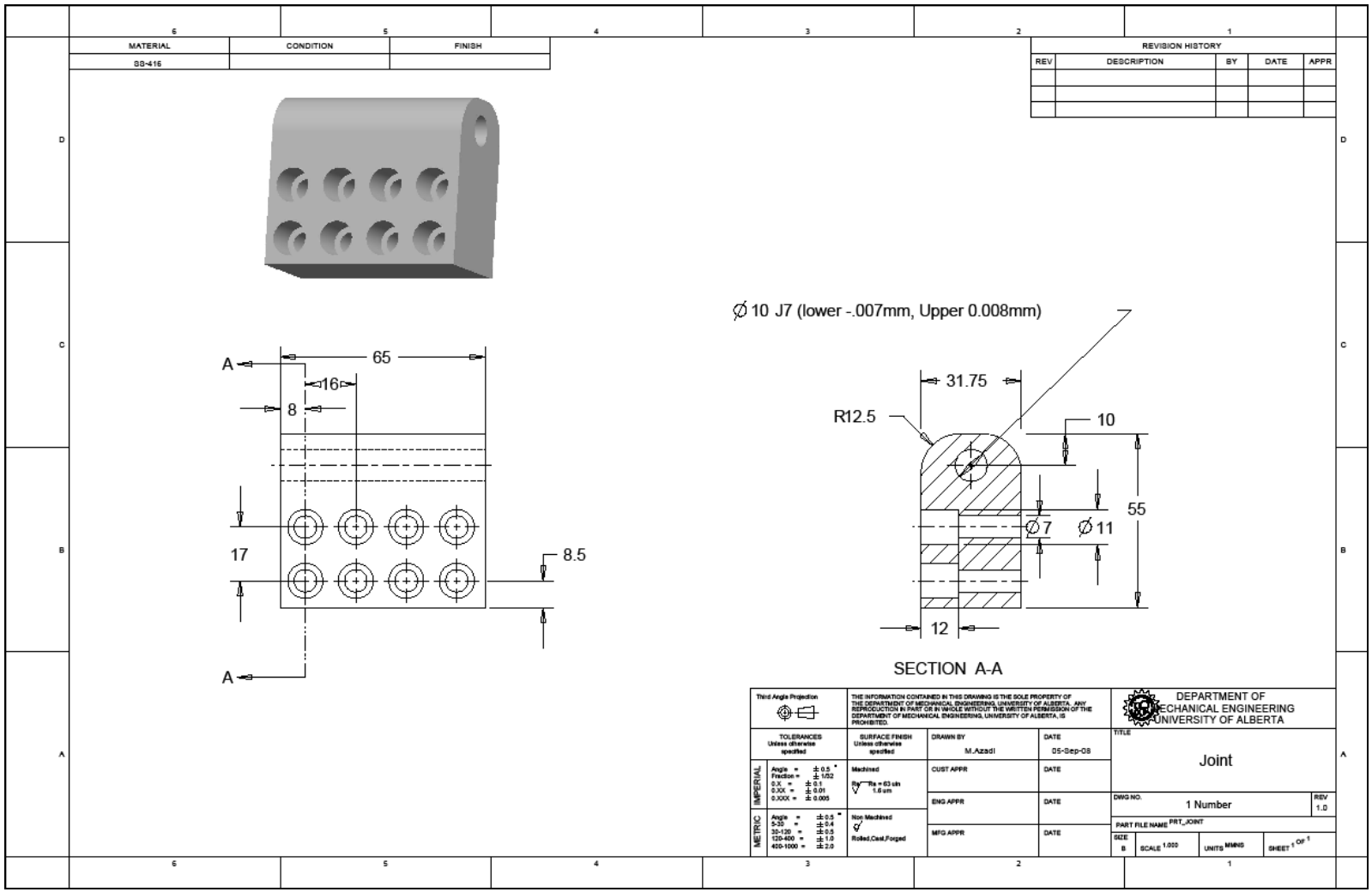
MATERIAL
SS-416
CONDITION
FINISH
REVISION HISTORY
REV
DESCRIPTION
BY
DATE
APPR
∅10 J7 (lower -.007mm, Upper 0.008mm)
65
16
8
17
8.5
A
A
31.75
R12.5
10
55
∅7
∅11
12
SECTION A-A
Third Angle Projection
THE INFORMATION CONTAINED IN THIS DRAWING IS THE SOLE PROPERTY OF THE DEPARTMENT OF MECHANICAL ENGINEERING, UNIVERSITY OF ALBERTA. ANY REPRODUCTION IN PART OR IN WHOLE WITHOUT THE WRITTEN PERMISSION OF THE DEPARTMENT OF MECHANICAL ENGINEERING, UNIVERSITY OF ALBERTA, IS PROHIBITED.
DEPARTMENT OF MECHANICAL ENGINEERING
UNIVERSITY OF ALBERTA
TOLERANCES
Unless otherwise specified
SURFACE FINISH
Unless otherwise specified
DRAWN BY
M.Azadi
DATE
05-Sep-08
CUST APPR
ENG APPR
MFG APPR
IMPERIAL
METRIC
Machined
Ra = 63 uin
1.6 um
Non Machined
Rolled,Cast,Forged
TITLE
Joint
DWG NO.
1 Number
REV
1.0
PART FILE NAME
PRT_JOINT
SIZE
B
SCALE 1.000
UNITS MMNS
SHEET 1 OF 1

Appendix B

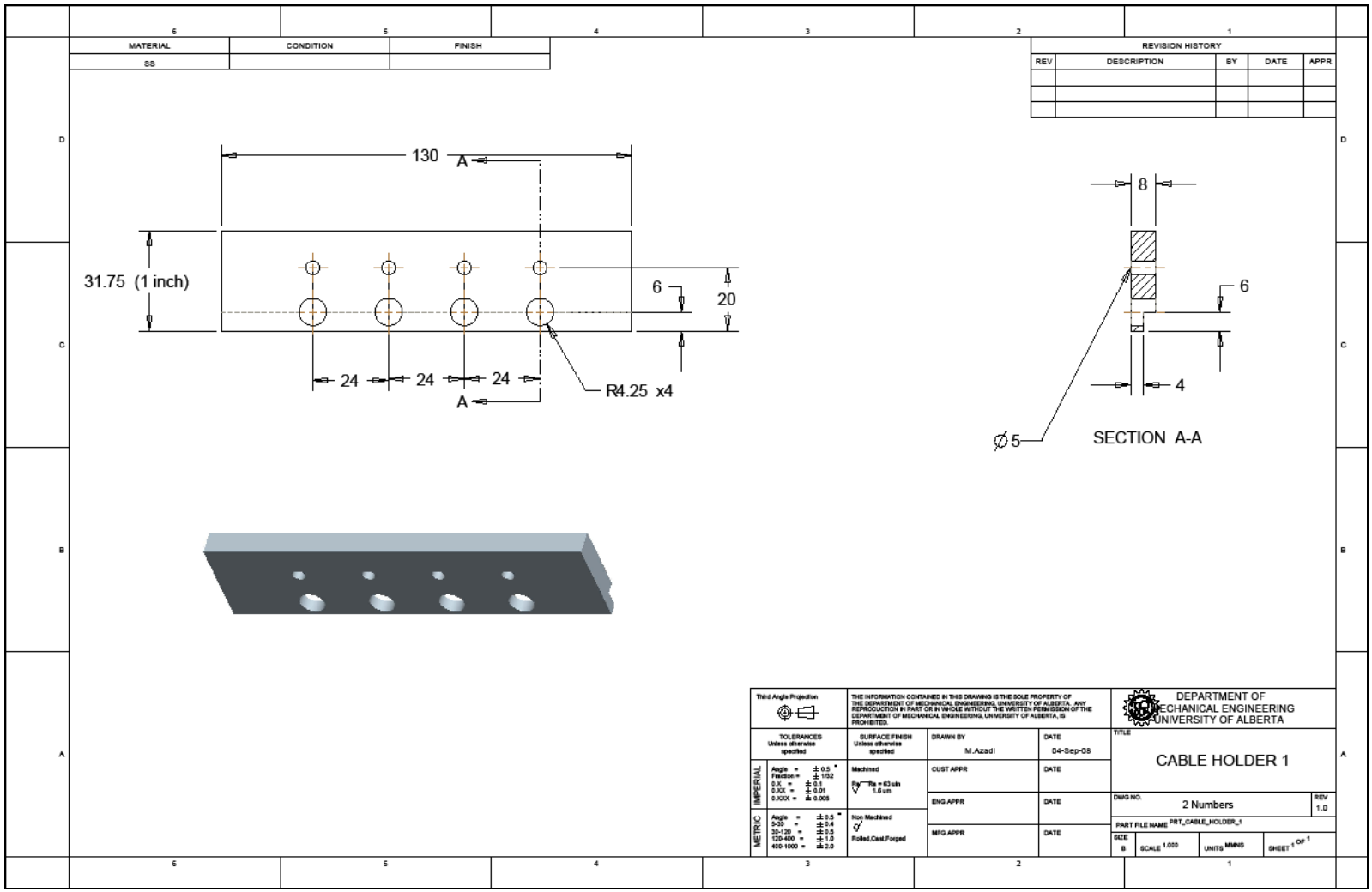
MATERIAL
CONDITION
FINISH
SS
REVISION HISTORY
REV
DESCRIPTION
BY
DATE
APPR
130
A
31.75 (1 inch)
6
20
24
24
24
R4.25 x4
A
8
6
4
Ø5
SECTION A-A
DEPARTMENT OF MECHANICAL ENGINEERING
UNIVERSITY OF ALBERTA
CABLE HOLDER 1
DRAWN BY
M.Azadi
04-Sep-08
2 Numbers
PART_CABLE_HOLDER_1
SCALE 1.000
UNITS MMNS

Appendix B

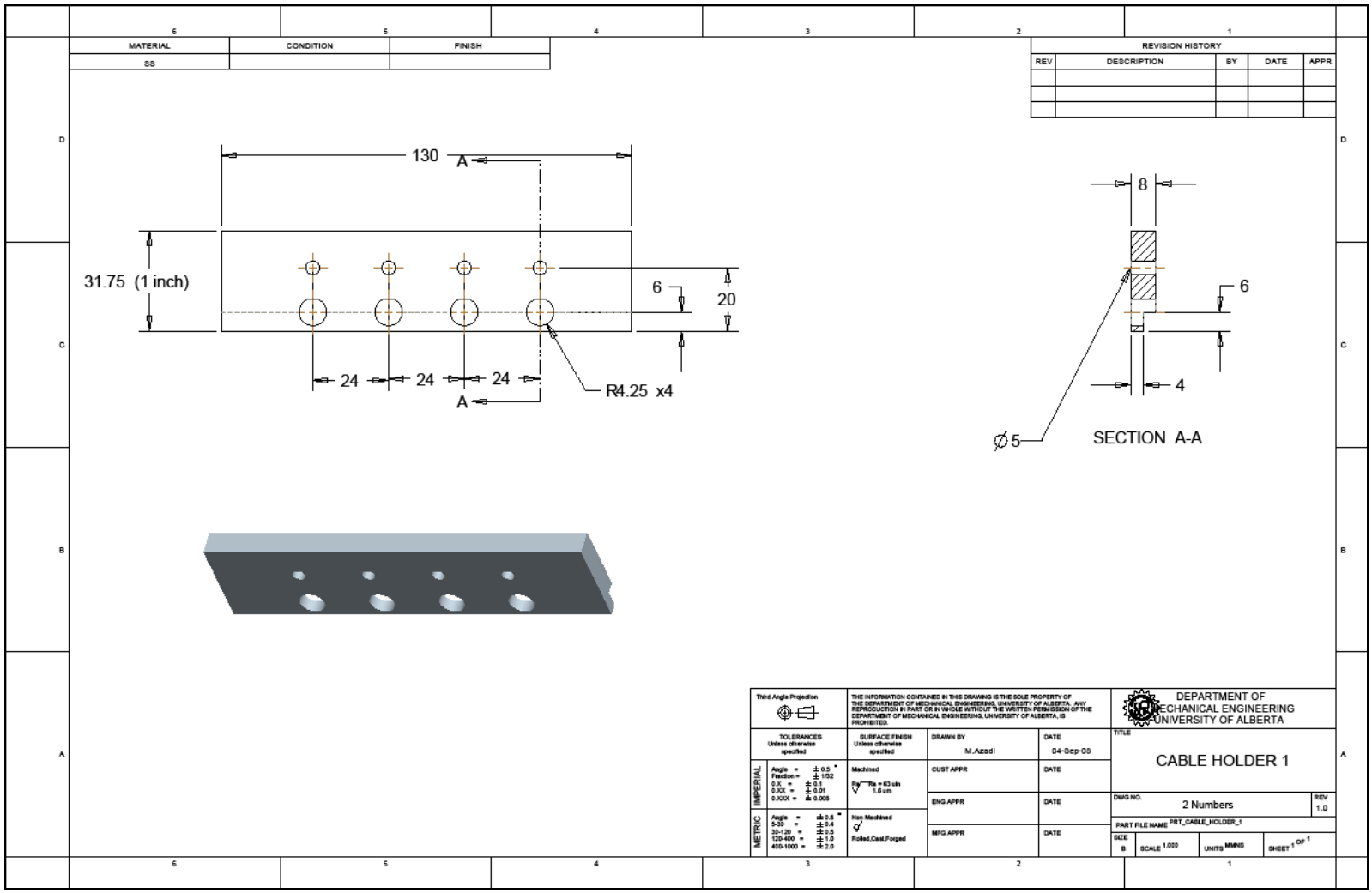
MATERIAL
CONDITION
FINISH
SS
REVISION HISTORY
REV
DESCRIPTION
BY
DATE
APPR
130
A
31.75 (1 inch)
6
20
24
24
24
R4.25 x4
A
8
6
4
Ø5
SECTION A-A
DEPARTMENT OF MECHANICAL ENGINEERING
UNIVERSITY OF ALBERTA
CABLE HOLDER 1
DRAWN BY
M.Azadi
04-Sep-08
2 Numbers
PART FILE NAME PRT_CABLE_HOLDER_1
SIZE B
SCALE 1.000
UNITS MMNS
SHEET 1 OF 1

Appendix B

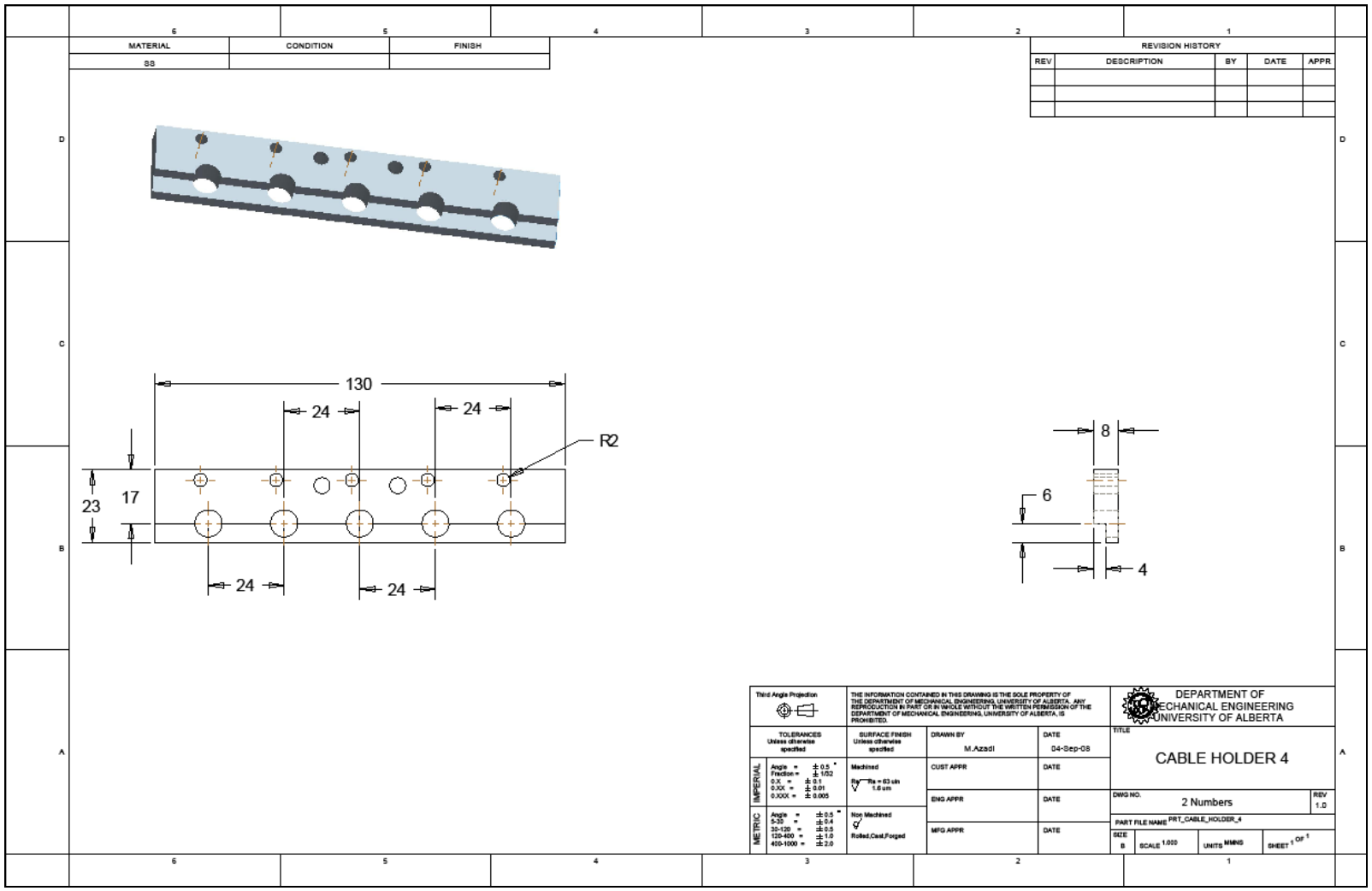
MATERIAL
SS
CONDITION
FINISH
REVISION HISTORY
REV
DESCRIPTION
BY
DATE
APPR
130
24
24
R2
23
17
24
24
8
6
4
Third Angle Projection
THE INFORMATION CONTAINED IN THIS DRAWING IS THE SOLE PROPERTY OF THE DEPARTMENT OF MECHANICAL ENGINEERING, UNIVERSITY OF ALBERTA. ANY REPRODUCTION IN PART OR IN WHOLE WITHOUT THE WRITTEN PERMISSION OF THE DEPARTMENT OF MECHANICAL ENGINEERING, UNIVERSITY OF ALBERTA, IS PROHIBITED.
DEPARTMENT OF MECHANICAL ENGINEERING
UNIVERSITY OF ALBERTA
TOLERANCES
Unless otherwise specified
SURFACE FINISH
Unless otherwise specified
DRAWN BY
M.Azadi
DATE
04-Sep-08
IMPERIAL
METRIC
Machined
Non Machined
Rolled,Cast,Forged
CUST APPR
ENG APPR
MFG APPR
TITLE
CABLE HOLDER 4
DWG NO.
2 Numbers
REV
1.0
PART FILE NAME
PRT_CABLE_HOLDER_4
SIZE
B
SCALE 1.000
UNITS MMNS
SHEET 1 OF 1

Appendix B

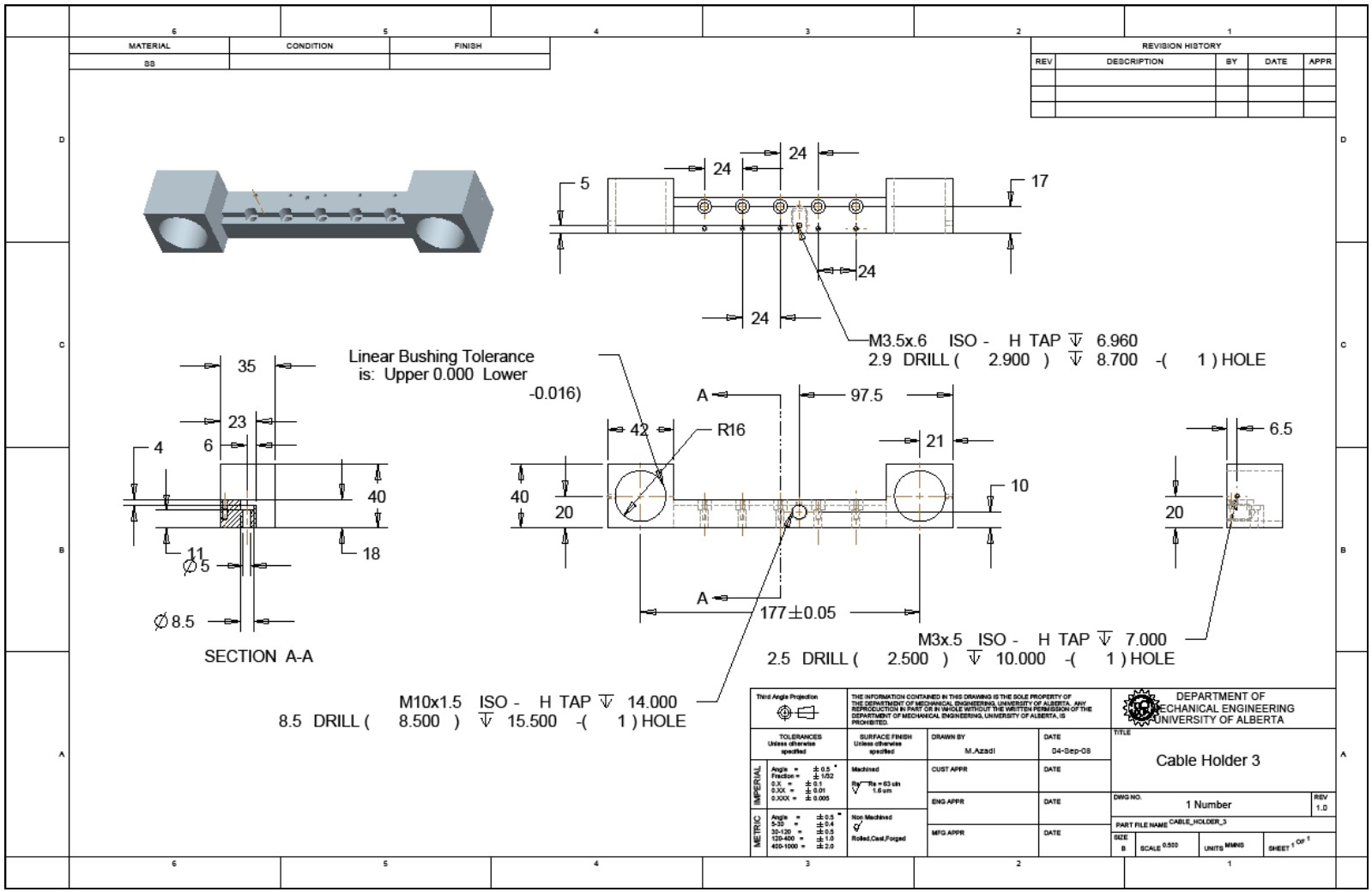
MATERIAL
SS
CONDITION
FINISH
REVISION HISTORY
REV
DESCRIPTION
BY
DATE
APPR
24
24
5
17
24
24
M3.5x.6 ISO - H TAP 6.960
2.9 DRILL (2.900) 8.700 -(1) HOLE
Linear Bushing Tolerance
is: Upper 0.000 Lower
-0.016)
35
23
6
4
40
18
11
Ø5
Ø8.5
SECTION A-A
A
97.5
42
R16
21
10
40
20
A
177±0.05
6.5
20
M3x.5 ISO - H TAP 7.000
2.5 DRILL (2.500) 10.000 -(1) HOLE
M10x1.5 ISO - H TAP 14.000
8.5 DRILL (8.500) 15.500 -(1) HOLE
Third Angle Projection
THE INFORMATION CONTAINED IN THIS DRAWING IS THE SOLE PROPERTY OF THE DEPARTMENT OF MECHANICAL ENGINEERING, UNIVERSITY OF ALBERTA. ANY REPRODUCTION IN PART OR IN WHOLE WITHOUT THE WRITTEN PERMISSION OF THE DEPARTMENT OF MECHANICAL ENGINEERING, UNIVERSITY OF ALBERTA, IS PROHIBITED.
DEPARTMENT OF MECHANICAL ENGINEERING
UNIVERSITY OF ALBERTA
TOLERANCES
Unless otherwise specified
SURFACE FINISH
Unless otherwise specified
DRAWN BY
M.Azadi
DATE
04-Sep-08
CUST APPR
DATE
ENG APPR
DATE
MFG APPR
DATE
IMPERIAL
METRIC
Machined
Non Machined
Rolled,Cast,Forged
TITLE
Cable Holder 3
DWG NO.
1 Number
REV
1.0
PART FILE NAME
CABLE_HOLDER_3
SIZE
B
SCALE
0.500
UNITS
MMNS
SHEET
1 OF 1

Appendix B

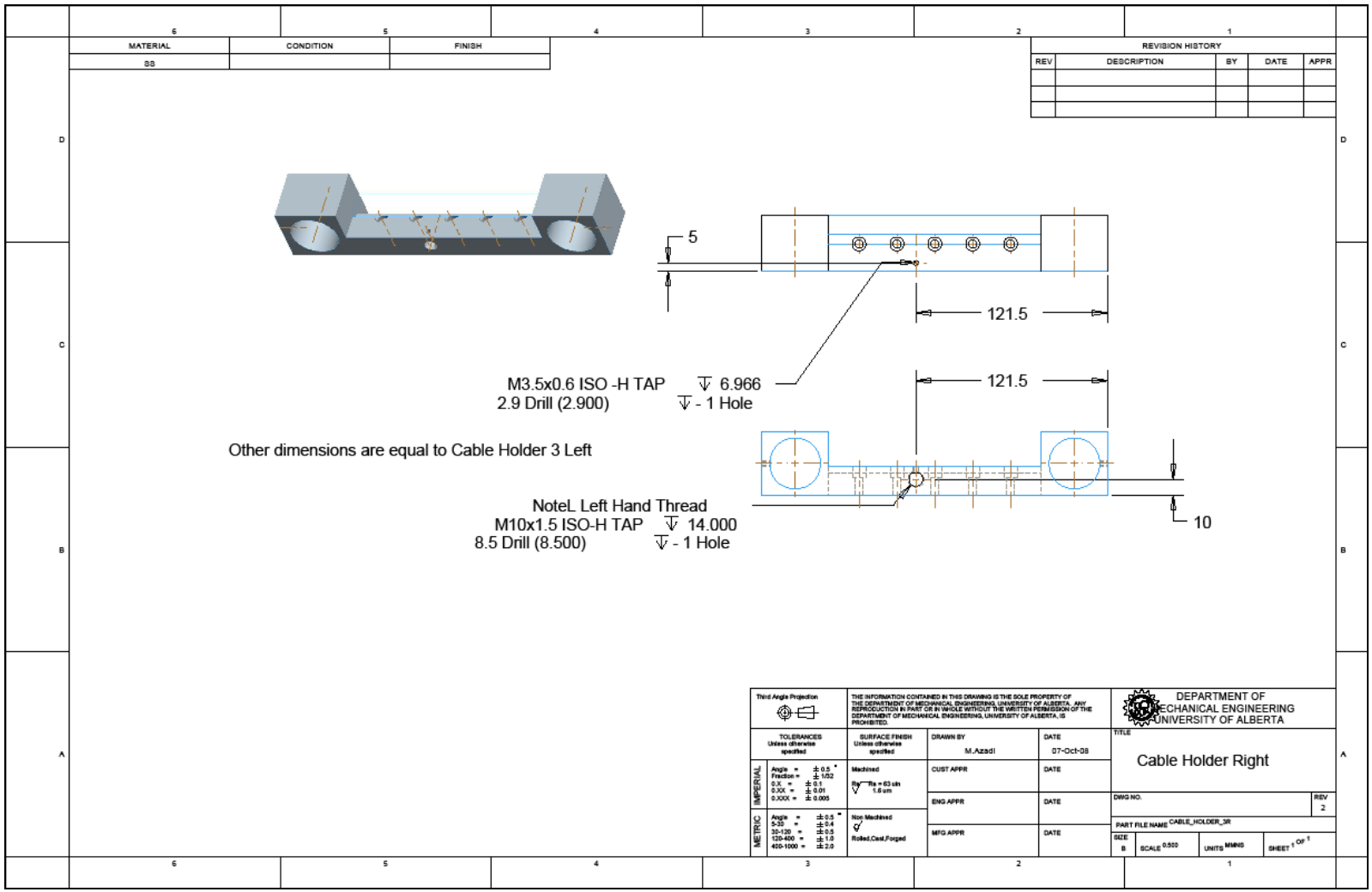
MATERIAL
CONDITION
FINISH
SS
REVISION HISTORY
REV
DESCRIPTION
BY
DATE
APPR
5
121.5
121.5
M3.5x0.6 ISO -H TAP ↧ 6.966
2.9 Drill (2.900) ↧ - 1 Hole
Other dimensions are equal to Cable Holder 3 Left
NoteL Left Hand Thread
M10x1.5 ISO-H TAP ↧ 14.000
8.5 Drill (8.500) ↧ - 1 Hole
10
Third Angle Projection
THE INFORMATION CONTAINED IN THIS DRAWING IS THE SOLE PROPERTY OF THE DEPARTMENT OF MECHANICAL ENGINEERING, UNIVERSITY OF ALBERTA. ANY REPRODUCTION IN PART OR IN WHOLE WITHOUT THE WRITTEN PERMISSION OF THE DEPARTMENT OF MECHANICAL ENGINEERING, UNIVERSITY OF ALBERTA, IS PROHIBITED.
DEPARTMENT OF MECHANICAL ENGINEERING
UNIVERSITY OF ALBERTA
TOLERANCES
Unless otherwise specified
SURFACE FINISH
Unless otherwise specified
DRAWN BY
M.Azadi
DATE
07-Oct-08
CUST APPR
ENG APPR
MFG APPR
IMPERIAL
METRIC
Machined
Ra = 63 uin
1.6 um
Non Machined
Rolled,Cast,Forged
TITLE
Cable Holder Right
DWG NO.
REV
2
PART FILE NAME
CABLE_HOLDER_3R
SIZE
B
SCALE 0.500
UNITS MMNS
SHEET 1 OF 1

Appendix B

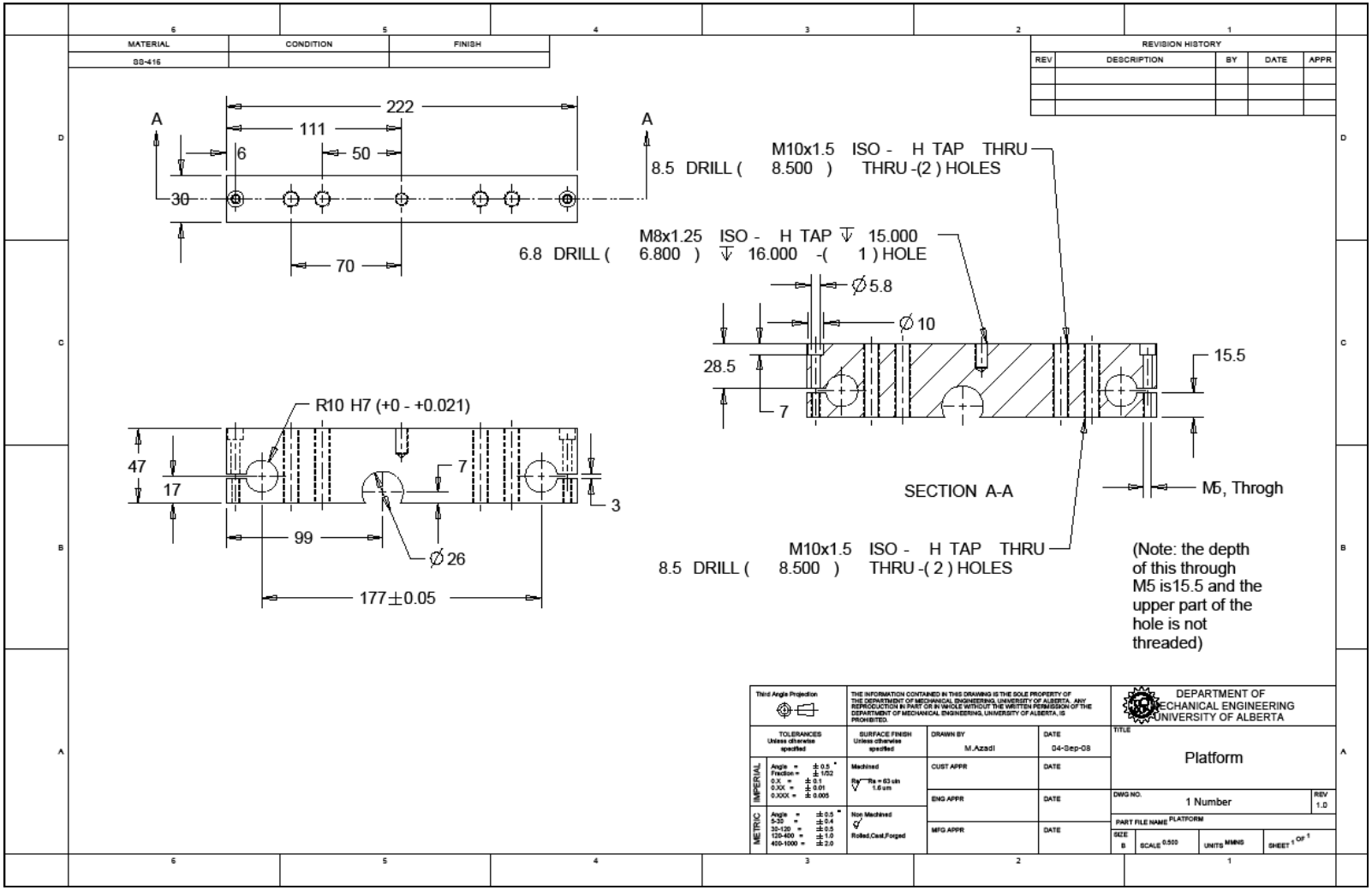
MATERIAL
CONDITION
FINISH
SS-416
REVISION HISTORY
REV
DESCRIPTION
BY
DATE
APPR
222
111
6
50
30
70
A
A
8.5 DRILL (8.500) THRU -(2) HOLES
M10x1.5 ISO - H TAP THRU
M8x1.25 ISO - H TAP ↧ 15.000
6.8 DRILL (6.800) ↧ 16.000 -(1) HOLE
Ø5.8
Ø10
28.5
7
15.5
M5, Throgh
SECTION A-A
R10 H7 (+0 - +0.021)
47
17
7
3
99
Ø26
177±0.05
M10x1.5 ISO - H TAP THRU
8.5 DRILL (8.500) THRU -(2) HOLES
(Note: the depth of this through M5 is15.5 and the upper part of the hole is not threaded)
Third Angle Projection
THE INFORMATION CONTAINED IN THIS DRAWING IS THE SOLE PROPERTY OF THE DEPARTMENT OF MECHANICAL ENGINEERING, UNIVERSITY OF ALBERTA. ANY REPRODUCTION IN PART OR IN WHOLE WITHOUT THE WRITTEN PERMISSION OF THE DEPARTMENT OF MECHANICAL ENGINEERING, UNIVERSITY OF ALBERTA, IS PROHIBITED.
DEPARTMENT OF MECHANICAL ENGINEERING UNIVERSITY OF ALBERTA
TOLERANCES Unless otherwise specified
SURFACE FINISH Unless otherwise specified
DRAWN BY M.Azadi
DATE 04-Sep-08
CUST APPR
ENG APPR
MFG APPR
TITLE Platform
DWG NO. 1 Number
REV 1.0
PART FILE NAME PLATFORM
SIZE B
SCALE 0.500
UNITS MMNS
SHEET 1 OF 1

Appendix B

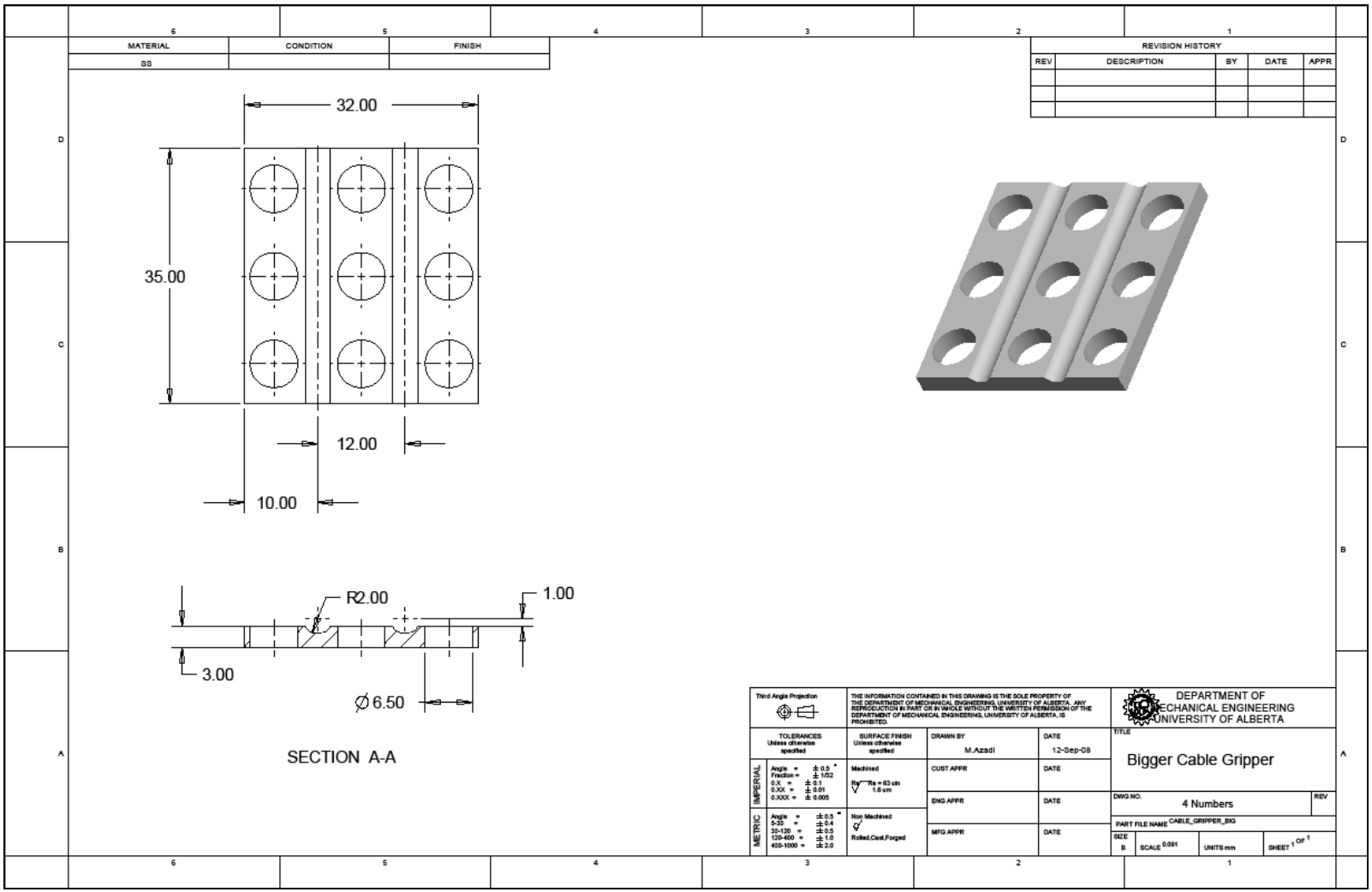
MATERIAL
CONDITION
FINISH
SS
REVISION HISTORY
REV
DESCRIPTION
BY
DATE
APPR
32.00
35.00
12.00
10.00
R2.00
1.00
3.00
Ø6.50
SECTION A-A
Third Angle Projection
THE INFORMATION CONTAINED IN THIS DRAWING IS THE SOLE PROPERTY OF THE DEPARTMENT OF MECHANICAL ENGINEERING, UNIVERSITY OF ALBERTA. ANY REPRODUCTION IN PART OR IN WHOLE WITHOUT THE WRITTEN PERMISSION OF THE DEPARTMENT OF MECHANICAL ENGINEERING, UNIVERSITY OF ALBERTA, IS PROHIBITED.
DEPARTMENT OF MECHANICAL ENGINEERING
UNIVERSITY OF ALBERTA
TOLERANCES
Unless otherwise specified
SURFACE FINISH
Unless otherwise specified
DRAWN BY
M.Azadi
DATE
12-Sep-08
IMPERIAL
METRIC
Machined
Non Machined
Rolled,Cast,Forged
CUST APPR
ENG APPR
MFG APPR
TITLE
Bigger Cable Gripper
DWG NO.
4 Numbers
REV
PART FILE NAME
CABLE_GRIPPER_BIG
SIZE
B
SCALE 0.091
UNITS mm
SHEET 1 OF 1

Appendix B

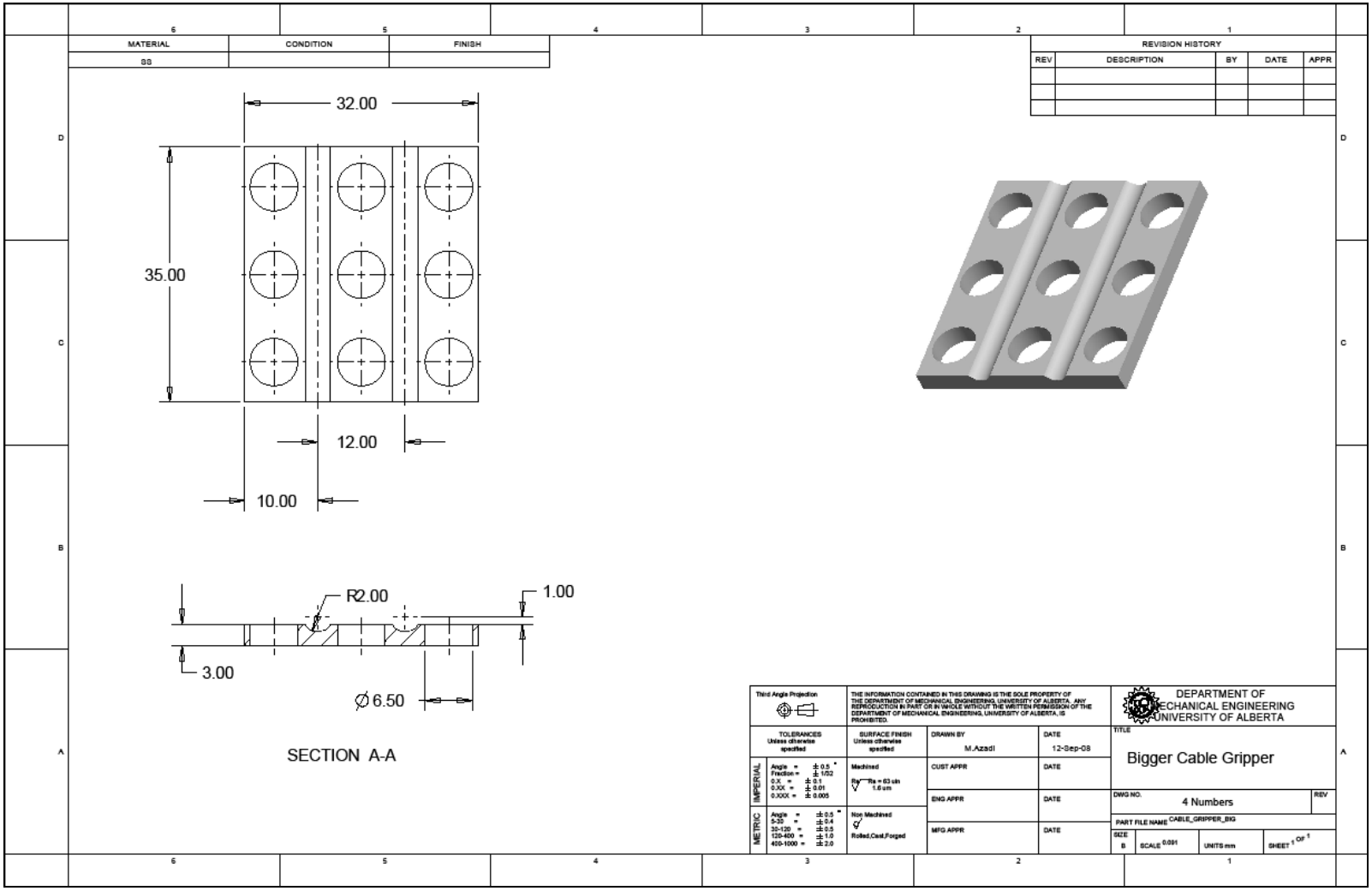
MATERIAL
CONDITION
FINISH
SS
REVISION HISTORY
REV
DESCRIPTION
BY
DATE
APPR
32.00
35.00
12.00
10.00
R2.00
1.00
3.00
Ø6.50
SECTION A-A
Third Angle Projection
THE INFORMATION CONTAINED IN THIS DRAWING IS THE SOLE PROPERTY OF THE DEPARTMENT OF MECHANICAL ENGINEERING, UNIVERSITY OF ALBERTA. ANY REPRODUCTION IN PART OR IN WHOLE WITHOUT THE WRITTEN PERMISSION OF THE DEPARTMENT OF MECHANICAL ENGINEERING, UNIVERSITY OF ALBERTA, IS PROHIBITED.
DEPARTMENT OF MECHANICAL ENGINEERING
UNIVERSITY OF ALBERTA
TOLERANCES
Unless otherwise specified
SURFACE FINISH
Unless otherwise specified
DRAWN BY
M.Azadi
DATE
12-Sep-08
TITLE
Bigger Cable Gripper
IMPERIAL
METRIC
Machined
Non Machined
Rolled,Cast,Forged
CUST APPR
ENG APPR
MFG APPR
DWG NO.
4 Numbers
REV
PART FILE NAME
CABLE_GRIPPER_BIG
SIZE
B
SCALE 0.091
UNITS mm
SHEET 1 OF 1

Appendix B

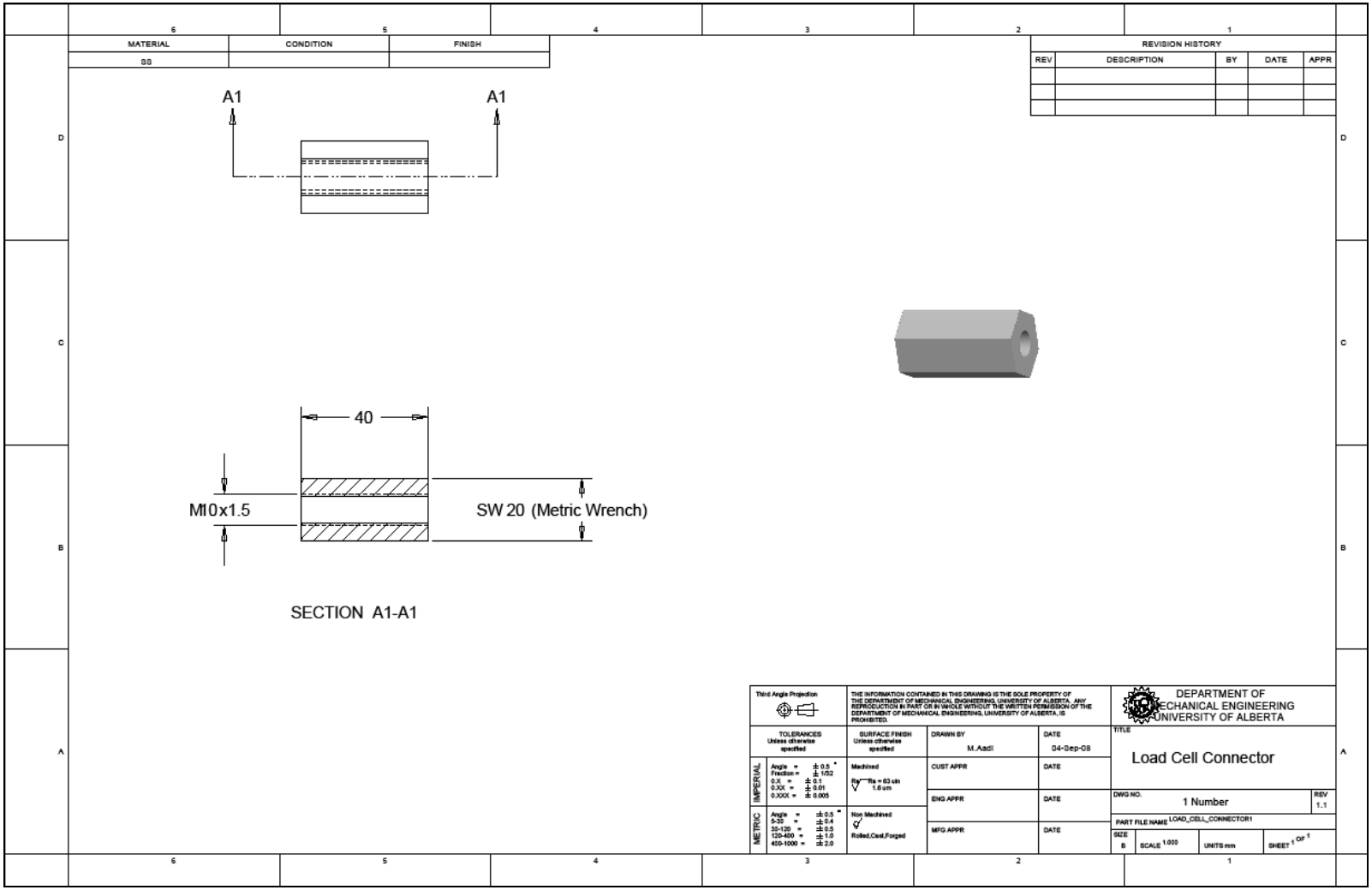
MATERIAL
SS
CONDITION
FINISH
REVISION HISTORY
REV
DESCRIPTION
BY
DATE
APPR
A1
A1
40
M10x1.5
SW 20 (Metric Wrench)
SECTION A1-A1
Third Angle Projection
THE INFORMATION CONTAINED IN THIS DRAWING IS THE SOLE PROPERTY OF THE DEPARTMENT OF MECHANICAL ENGINEERING, UNIVERSITY OF ALBERTA. ANY REPRODUCTION IN PART OR IN WHOLE WITHOUT THE WRITTEN PERMISSION OF THE DEPARTMENT OF MECHANICAL ENGINEERING, UNIVERSITY OF ALBERTA, IS PROHIBITED.
DEPARTMENT OF MECHANICAL ENGINEERING
UNIVERSITY OF ALBERTA
TOLERANCES
Unless otherwise specified
SURFACE FINISH
Unless otherwise specified
DRAWN BY
M.Aadil
DATE
04-Sep-08
IMPERIAL
METRIC
Machined
Non Machined
Rolled,Cast,Forged
CUST APPR
ENG APPR
MFG APPR
TITLE
Load Cell Connector
DWG NO.
1 Number
REV
1.1
PART FILE NAME
LOAD_CELL_CONNECTOR1
SIZE
B
SCALE 1.000
UNITS mm
SHEET 1 OF 1

Appendix B

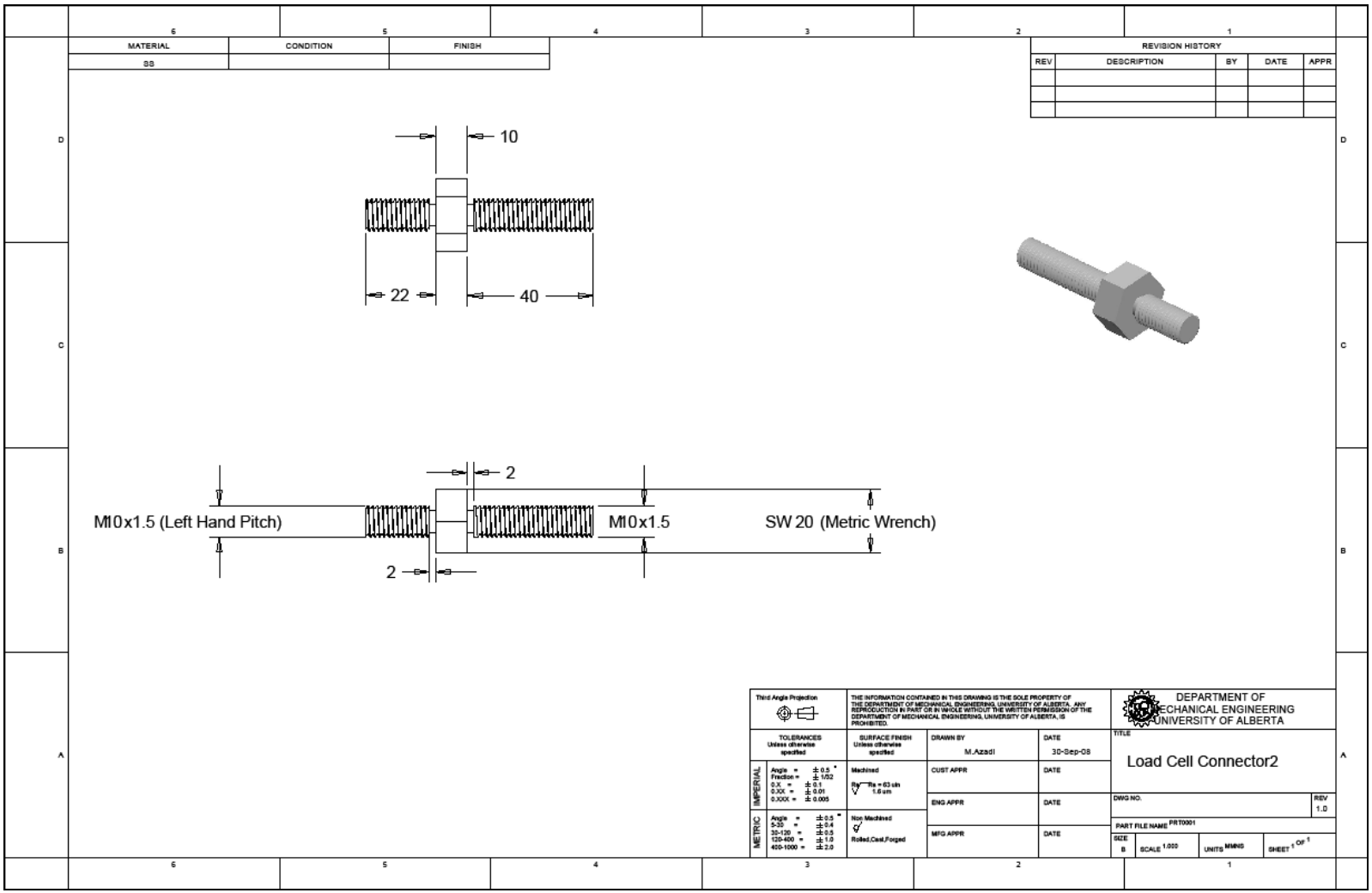
MATERIAL
CONDITION
FINISH
SS
REVISION HISTORY
REV
DESCRIPTION
BY
DATE
APPR
10
22
40
2
M10x1.5 (Left Hand Pitch)
M10x1.5
SW 20 (Metric Wrench)
2
Third Angle Projection
THE INFORMATION CONTAINED IN THIS DRAWING IS THE SOLE PROPERTY OF THE DEPARTMENT OF MECHANICAL ENGINEERING, UNIVERSITY OF ALBERTA. ANY REPRODUCTION IN PART OR IN WHOLE WITHOUT THE WRITTEN PERMISSION OF THE DEPARTMENT OF MECHANICAL ENGINEERING, UNIVERSITY OF ALBERTA, IS PROHIBITED.
DEPARTMENT OF MECHANICAL ENGINEERING
UNIVERSITY OF ALBERTA
TOLERANCES
Unless otherwise specified
SURFACE FINISH
Unless otherwise specified
DRAWN BY
M.Azadi
DATE
30-Sep-08
IMPERIAL
METRIC
Machined
Non Machined
Rolled,Cast,Forged
CUST APPR
ENG APPR
MFG APPR
TITLE
Load Cell Connector2
DWG NO.
REV
1.0
PART FILE NAME PRT0001
SIZE
B
SCALE 1.000
UNITS MMS
SHEET 1 OF 1

Appendix B

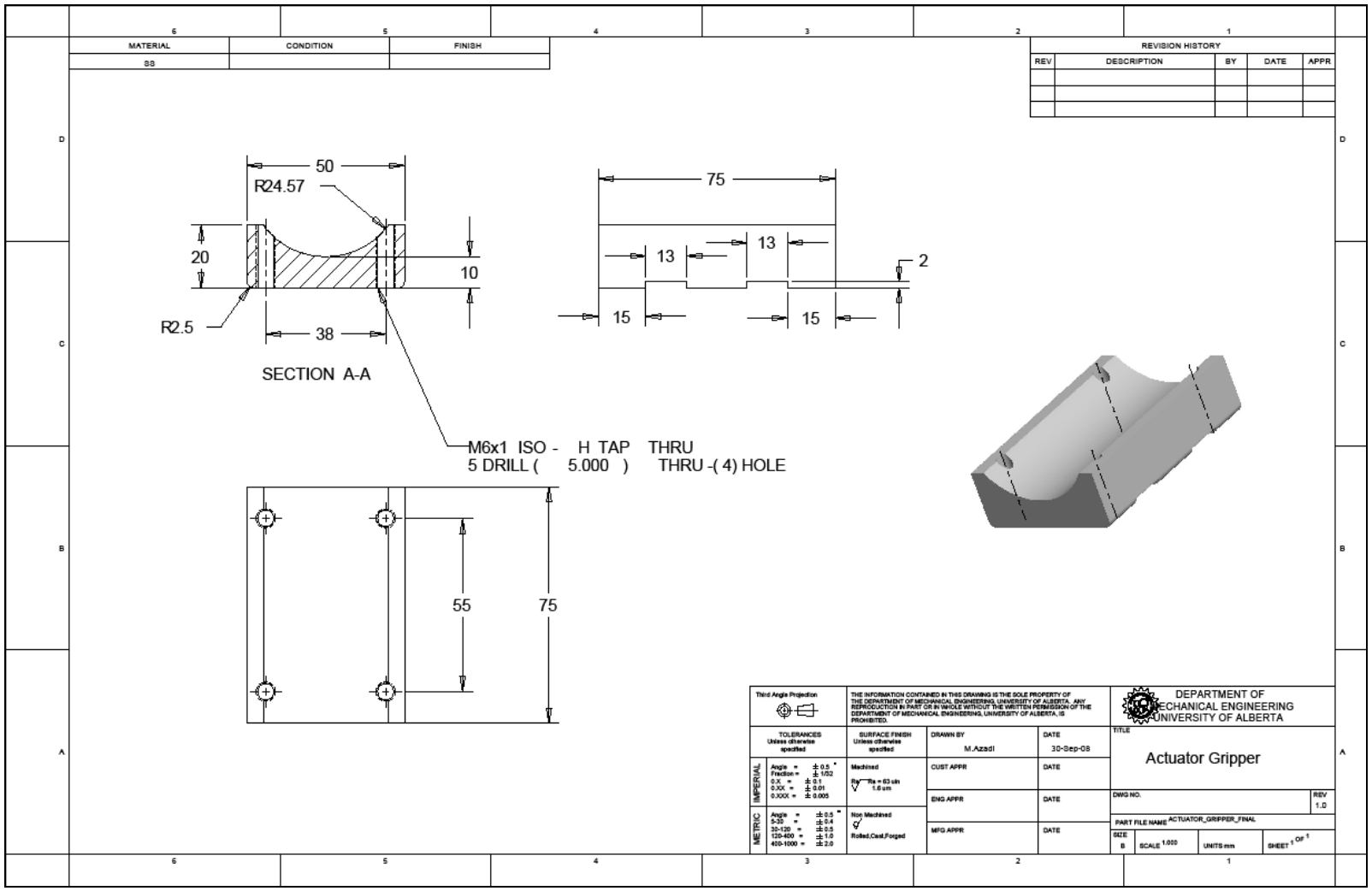
MATERIAL
CONDITION
FINISH
SS
REVISION HISTORY
REV
DESCRIPTION
BY
DATE
APPR
50
R24.57
20
10
R2.5
38
SECTION A-A
75
13
13
2
15
15
M6x1 ISO - H TAP THRU
5 DRILL (5.000) THRU -(4) HOLE
55
75
Third Angle Projection
THE INFORMATION CONTAINED IN THIS DRAWING IS THE SOLE PROPERTY OF THE DEPARTMENT OF MECHANICAL ENGINEERING, UNIVERSITY OF ALBERTA. ANY REPRODUCTION IN PART OR IN WHOLE WITHOUT THE WRITTEN PERMISSION OF THE DEPARTMENT OF MECHANICAL ENGINEERING, UNIVERSITY OF ALBERTA, IS PROHIBITED.
DEPARTMENT OF MECHANICAL ENGINEERING
UNIVERSITY OF ALBERTA
TOLERANCES
Unless otherwise specified
SURFACE FINISH
Unless otherwise specified
DRAWN BY
M.Azadi
DATE
30-Sep-08
IMPERIAL
METRIC
Machined
Non Machined
Rolled,Cast,Forged
CUST APPR
ENG APPR
MFG APPR
TITLE
Actuator Gripper
DWG NO.
REV
1.0
PART FILE NAME
ACTUATOR_GRIPPER_FINAL
SIZE
B
SCALE 1.000
UNITS mm
SHEET 1 OF 1

Appendix B

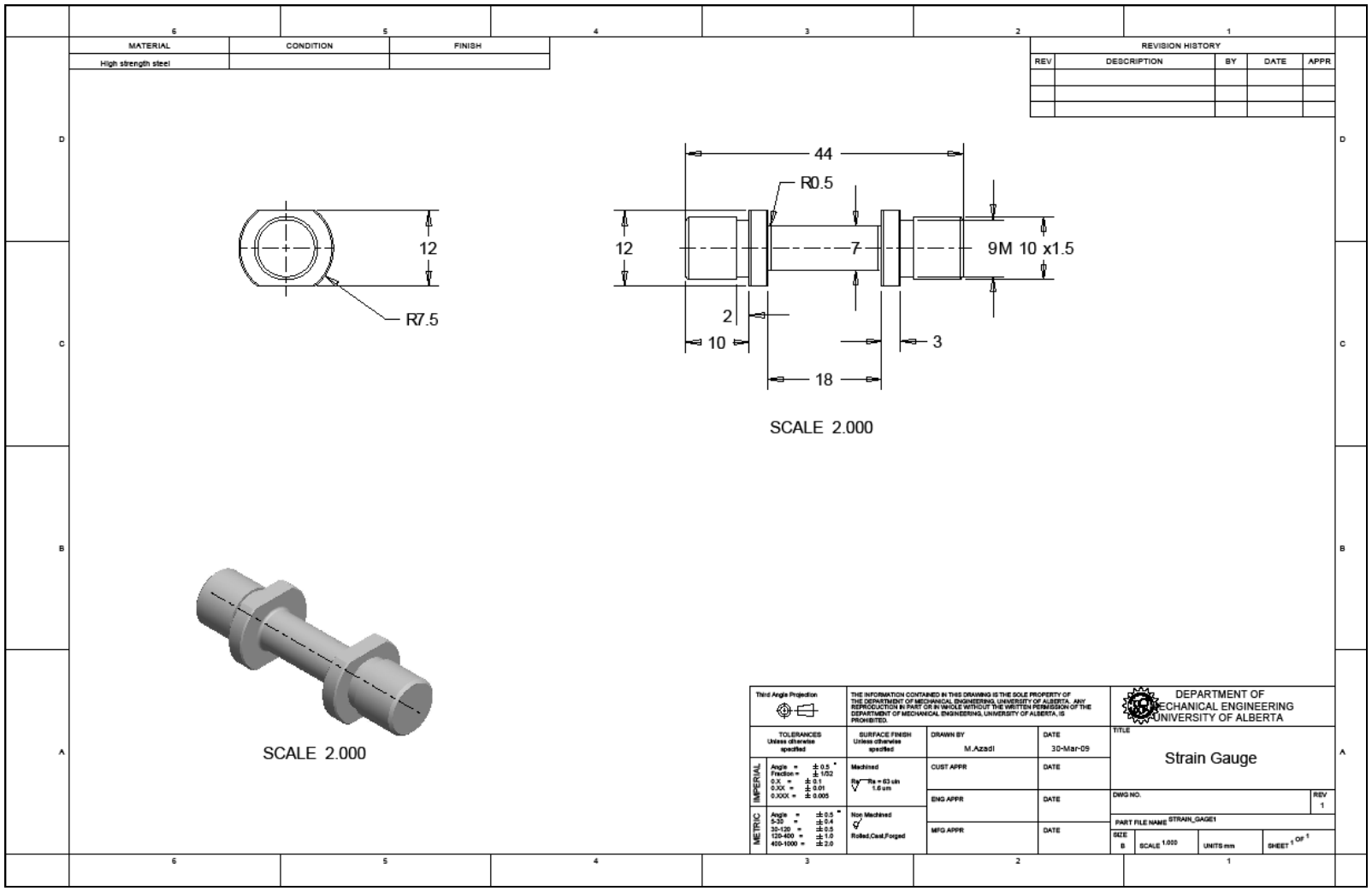
MATERIAL
CONDITION
FINISH
High strength steel
REVISION HISTORY
REV
DESCRIPTION
BY
DATE
APPR
44
R0.5
12
12
7
9M 10 x1.5
R7.5
2
10
3
18
SCALE 2.000
SCALE 2.000
Third Angle Projection
THE INFORMATION CONTAINED IN THIS DRAWING IS THE SOLE PROPERTY OF THE DEPARTMENT OF MECHANICAL ENGINEERING, UNIVERSITY OF ALBERTA. ANY REPRODUCTION IN PART OR IN WHOLE WITHOUT THE WRITTEN PERMISSION OF THE DEPARTMENT OF MECHANICAL ENGINEERING, UNIVERSITY OF ALBERTA, IS PROHIBITED.
DEPARTMENT OF MECHANICAL ENGINEERING
UNIVERSITY OF ALBERTA
TOLERANCES
Unless otherwise specified
SURFACE FINISH
Unless otherwise specified
DRAWN BY
M.Azadi
DATE
30-Mar-09
TITLE
Strain Gauge
IMPERIAL
METRIC
Machined
Non Machined
Rolled,Cast,Forged
CUST APPR
ENG APPR
MFG APPR
DATE
DWG NO.
REV
1
PART FILE NAME
STRAIN_GAGE1
SIZE
B
SCALE 1.000
UNITS mm
SHEET 1 OF 1

Appendix B

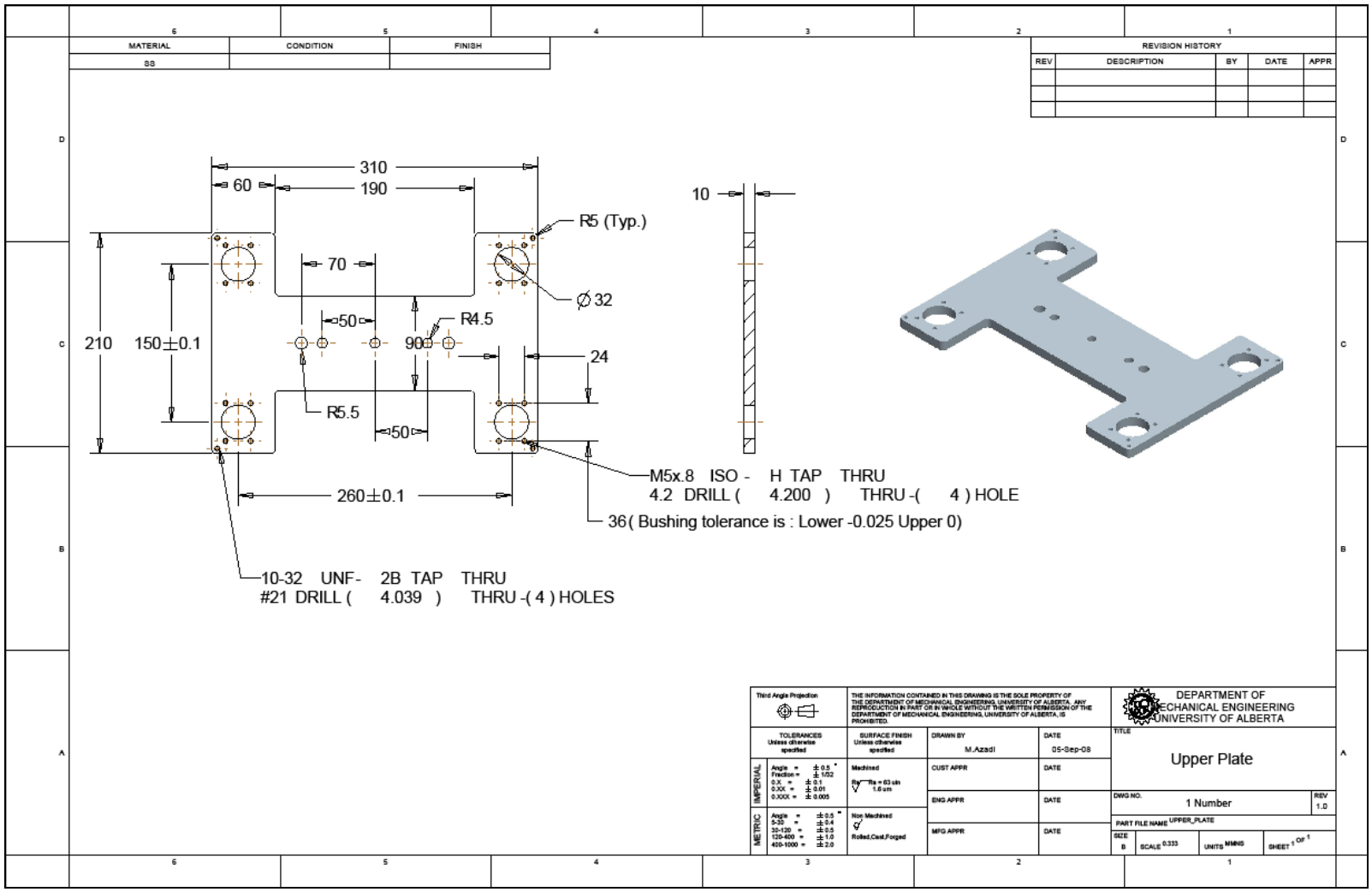
MATERIAL
CONDITION
FINISH
SS
REVISION HISTORY
REV
DESCRIPTION
BY
DATE
APPR
310
60
190
70
50
50
90
210
150±0.1
260±0.1
R5 (Typ.)
Ø32
R4.5
R5.5
24
10
M5x.8 ISO - H TAP THRU
4.2 DRILL (4.200) THRU -(4) HOLE
36 (Bushing tolerance is : Lower -0.025 Upper 0)
10-32 UNF- 2B TAP THRU
#21 DRILL (4.039) THRU -(4) HOLES
Third Angle Projection
THE INFORMATION CONTAINED IN THIS DRAWING IS THE SOLE PROPERTY OF THE DEPARTMENT OF MECHANICAL ENGINEERING, UNIVERSITY OF ALBERTA. ANY REPRODUCTION IN PART OR IN WHOLE WITHOUT THE WRITTEN PERMISSION OF THE DEPARTMENT OF MECHANICAL ENGINEERING, UNIVERSITY OF ALBERTA, IS PROHIBITED.
DEPARTMENT OF MECHANICAL ENGINEERING
UNIVERSITY OF ALBERTA
TOLERANCES
Unless otherwise specified
SURFACE FINISH
Unless otherwise specified
DRAWN BY
M.Azadi
DATE
05-Sep-08
IMPERIAL
METRIC
Machined
Non Machined
Rolled,Cast,Forged
CUST APPR
ENG APPR
MFG APPR
DATE
TITLE
Upper Plate
DWG NO.
1 Number
REV
1.0
PART FILE NAME
UPPER_PLATE
SIZE
B
SCALE
0.333
UNITS
MMNS
SHEET
1 OF 1

Appendix B

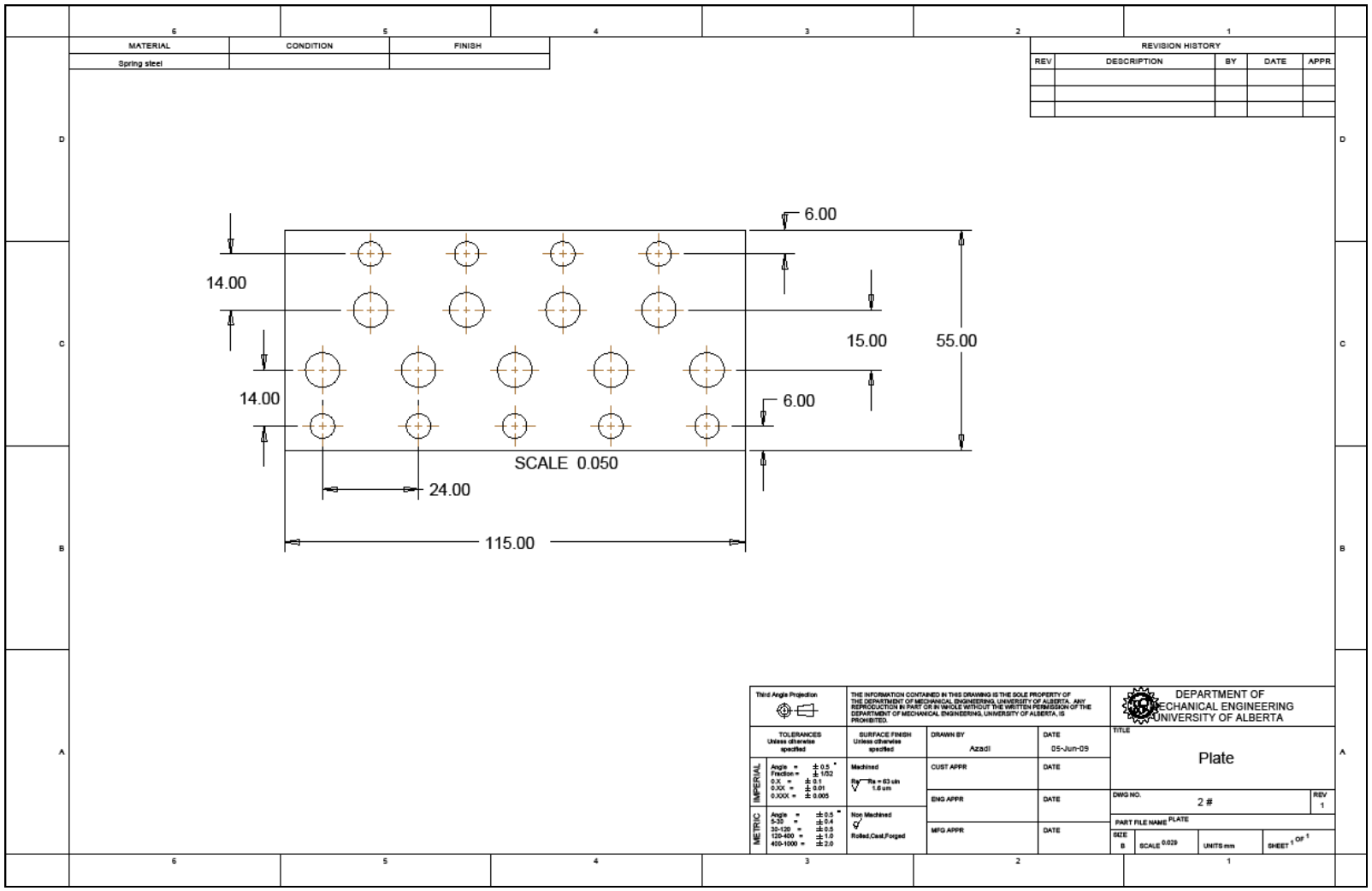
MATERIAL
CONDITION
FINISH
Spring steel
REVISION HISTORY
REV
DESCRIPTION
BY
DATE
APPR
6.00
14.00
15.00
55.00
14.00
6.00
SCALE 0.050
24.00
115.00
Third Angle Projection
THE INFORMATION CONTAINED IN THIS DRAWING IS THE SOLE PROPERTY OF THE DEPARTMENT OF MECHANICAL ENGINEERING, UNIVERSITY OF ALBERTA. ANY REPRODUCTION IN PART OR IN WHOLE WITHOUT THE WRITTEN PERMISSION OF THE DEPARTMENT OF MECHANICAL ENGINEERING, UNIVERSITY OF ALBERTA, IS PROHIBITED.
DEPARTMENT OF MECHANICAL ENGINEERING
UNIVERSITY OF ALBERTA
TOLERANCES
Unless otherwise specified
SURFACE FINISH
Unless otherwise specified
DRAWN BY
Azadi
DATE
05-Jun-09
IMPERIAL
METRIC
Machined
Non Machined
Rolled,Cast,Forged
CUST APPR
ENG APPR
MFG APPR
TITLE
Plate
DWG NO.
2 #
REV
1
PART FILE NAME
PLATE
SIZE
B
SCALE 0.029
UNITS mm
SHEET 1 OF 1